Photo Activated Ruthenium-containing Polymer Micelles to Overcome Multidrug Resistance

Dissertation
Zur Erlangung des Grades
„Doktor der Naturwissenschaften“
am FB 09 Chemie, Pharmazie, Geographie und Geowissenschaften
der Johannes Gutenberg-Universität Mainz

Von
Mingjia Chen
geboren in Chongqing, P.R. China

Mainz, 2020

Die vorliegende Arbeit wurde in der Zeit von September 2016 bis Juni 2020 unter der Betreuung von Prof. Dr. Hans-Jürgen Butt und Prof. Dr. Si Wu am Max-Planck-Institut für Polymerforschung in Mainz angefertigt.

Tag der Prüfung: 05.08.2020
Dekan: Prof. Dr. Tobias Reich
1. Berichterstatter: Prof. Dr. Hans-Jürgen Butt
2. Berichterstatter: Prof. Dr. Rudolf Zentel
Dissertation an der Universität Mainz (D77)

For my grandmother

Table of Contents

Chapter 1: Motivation

Cancer is one of the leading causes of human death in the world. Although significant improvement has been made in chemotherapy for cancer treatment, complete regression is still challenging. A great obstacle in chemotherapy is the acquired resistance when chemotherapeutics are used, inducing tumor recurrence and therapeutic failure. A main mechanism of multidrug resistance (MDR) is via expression of drug efflux transporters on the surface of tumor cells such as permeability glycoprotein (P-gp). They not only inhibit the uptake of chemotherapeutics, but also pumps them out from tumor cells. Moreover, high systemic toxicity of chemotherapeutics is another problem that hurdles the clinical treatment of cancer.

The development of nanocarriers brings new hope for chemotherapy. They exhibit a long circulation time in the bloodstream and can deliver drugs to tumor cells through nanotechnology-mediated passive or active targeting. What is important, in the process of uptake: nanocarriers can bypass P-gp so that the drugs are not recognized by P-gp as substrates. Thus, the drugs escape from the capture of the transporters, allowing a high intracellular drug accumulation. Although substantial progress has been made using nanocarriers, the entire eradication and cure of cancer remains a challenge. Nanocarriers need combine with other strategies to overcome MDR.

Compared to other external stimuli, light-triggered drug release has the potential advantage of its noninvasive nature and ease of spatiotemporal control. Most phototherapy studies used ultraviolet (UV) light or short-wavelength visible light to trigger the release of drugs. However, the depth of light penetration into tissue depends on the wavelength. When setting the the same light intensity, the light penetrates only ~1.00 mm at wavelength of 408 nm, but ~6.3 mm at wavelength of 633 nm and ~7.5 mm at wavelength of 705 nm. UV light or short-wavelength visible light not only shows limited penetration depth into tissue but also has the risk of photodamage to biological systems. In contrast, red or near infrared radiation (NIR) light can penetrate deeper into tissue and cause less photodamage, which is more suitable for *in vivo* applications.

The success of platinum (Pt) complexes such as cisplatin in cancer treatment motivates the development of new metallodrugs. Some Ruthenium (Ru) complexes are promising metallodrugs for anticancer therapy. More than three of them are in clinical trials. Photoactivation is a way to improve selectivity of Ru complexes in cancer therapy. Some of them are responsive to red or NIR light. The successful delivery of photoactivatable Ru complexes to cancer cells requires that they must be stable in the dark under physiological conditions. However, the ligands of photoactivatable Ru

complexes may be substituted by water and biomolecules such as dissolved proteins before they are delivered to cancer cells.

Therefore, the question arise: what need to do for overcoming MDR of cancer cells more efficiently? Combined nanocarriers with phototherapy of Ru complexes using red light may settle this problem. The aim of this thesis is a prerequisite to answer the question, namely to improve the stability of photoactivatable Ru complexes under physiological conditions.

In this thesis, I first systematically studied the stabilities of two Ru-containing block polymers and their corresponding Ru complexes under imitated physiological conditions. I concluded from results that in the different media, the corresponding Ru complexes were stabilized by their Ru-containing polymer assemblies, which made these assemblies potential candidates for biomedical applications.

Then, red-light-triggered Ru-containing block copolymer (PEG-*b*-P(CPH-*co*-RuCHL)) micelles with doxorubicin (DOX) encapsulation (DOX@PEG-*b*-P(CPH-*co*-RuCHL)) were designed. Red light induced the destruction of DOX@PEG-*b*-P(CPH-*co*-RuCHL) micelles, resulting in the release of Ru complexes and DOX simultaneously.

Finally, DOX@PEG-*b*-P(CPH-*co*-RuCHL) micelles were used to overcome MDR. After bypass P-gp, DOX@PEG-*b*-P(CPH-*co*-RuCHL) micelles were accumulated in drug-resistant Michigan Cancer Foundation-7 (MCF-7R) breast cells. The intracellular release of DOX was controlled by red light. Deoxyribonucleic acid (DNA) damage was caused via DOX interacted with DNA by intercalation and Ru complexes crosslinked with DNA by photobinding. I also studied the effect of overcoming MDR *in vitro* and *in vivo*. DOX@PEG-*b*-P(CPH-*co*-RuCHL) micelles that were activated by red light irradiation induced the significant death of MCF-7R cells and the excellent inhibition of the growth of MCF-7R tumor. I believe that the design of the controlled release of dual drugs from red-light-responsive Ru-containing polymer micelles will open up an avenue for photochemotherapy to overcome MDR.

Chapter 2: Introduction

2.1 Nanocarriers to overcome multidrug resistance

2.1.1 Multidrug resistance

Cancer is a devastating disease that arises from cellular abnormalities and genetic alterations. The mutated cells proliferate indefinitely and escape from the apoptosis, leading to tumor formation and high mortality in patients.[1-4] More than 10 million new cases of cancer take place every year.[5] Advanced cancer requires systemic treatment.[6] Chemotherapeutic drugs as one of the standard methods are used effectively to treat cancer by targeting specific multiple pathways.[7-9] However, many defects of traditional systemic chemotherapy including the ineffective delivery of the drug agents to the specific tumor site and the subsequent toxicity to healthy tissues, limit the treatment of the disease.[10, 11] Moreover, repeated use of the drug agents can result in dose-dependent adverse conditions or develop to MDR.[12]

Because of the pharmacological features of the drug agents, the dose-dependent cumulative adverse effects are not tissue-specific, but refer to all tissues in a general manner. What's more, the high turnover rates of the gastro-intestinal system and skin induce the increased toxicity of the drug agents, which are the most common dose-restraining cumulative adverse effects during chemotherapy.[13]

The appearance of MDR in tumor cells is a major challenge, inducing the failure of tumor standard therapeutic and the relapse in patients undergoing metastatic cancer conditions.[14] The biological paths by which tumor cells are capable of escaping death by chemotherapy are multitudinous and complicated. The main mechanism of MDR is reported as follows: (a) over expression of drug efflux transporters on the surface such as P-gp, which not only inhibits the uptake of chemotherapeutics, but also pumps them out of tumor cells;[15-17] (b) modification of drug targets by up-regulated expression of target enzymes such as β-catenin and thymidylate synthase;[18, 19] (c) enhanced DNA repair capacity by exacerbated activity of excision repair cross-complementing protein following tumor cell DNA damage;[20, 21] (d) apoptotic pathway defects by activation of transcription hypoxia-inducible factor-1 to strengthen the expression of MDR-related genes such as adenosine triphosphate (ATP)-binding cassette (ABC) transporters, metallothionein, glutathione and B-cell lymphoma 2 (Bcl-2) protein family.[22-26] The mentioned chemoresistance pathways in tumor cell are summarized in Figure 1.

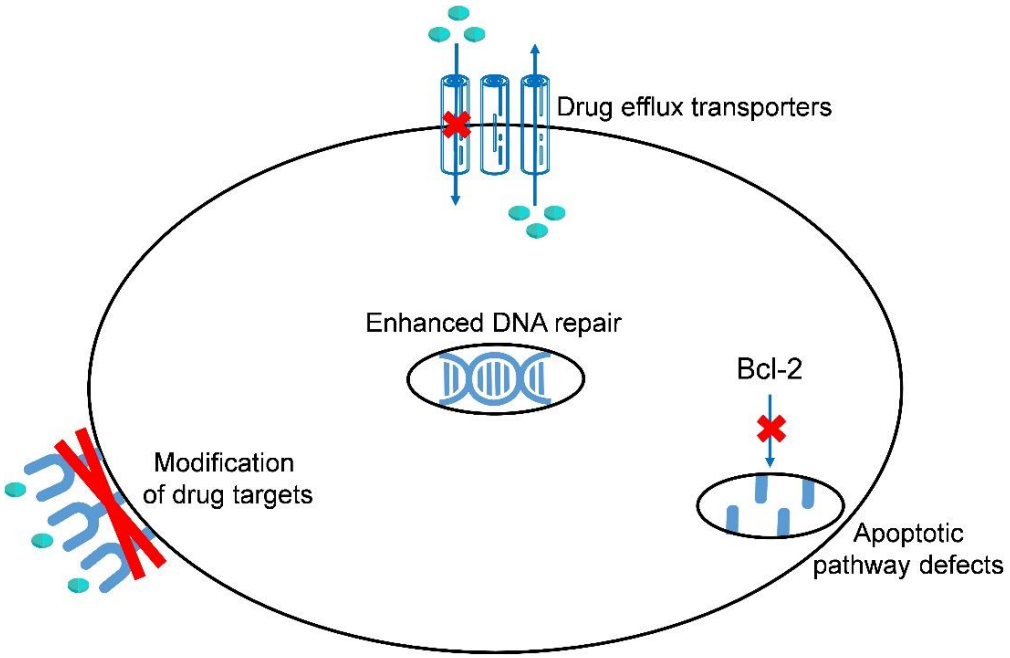

Figure 1. Mechanism of multidrug resistance in tumor cell.

2.1.2 Properties of nanocarriers

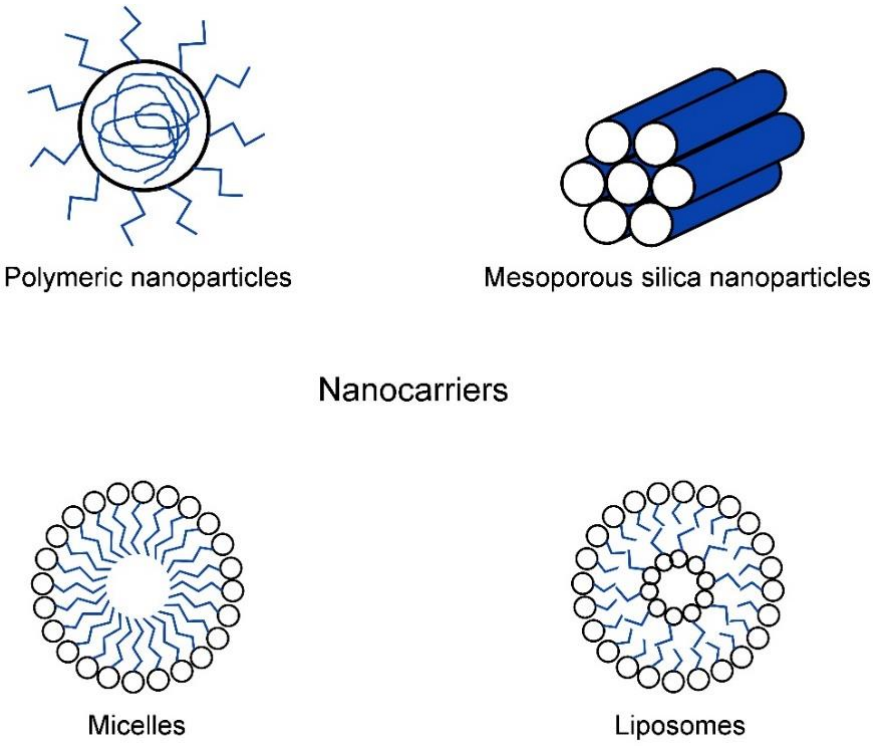

Figure 2. Major classes of nanocarriers utilized for overcoming multidrug resistance.

Nanocarriers for anticancer drugs are being investigated in anticancer therapy, which aim to enhance treatment efficacy, decrease side effects, and overcome MDR.[27, 28] The most common nanocarriers include polymeric nanoparticles, mesoporous silica nanoparticles (MSNs), micelles, liposomes etc (Figure 2). They exhibit stable, non-toxic and biocompatible properties, that are applied for drug delivery in cancer imaging, diagnosis and treatment.[26, 29, 30]

2.1.2.1 Permeability and retention effect

The higher porosity of surrounding angiogenesis and impaired lymphatic drainage are caused by the formation of tumor.[31] Various nanocarriers rely on the tumor characteristics to accumulate drug efficiently at the tumor site, which are regarded to be passively targeted. Nanocarriers that are 10-200 nm in diameter contribute to drug uptake into tumor via enhanced permeability and retention (EPR) effect.[32-34] However, the size of pores in blood vessels are not the same in different tumor species or even a same tumor, inducing that the drug is unpredictably accumulated in only certain areas at tumor. The EPR effect is also affected by the size and location of the tumor, the neighboring stroma, the infiltration number of macrophages, and patient features. Current clinical data comes from the passive target to liposomes, but numerous nanocarriers for active targeting are also being developed in clinic.[35] Still, the accumulation of nanocarriers by EPR effect within a tumor is better than the enrichment of free drugs such as DOX, paclitaxel, salinomycin, rapamycin, thiostrepton etc.[36-40]

2.1.2.2 Attachment of polyethylene glycol

Traditional chemotherapeutic agents may be quickly cleared from the body because of non-targeting and poor bioavailability. Their short half-life in blood leads to low therapeutic efficiency. Moreover, they do not accumulate at tumor sites, leading to the subsequent toxicity to healthy tissues. Nanocarriers conjugated to polyethylene glycol (PEG) show a reduction of the extravasation into normal tissues,[41-43] and an extension of circulation time *in vivo*.[44, 45] Specifically, this strategy can lower opsonization, promote the protein adsorption, avoid aggregation, stabilize the lipid layers, and restrict the binding of reticuloendothelial system cells which may clear nanocarriers.[46] Doxil®/Caelyx® Liposomal DOX is the first PEGylated nanocarrier approved in the USA and Europe. It can be utilized for treatment of recurrent ovarian cancer,[47] multiple myeloma,[48] and Kaposi's sarcoma.[49] Whereas, the conjugation of PEG to nanocarriers may also induce the side effect of immunological response by complement activation.[50]

2.1.2.3 Bypass of drug efflux pumps

Nearly all free drugs enter tumor cells by diffusion via membranes. The membrane-bound ABC transporters such as P-gp can pump them out from tumor cells, resulting in MDR. However, nanocarriers can effectively enter tumor cells through endocytosis. P-gp cannot recognize the drugs, chemical conjugating or encapsulated into nanocarriers as substrates. Thus, drugs inside nanocarriers escape the capture of the transporters, permitting the high intracellular drug accumulation.[51] After endosomal and lysosomal transport,[52] the active drugs are released from nanocarriers to the perinuclear area of the cytoplasm (Figure 3).

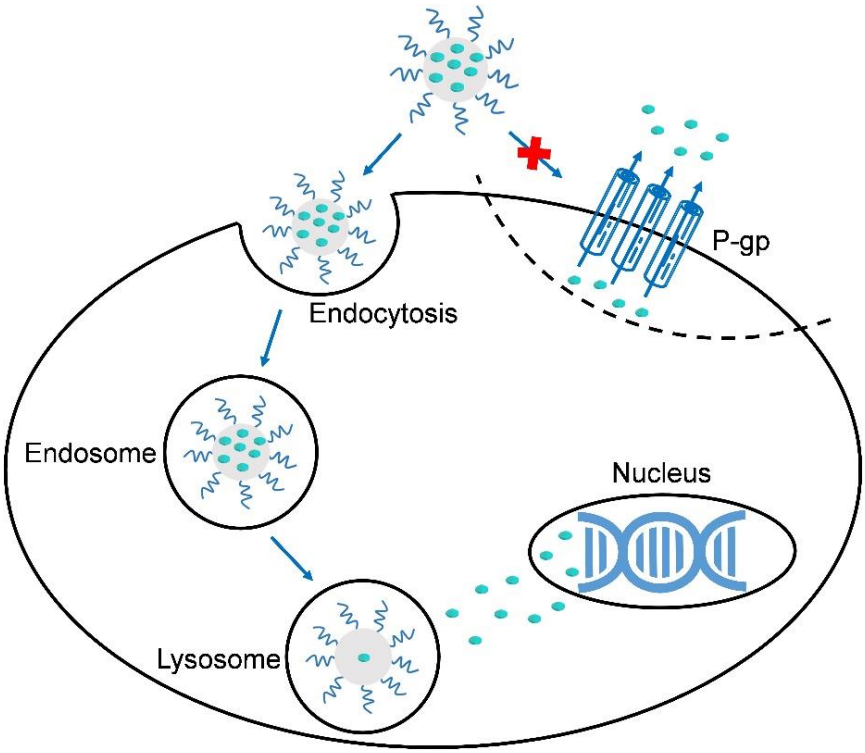

Figure 3. Schematic illustration of the bypass P-gp of nanocarriers to overcome multidrug resistance in tumor cell.

2.1.3 Combined treatment strategies based on nanocarriers

Although substantial progress has been made to overcome MDR using nanocarriers, the entire eradication and cure of cancer remain a tough challenge. Therefore, multifunctional nanocarriers are fast developing and providing a multi-modality therapeutic approach for fulfilling a favorable outcome.[53] The strategies include synergistic co-delivering of a chemotherapeutic agent with a proper chemosensitizer, such as an inhibitor of drug efflux pumps or a mitochondria-targeted agent or a gene-silencing agent of MDR; endosomal decomposition by incorporating carbon dioxide

(CO_2)-generating ingredients to reinforce intracellular drug accumulation.

2.1.3.1 Delivery of inhibitor of drug efflux pumps

The first identified transporter relevant for MDR is P-gp, that is most characterized and certified as a feasible target to overcome MDR.[54] In spite of the efficient uptake of nanocarriers into tumor cells via ‘‘P-gp bypass effect’’, numerous P-gp also distribute inside cells, such as intracellular membranes, Golgi apparatus, intracytoplasmic vesicles, nuclear envelope.[55-57] Therefore, the released drugs are also hard to reach their intracellular targets and unfold their activity. Currently, synergistic co-delivery of anticancer drugs and P-gp inhibitors by nanocarriers is developed for a good option to overcome MDR.[58, 59]

Tang et al. reported that a redox-sensitive liposome was prepared to co-encapsulate DOX and a P-gp inhibitor of verapamil (Figure 4).[60] Combining ‘‘P-gp bypass effect’’ and ‘‘P-gp inhibition effect’’, the system could inactivate the P-gp, which localized in membrane and nuclear envelope of tumor cells, resulting in the improved intracellular DOX accumulation and then killing the cells effectively.

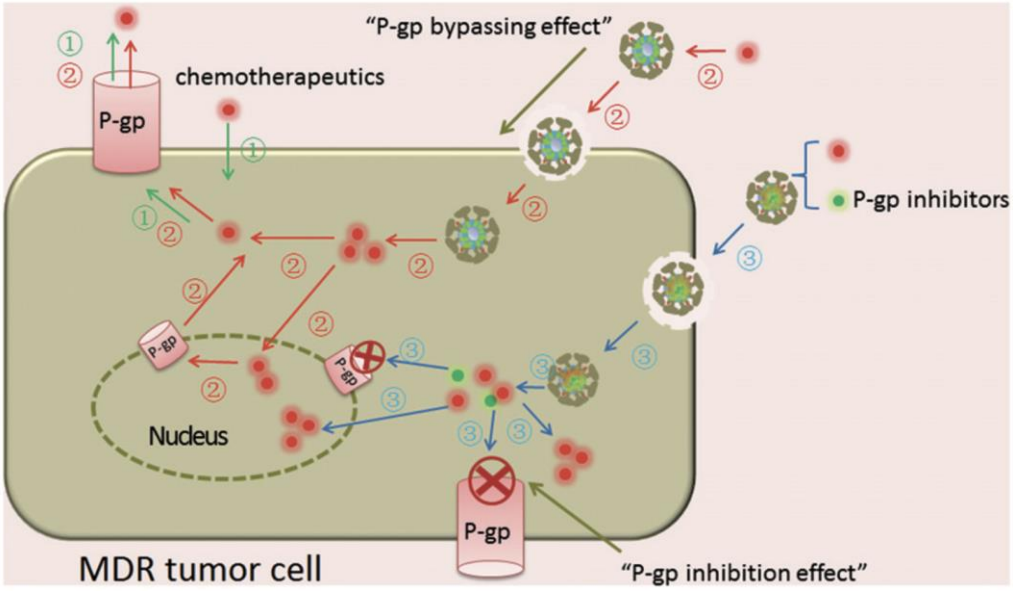

Figure 4. The intracellular delivery routes of different drug formulations in MDR cells. Drugs are ejected by P-gp (route 1). Although the uptake of nanocarriers via ‘‘P-gp bypass effect’’, the released drugs are ejected again by P-gp (route 2). DOX and a P-gp inhibitor co-loading nanocarriers can enhance drug accumulation and target organelles under the synergy of ‘‘P-gp bypass effect’’ and ‘‘P-gp inhibition effect’’ (route 3). Reproduced by permission of ref 60. Copyright 2016 Taylor & Francis.

2.1.3.2 Delivery of mitochondria-targeted agent

ATP is the energy source of tumor cells. Oxidation of glucose can produce a high proportion of ATP. The mitochondria are the cellular power stations, where ATP is primarily generated. Since drug efflux pumps show a high energy requirement, targeting the mitochondria seems to be an appealing solution to overcome MDR.[61] Besides the relevant role in survival of tumor cells, the mitochondria are crucial regulators of apoptotic pathway.[62] They control some effector cascades by releasing pro-apoptotic proteins such as cytochrome c, apoptotic protease activating factor 1 and diablo homolog, which normally dwell in the inter-membranous area. Therefore, the characters of the mitochondria make them ideal targets to overcome MDR.[63]

Chen and colleagues reported an intracellular transformable nanomedicine accompanied by programmed therapeutic effect for reversal of MDR (Figure 5).[64] The micellar nanoparticles were triggered to switch to drug nanofibers in response of overexpressed matrix metalloproteinases in tumor, inducing the enhanced intracellular drug retention. In addition, the release of proapoptotic peptide $(KLAKLAK)_2$ could decrease ATP production by the damage of targeted-mitochondria, that further blocked the drug efflux pumps and prolonged the drug residence time. This integrated approach significantly improved the bioavailability of chemotherapeutic agents.

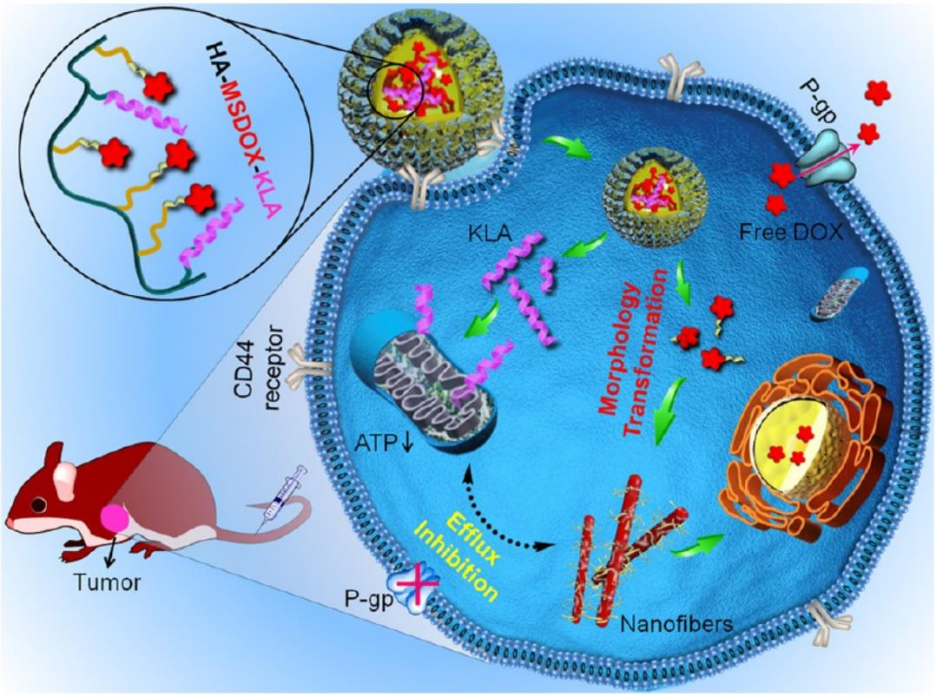

Figure 5. Schematic illustration of the integrated strategy to overcome MDR by the tumor-triggered transformable nanomedicine. Reproduced by permission of ref 64. Copyright 2016 American Chemical Society.

2.1.3.3 Delivery of gene-silencing agent

An important mechanism that cause MDR is apoptotic pathway defects.[65] Simple nanocarriers cannot address the activation of anti-apoptotic pathways. Small interference ribonucleic acid (siRNA) can disrupt cellular pathways, providing a new approach for treatments of diseases resulted from aberrant gene expression.[66, 67] However, siRNA will be rapid degraded by ribonuclease enzymes in the bloodstream and cleared by the renal system, reducing the treatment effect.[67] If siRNA and chemotherapeutic drugs are co-encapsulated into nanocarriers, their synergistic effectiveness may be improved. Nanocarriers can protect them until the uptake by tumor cells. siRNA silences the genes that are responsible for MDR, making the cells more sensitive to chemotherapeutic drugs.[68]

Chen and colleagues reported use of MSNs as a nanocarrier to simultaneously release DOX and Bcl-2-targeted siRNA in MDR cancer cells for increased efficacy of chemotherapy (Figure 6).[69] DOX was primarily concentrated at perinuclear region after internalization, because of bypassing pump resistance via MSNs. The Bcl-2 mRNA was effectively silenced and non-pump resistance was significantly suppressed by the Bcl-2 siRNA, which elevated the anticancer activity of DOX.

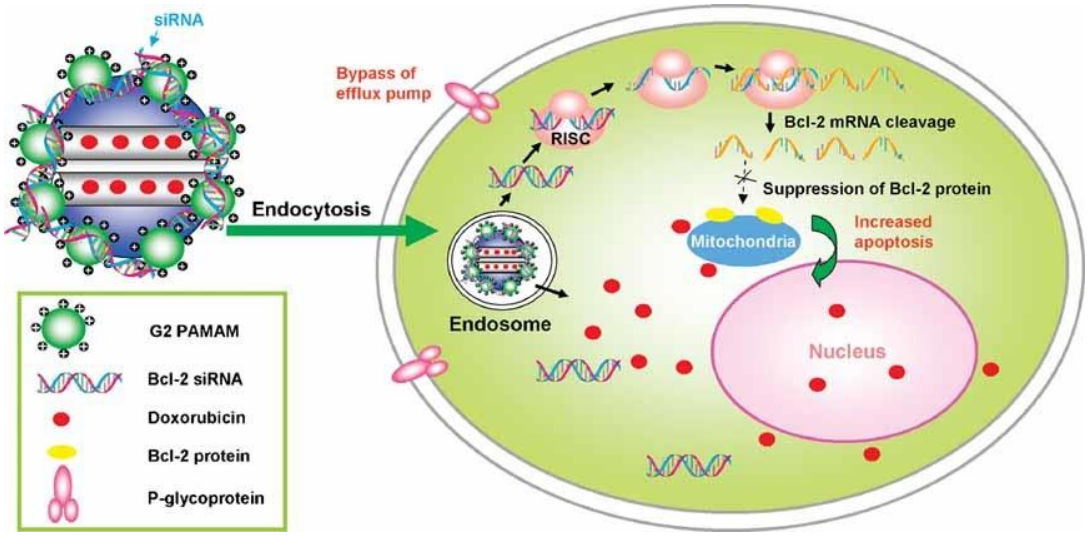

Figure 6. Schematic illustration of a co-delivery system based on MSNs to deliver DOX and Bcl-2-targeted siRNA simultaneously to A2780/AD human ovarian cancer cells for enhanced chemotherapy efficacy. Reproduced by permission of ref 69. Copyright 2009 WILEY-VCH.

2.1.3.4 Generation of carbon dioxide

Poly(lactic-co-glycolic) acid (PLGA) is known as an efficient and biomedically safe copolymer. It shows a tunable structure, an encapsulated capacity of diverse agents,

biocompatibility and biodegradation. Food and drug administration approve its application in drug delivery systems. Besides, PLGA can influence the regulation of P-gp, which may assist to overcome MDR.[70] However, the release of drug from PLGA nanocarriers in tumor cells may continue from days to months, because of the slow diffusion process. Thus, the drug concentration of the optimum therapeutic threshold cannot be reached, resulting in the failure of overcomeing MDR.[71] In other hand, Bicarbonates can be loaded into nanocarriers for CO_2 gas-triggered drug release. Bicarbonates react with acid to produce a salt and carbonic acid, that effortlessly decomposes into water and CO_2.[72]

Ke and colleagues developed a pH-responsive PLGA hollow particle to overcome MDR (Figure 7).[73] DOX and $NaHCO_3$ were encapsulated in the core of PLGA hollow particles, which experienced a progressively acidic environment after uptake by cells. Because of the increasing acidification, CO_2 bubbles were produced from $NaHCO_3$ in the late endosomes/lysosomes, inducing the particle disturbances and the accelerated DOX release. Finally, DOX accumulated in the nuclei and killed MDR cells.

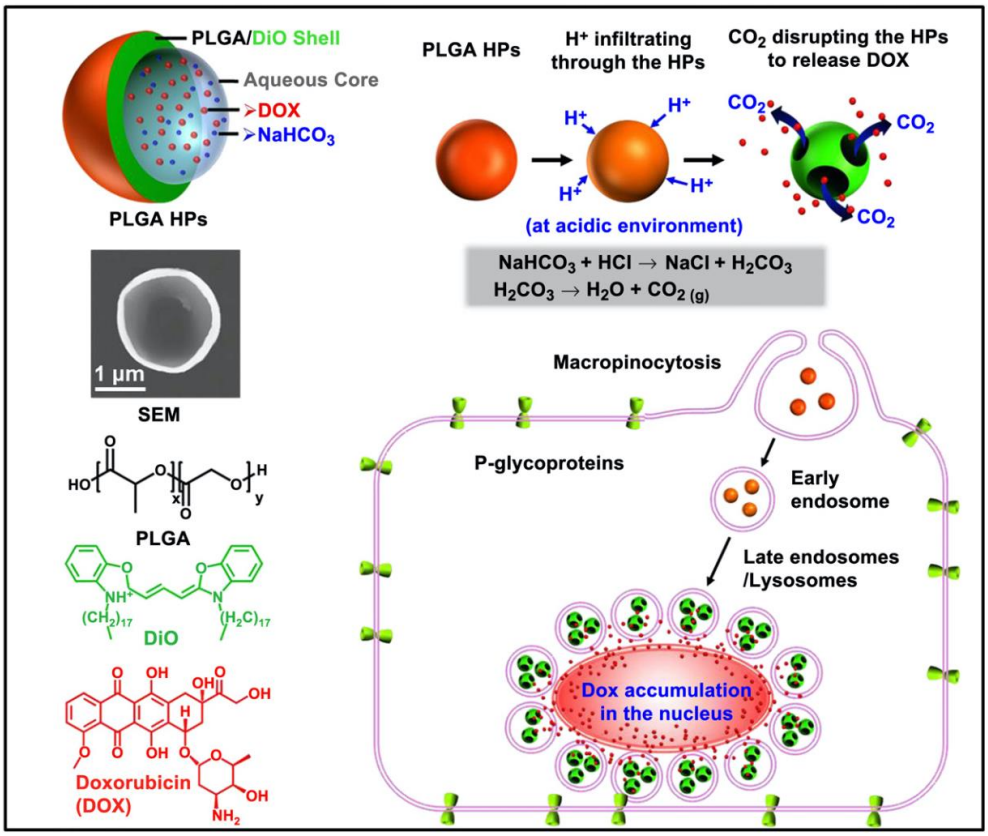

Figure 7. The structure of the PLGA hollow particle and its pH-response to overcome MDR. Reproduced by permission of ref 73. Copyright 2013 Elsevier.

2.2 Phototherapy in nanocarriers to overcome multidrug resistance

Stimulus-sensitive nanocarriers that can respond to particular stimuli of endogeneity such as pH, redox, enzymes, overexpression of biomolecules (e.g., glutathione, adenosine triphosphate)[74] or stimuli of exogeneity such as temperature, ultrasound, light, mechanical force, and magnetic field,[75] have been developed to control the delivery and trigger the release of drugs. Among the external stimuli, light is particularly attractive because of its noninvasive nature, ease of production and spatiotemporal control.[76]

Different wavelengths of light such as UV, visible, and NIR light can be utilized to trigger light-responsive drug release.[77] UV light is considered to be hazardous for clinical application since it can damage of nucleic acids, proteins and other biomolecules.[78] Because of decreased absorption in tissue, less reflection and scattering, red or NIR light that localized in the phototherapeutic window can penetrate deeper into living tissue than UV or visible light (Figure 8).[79, 80] Thus, red or NIR light is the optimal choice for deep tissue treatment.

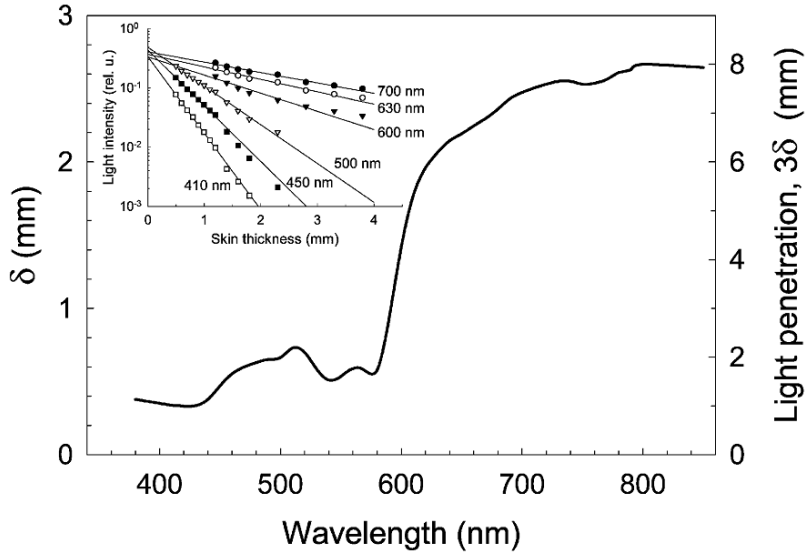

Figure 8. The light penetration depth in the rat skin. Insert: light influence presented for some of the wavelengths. Reproduced by permission of ref 80. Copyright 2002 Royal Society of Chemistry.

To overcome MDR, phototherapy in nanocarriers can be divided into three different categories: photothermal therapy (PTT), photodynamic therapy (PDT), and photo-activated chemotherapy (PACT).[81, 82]

2.2.1 Photothermal therapy in nanocarriers

PTT uses light (most in infrared wavelengths) as the source, bringing the phototherapy agent to an excited state and then generating a high temperature.[83, 84] The high temperature causes lysis and release of digestive enzymes, resulting in the necrosis of tumor cells.[85] Figure 9 illustrates the cellular destruction at different temperatures. An advantage of the heating effect is that the dose of light can be restricted to prevent the damage of normal tissues. The principle of PTT approach in nanocarriers is that nanocarriers can efficiently transform the absorbed light into localized heat, that cause hyperthermia around the nanocarriers.[85, 86] The ease of this approach provides the possibility to combine it with other approaches to overcome MDR.

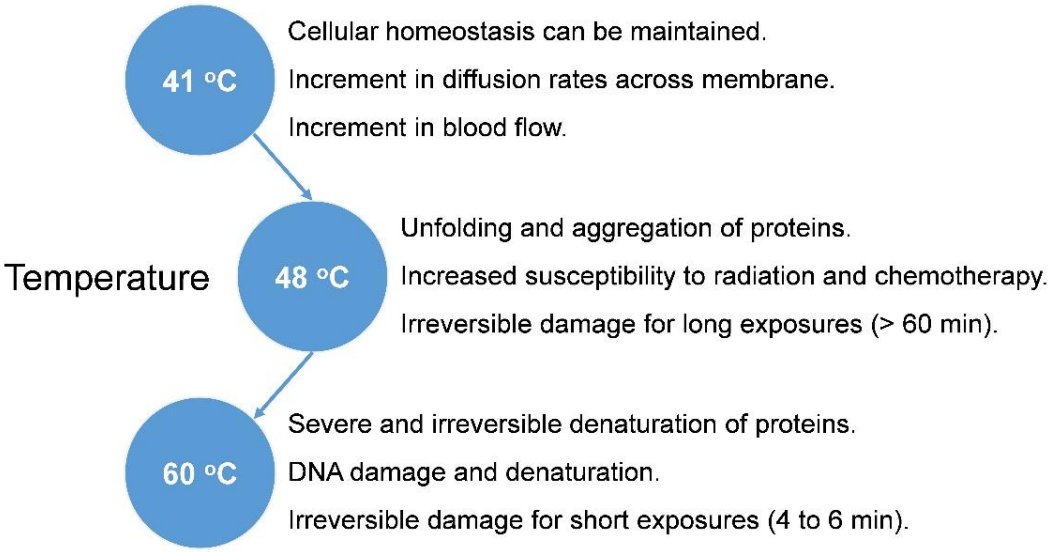

Figure 9. Different temperatures mediated cellular destruction.

Li et al. prepared an IR-780 loaded polymeric prodrug micelle with pH responsiveness and NIR photothermal effect to conduct chemo-photothermal therapy for reversal of MDR (Figure 10).[87] The micelles exhibited the rapid release of DOX in acidic condition and significant hyperthermia under NIR laser irradiation. The temperature elevation integrated with acid-sensitive prodrugs enhanced the intracellular DOX accumulation, inducing apoptosis of MCF-7R cells and the suppression of the growth of MCF-7R tumor. The synergistic PTT and chemotherapy of the micelles presented a potential strategy to overcome MDR.

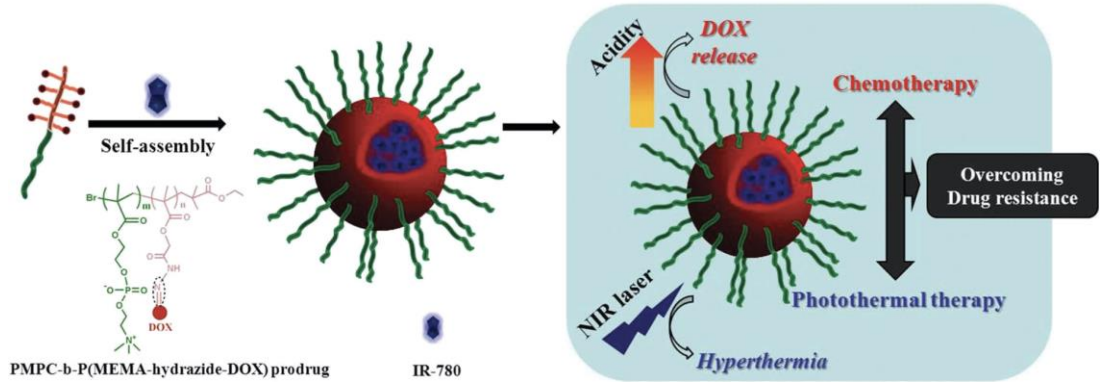

Figure 10. Schematic representation of an IR-780 loaded polymeric prodrug micelle for chemo-photothermal therapy to overcome MDR. Reproduced by permission of ref 87. Copyright 2016 Wiley-VCH.

2.2.2 Photodynamic therapy in nanocarriers

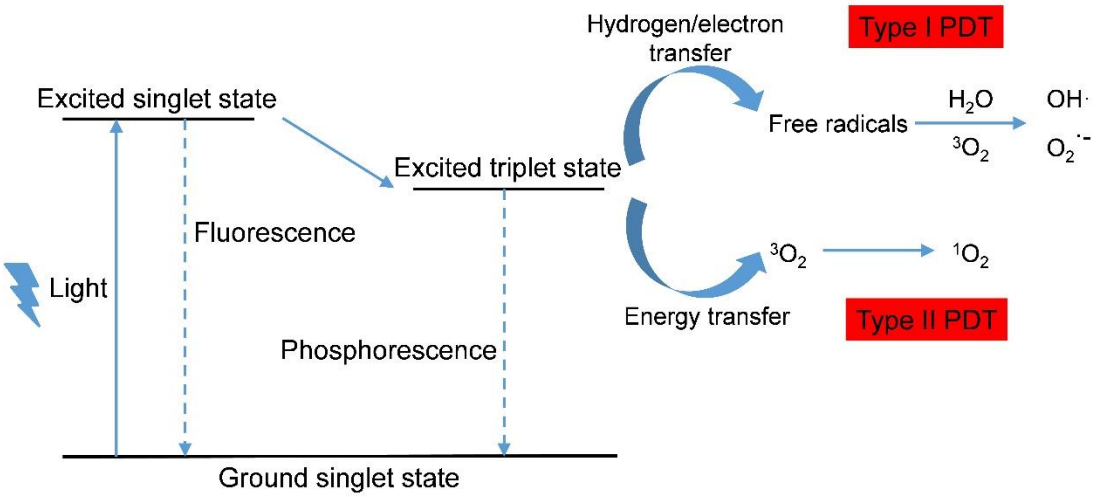

Figure 11. Scheme of the photochemical reactions for type I and type II PDT.

PDT is a photoactivation form for cancer treatment. Spatial confined light excites photosensitizer, that can generate reactive oxygen species (ROS) including singlet oxygen ($^1O_2$) and oxygen free radicals to induce the selective death of tumor cells.[88-90] Although the processes of PDT are oxygen-dependent in most cases, some PDT can occur under hypoxia, without oxygen involvement.[91-93] There are usually two types of reactions leading to ROS (Figure 11). The photosensitizer absorbs light, resulting in the transition from ground singlet state to excited singlet state. Then it transfers to excited triplet state via intersystem crossing. [94, 95] During process of type I PDT, the excited triplet state interacts with a biological substrate to generate free radicals by transfer of

a proton or an electron. Following that, these radicals interact with water and triplet oxygen ($^3O_2$) to produce hydroxyl radicals and superoxide anions, respectively.[96, 97] For type II PDT, energy is directly transferred from the excited triplet state to the surrounding $^3O_2$, converting $^3O_2$ into $^1O_2$.[98-100] Thus, type I PDT can take place under hypoxia, while well-oxygenated environment is precondition for type II PDT. However, PDT has some limitations such as low depth of penetration and poor water solubility of photosensitizer. Comparable with PTT, PDT is also applied in combination with other strategies in nanocarriers to improve its performance and overcome MDR.[101]

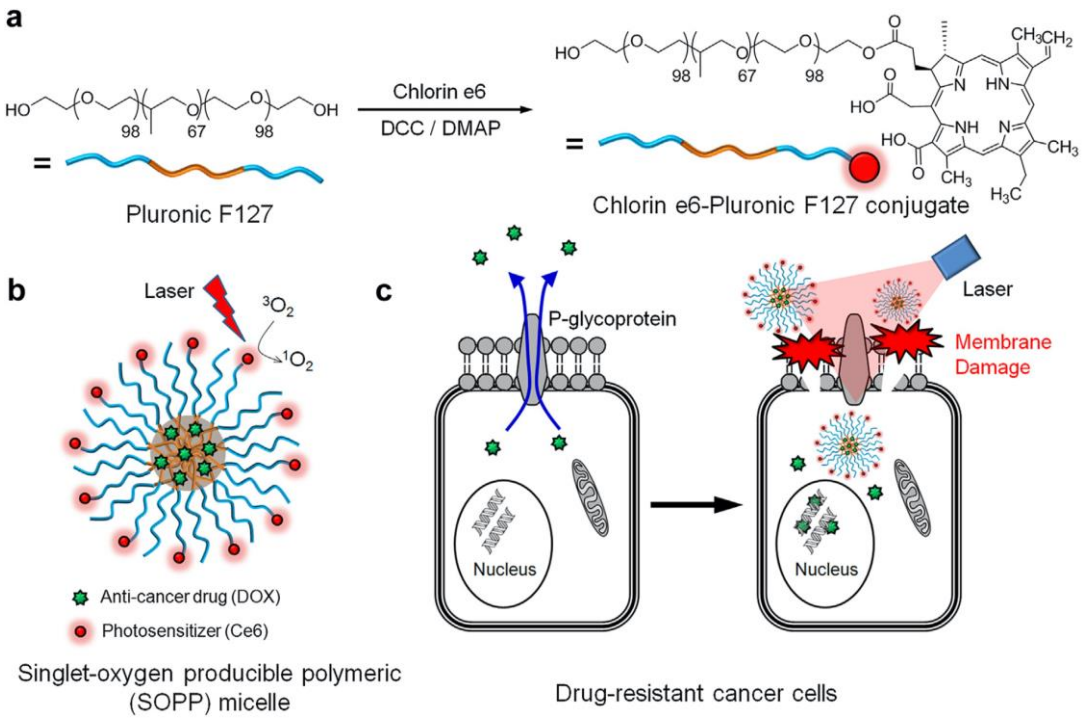

Figure 12. (a) Synthetic route to amphiphilic copolymer conjugated with chlorin e6. (b) Schematic illustration of the generation of singlet oxygen by micelle upon laser irradiation. (c) Schematic illustration of strategy for overcoming MDR in cancer cells via singlet-oxygen-mediated cellular membrane damage. Reproduced by permission of ref 102. Copyright 2014 Elsevier.

Park et al. demonstrated a singlet-oxygen producible polymeric micelle based on amphiphilic copolymer conjugated with chlorin e6 as photosensitizer by photochemical internalization. DOX was loaded with the micelles to overcome MDR (Figure 12).[102] The micelles displayed increased cancer-targeting effectiveness. Under laser irradiation, the photosensitizer moiety damaged the cellular membrane by singlet-oxygen-mediation, causing enhanced cell membrane permeability and rapid DOX accumulation,

thus exhibiting significant chemotherapeutic efficiency to overcome MDR.

2.2.3 Photo-activated chemotherapy in nanocarriers

PACT can use light to cleave the photolabile chemical bonds, which combine chromophores with anticancer agents or other toxic molecules, and then release the agents at a specific site to induce the death of tumor cells.[103, 104] Generally, chromophores exhibit low toxicity to cells when they are transported in the dark. After irradiation by light, they are converted from a ground state to an excited singlet state, which is not unstable. Subsequently, they decay back to the ground state in a nonradiative manner during a short time period.[104] Ligand dissociation occurs within this decay pathway, causing the release of compounds. For some chromophores such as transition metal complexes, their residuals after light irradiation can covalent bonds with DNA, distort the structure and finally kill the tumor cells.[105] Two representative PACT of transition metal complexes, Pt complexes and Ru complexes, are illustrated in Figure 13.[82, 106] They appear to be non-toxic to cells in the dark but are activated by the light. As a result, they become toxic to cellular components, such as DNA and proteins. Moreover, unlike PDT, the reaction of PACT does not demand oxygen, thus it can work under normoxia and hypoxia.

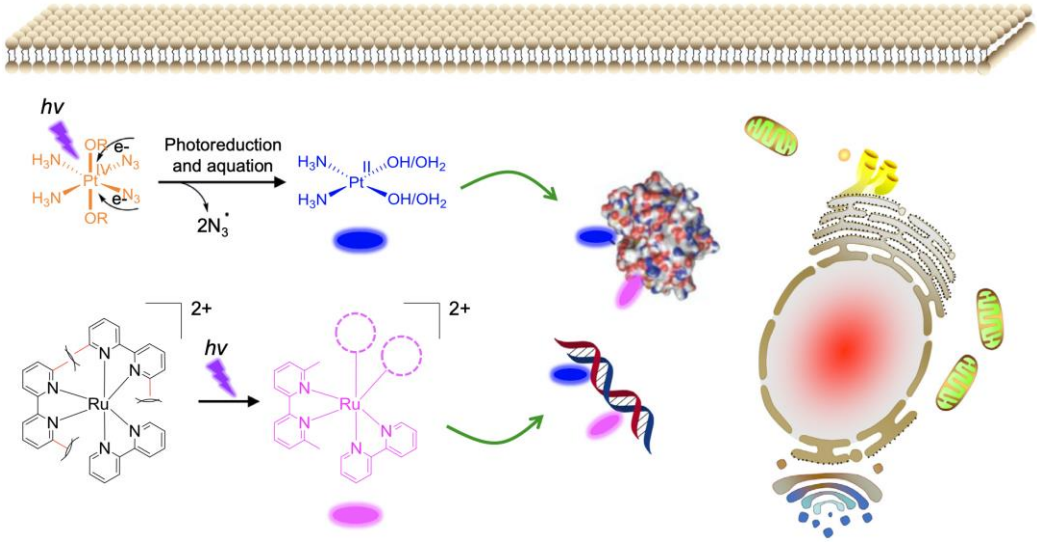

Figure 13. Schematic representation of two kinds of metal complexes for PACT. Reproduced by permission of ref 82. Copyright 2019 Elsevier.

Song and colleagues reported a sterically hindered photosensitive Pt(IV) prodrug that was conjugated to biodegradable polymers. It achieved a great enhancement of the anticancer efficacy to cisplatin resistant cancer cells (Figure 14).[107] The polymer

conjugates self-assembled into nanoparticles to inhibit premature binding and thiol detoxification of Pt drugs. The nanoparticles showed > 100 times more effective upon photo-activation, compared to cisplatin. This simple approach could open an avenue for designing new Pt(IV) agents to overcome MDR.

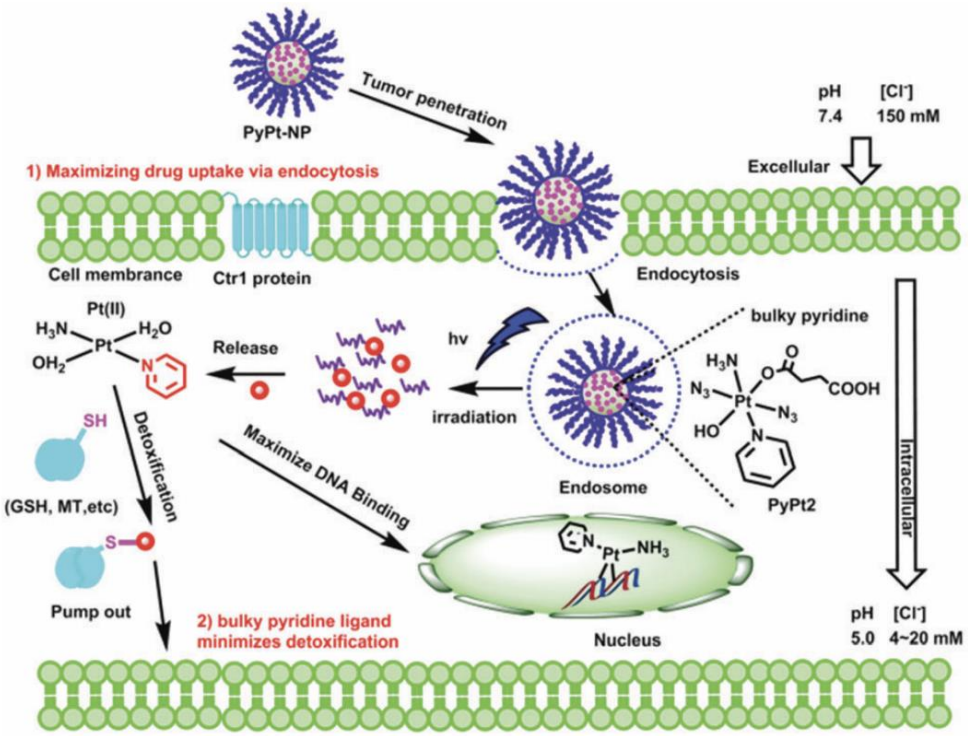

Figure 14. Schematic of intracellular pathway of sterically hindered photosensitive Pt drugs. Adapted by permission of ref 107. Copyright 2016 Royal Society of Chemistry.

Nitric oxide (NO) is a colorless, odorless, diffusible, lipophilic, short-lived radical molecule, playing a crucial role in the process of physiology and pathology.[108] NO can react with ROS to relieve oxidative stress, that may restrict the scavenging and tolerance systems in MDR tumor cells.[109, 110] Additionally, NO can suppress the P-gp expression to return the cytotoxicity of drugs in MDR cells.[111, 112] Hence, PACT combined with NO generation is a potential strategy to overcome MDR.

Fan et al. constructed a biodegradable nanomedicine wrapped with DOX and the UV/vis light-responsive *N,N′*-di-sec-Butyl-*N,N′*-dinitroso-1,4-phenylenediamine (BNN6), that acted as nitric oxide donor (Figure 15).[113] This nanomedicine was stable under physiological conditions. After UV/vis light irradiation, the generated NO gas from BNN6 ruined the nanoparticle shell and accelerated the release of DOX. Furthermore, NO functioned to reverse the MDR of tumor cells, leading to an increase of chemosensitization of DOX.

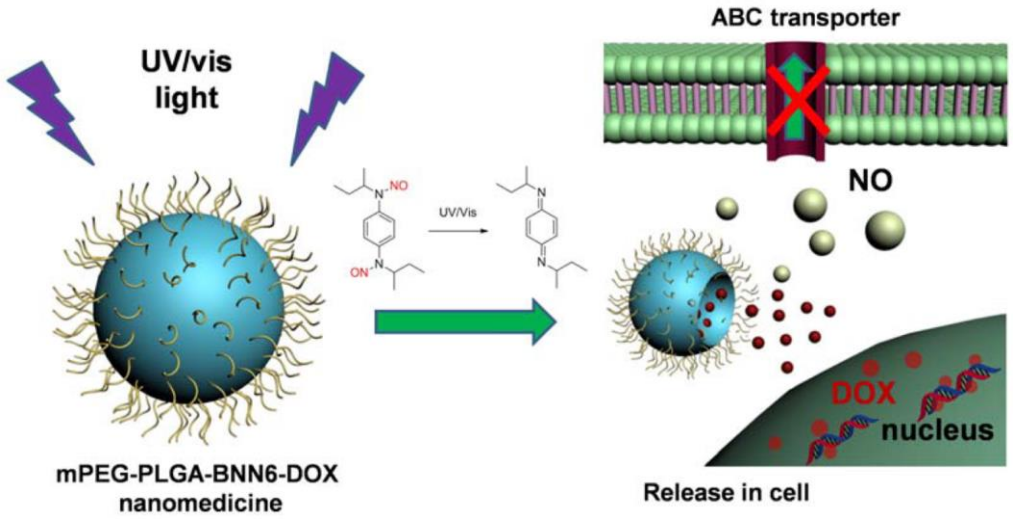

Figure 15. mPEG-PLGA-BNN6-DOX nanoparticles release NO and DOX inside cells. Reproduced by permission of ref 113. Copyright 2016 American Chemical Society.

2.3 Ruthenium-containing materials for phototherapy

2.3.1 Ruthenium complexes as anticancer therapeutics

Metallotherapeutics has attracted mounting attention after the discovery and advancement of Pt compounds.[114, 115] Their metal scaffolds can trigger the damage of DNA and the disruption of DNA repair process, causing cell apoptosis.[116-118] Cisplatin is one of the most common metallotherapeutics, that are applied in the clinic to treat manifold forms of human cancers. However, the serious side effects and increasing drug resistance of cisplatin limit its therapeutic value.[119] This motivates the development of new metallotherapeutics. Ru complexes are promising candidates as antitumor therapeutics.[120]

Due to different ligand exchange kinetics, high biological activity and low genotoxicity, some Ru-based therapeutics are successfully used in clinical trials, including Ru(III) species (KP1019, KP1339 and NAMI-A) (Figure 16) and Ru(II) species (TLD1433).[121-123] Their activation mechanisms have been reported.[124, 125]

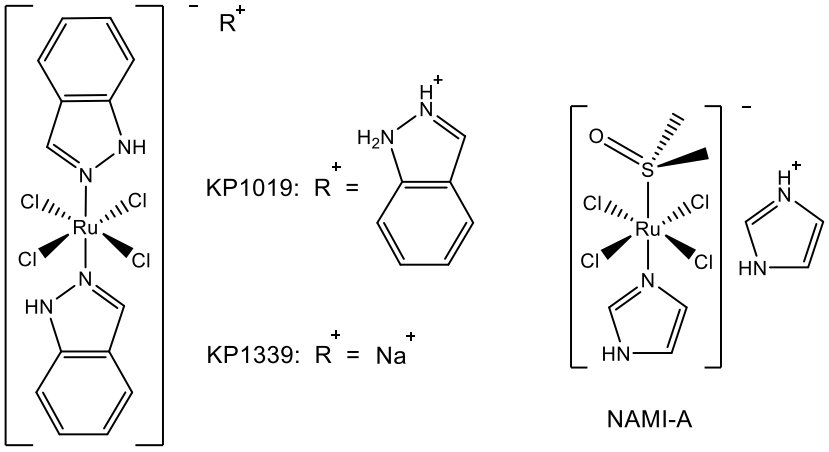

Figure 16. Structures of Ru(III) complexes in clinical trials.

KP1019 has been studied for its hydrolysis behavior and protein binding ability (Figure 17A).[126-128] The large-scale binding to serum proteins in the blood regulated its tumor-specific activity. In electron paramagnetic resonance experiment, the interaction of transient hydrophobicity was found between KP1019 and human serum albumin, which converted to the interaction of coordination at a slow pace.[129] The hypoxia in cancer cells may induce the generation of reactive Ru(II) species, which eventually bind to DNA or cellular proteins causing the death of cancer cells. The preclinical report underlined that KP1019 possesses clinical activity to different type tumors, when reaching high enough concentrations.[130] The binding of NAMI-A to biomolecules was detected using X-ray diffraction (Figure 17B).[128] The phase I studies of NAMI-A in clinical trials were completed in 2004.[131]

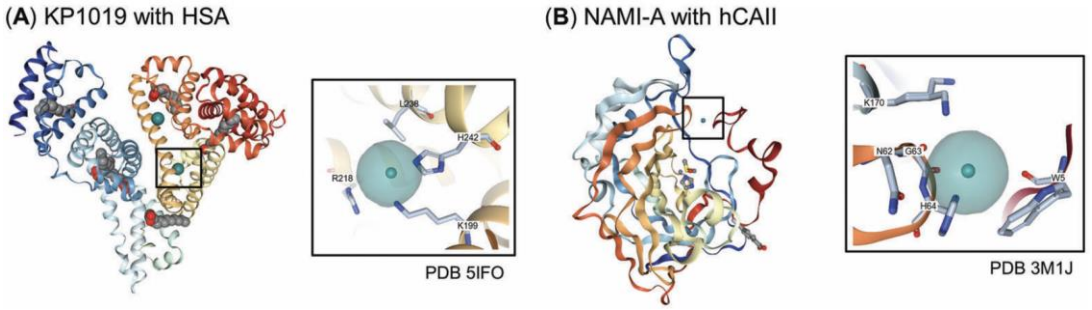

Figure 17. Molecular information derived from X-ray diffraction studies on the binding mode of Ru anticancer drug candidates to biomolecules: (A) KP1019 exposed to human serum albumin (HSA) and (B) NAMI-A to human carbonic anhydrase II (hCAII). Both Ru(III) compounds undergo extensive ligand exchange reactions. Adapted by permission of ref 128. Copyright 2017 Royal Society of Chemistry.

2.3.2 Ruthenium complexes for phototherapy

Photoactivation is a vital feature of Ru complexes, that can improve their selectivity in cancer therapy. There are two types of photoactivated Ru complexes. The first type is Ru complex photosensitizers, which generates $_1O^2$ when illuminated. This can be used for PDT.[132-134] The other type is photo-induced release of toxic Ru moieties or ligands under light irradiation,[135, 136] which are potential candidates for PACT.[137-143].PACT and PDT can also be combined.[137, 139, 144]

2.3.2.1 Ruthenium complexes for photodynamic therapy

Ru complexes can be applied as photosensitizers. Due to their tunable photophysics, good photostability and long fluorescence lifetimes, those photosensitizers can generate ROS under light irradiation, that cleaves the supercoiled DNA and damages the certain biomarkers. The introduction of the intercalative ligand to Ru complexes is a reasonable approach to design the photosensitizers. That can enhance the affinity of the compounds for DNA, achieving a targeted delivery of $^1O_2$ to the genetic material.[145]

TLD1433 is the first Ru(II) complex as photosensitizer to enter human clinical trials.[122, 123] TLD1433 is based on a racemic (ΔΛ) monometallic Ru(II) dyad, bearing two 4,4′-dimethyl-2,2′-bipyridine co-ligands and an ionizable imidazo[4,5-f][1,10]phen-anthroline ligand conjugated to an α-terthienyl acting as the chromophore (Figure 18).α-Terthienyl and its analogues can produce ROS when irradiated with light, resulting in the photocytotoxicity.[146, 147] Introduction of α-Terthienyl to a Ru(II) dyad complex contributes to the indirect access to the photosensitizing 3ππ* states using visible light at long-wavelength.

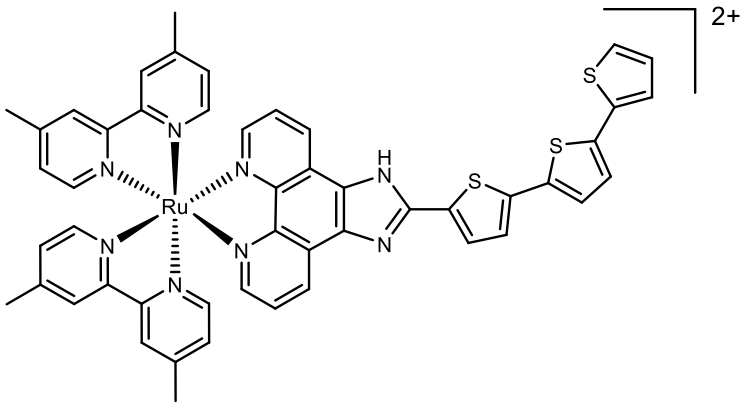

Figure 18. Structures of TLD1433 for PDT in clinical trials.

McFarland and co-workers modified the structures of the ligands coordinated with the Ru centre to tune the photophysical property. They developed Ru polypyridyl

photosensitizers derived from benzo[*i*]dipyrido[3,2-*a*:2′,3′-*c*]phenazine ligand (Figure 19).[148] The PDT activity of the compounds were characterized by blue, green, red, and NIR light in HL-60 cells and cell-free DNA media. Due to their excited states of triplet intraligand with low energy and extra-long lifetimes, they displayed extraordinary PDT effects in the therapeutic window.

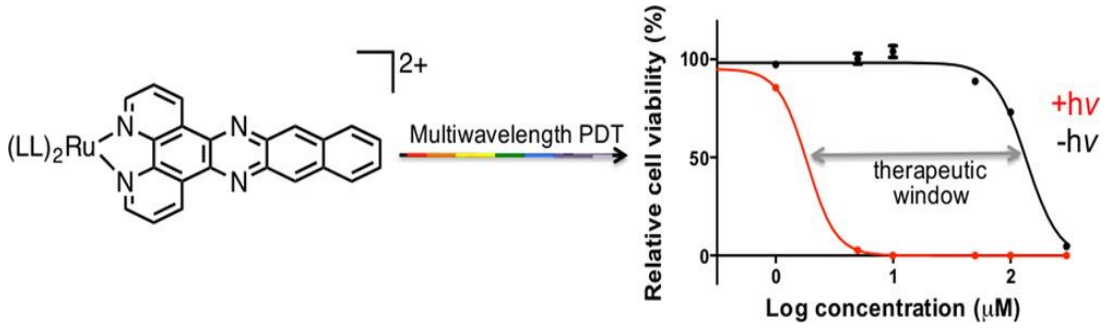

Figure 19. PDT of Ru(II) complexes derived from the π-expansive dppn ligand in the therapeutic window (LL: bidentate ancillary ligands). Reproduced by permission of ref 148. Copyright 2014 American Chemical Society.

2.3.2.2 Ruthenium complexes for photo-activated chemotherapy

As mentioned above, PACT is an oxygen-independent photo-activation approach, that allows for spatial and temporal control to induce cell death. PACT of Ru complexes can cleave the ligands when irradiated with light, permitting them to covalently bind with DNA to cause cell death.[149, 150]

Bonnet et al. synthesized two Ru(II) complex prodrugs by a 6,6′-bis[N-(isoquinolyl)1-amino]-2,2′-bipyridine ligand to coordinate with the Ru centre, binding to monodentate sulphur ligands at two trans coordination sites.[151] Their chemical structures are shown in Figure 20. When irradiated with green light, these sulphur ligands were photosubstituted by water, due to the trans geometry distortion of the coordination sphere. Two Ru(II) complexes were well taken up in cancer cells. They showed mild cytotoxicity in the dark, but increased to 22-fold under 520 nm green light irradiation. Cell-free DNA binding measurements concluded that the cell death was not induced by PDT, but instead by the binding of the Ru complexes to DNA.

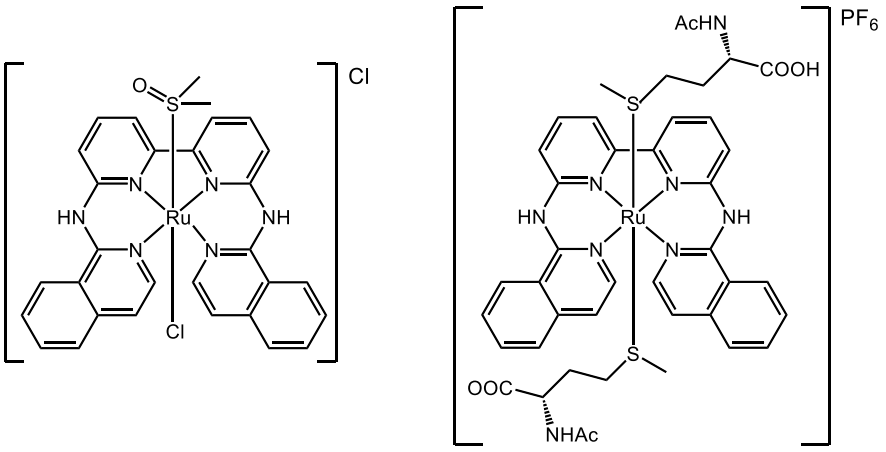

[1]Cl [2]PF_6

Figure 20. Structures of of [1]Cl and [2]PF_6.

Compared to their polypyridyl congeners, insertion of cyclometallating ligands to Ru(II) complexes induces a shift of the first oxidation and reduction potentials. A bathochromic shift of the lowest-energy absorption bands can be caused by those shifts. Therefore, the metal-to-ligand charge transfer (MLCT) absorption of Ru complexes can red-shift to the therapeutic window by cyclometalation.[152] Turro et al. focused on the phenylpyridine ligand and investigated the photoactivation of a cycloruthenated complex.[153] Its molecular structure is shown Figure 21. The CH_3CN ligand was cleaved from the Ru centre using 3 min light irradiation ($\lambda irr \geq 420$ nm), while 30 min are required for the cleavage of the second acetonitrile ligand. When the compounds were irradiated by 690 nm light at 5 J cm^{-2}, the death of human ovarian carcinoma cells increased to the 14-fold compared to dark circumstances, due to the photo-aquation. The agarose gel assay displayed the photobinding of the compounds to DNA, which caused the increase of toxicity.

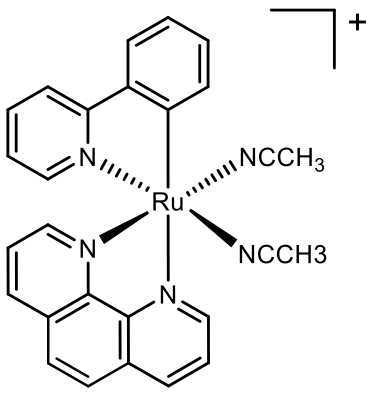

Figure 21. Structure of the cycloruthenated complex.

Drugs can be introduced to Ru complexes to increase the toxicity. Light activates the drug by photocleavage. Turro et al. used 5-cyanouracil as a therapeutic compound, which coordinated with a Ru complex (Figure 22).[154] The axial 5-cyanouracil ligands could be efficiently replaced by H_2O solvent molecules, when irradiated using visible light. The complex presented photoinitiated binding to DNA under irradiation with light ($\lambda_{irr} \geq 395$ nm). Due to the binding of DNA and the release of biologically active 5-cyanouracil simultaneously, the dual-action enhanced the toxicity, inducing the death of HeLa cancer cells.

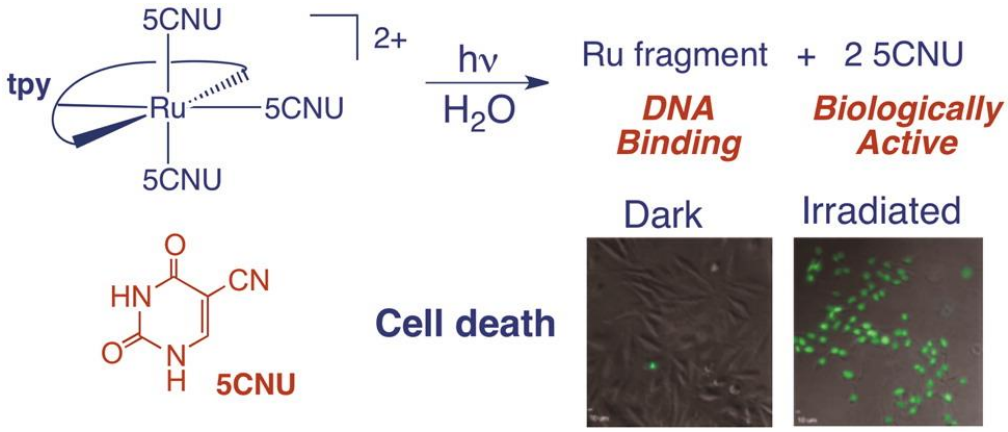

Figure 22. Photoreaction of the 5-cyanouracil-based Ru complex and its toxicity to cancer cells under light irradiation. Dead cancer cells show green fluorescence. Reproduced by permission of ref 154. Copyright 2013 American Chemical Society.

2.3.2.3 Ruthenium complexes combined photodynamic therapy and photo-activated chemotherapy

Combination PACT with PDT can lead to synergetic therapeutic effects[137, 139, 144]. Turro and co-workers synthesized a tris-heteroleptic Ru complex, being capable of generation of $^1O_2$ and exchange of ligand to covalently bind to DNA or other biomolecules when irradiated with light (Figure 23).[155] Upon irradiation, the complex showed a greater photocytotoxicity in HeLa cancer cells compare to the control groups, which produced $^1O_2$ or underwent the ligand exchange, separately. This dual-action contributed to increase of the phototherapy effect.

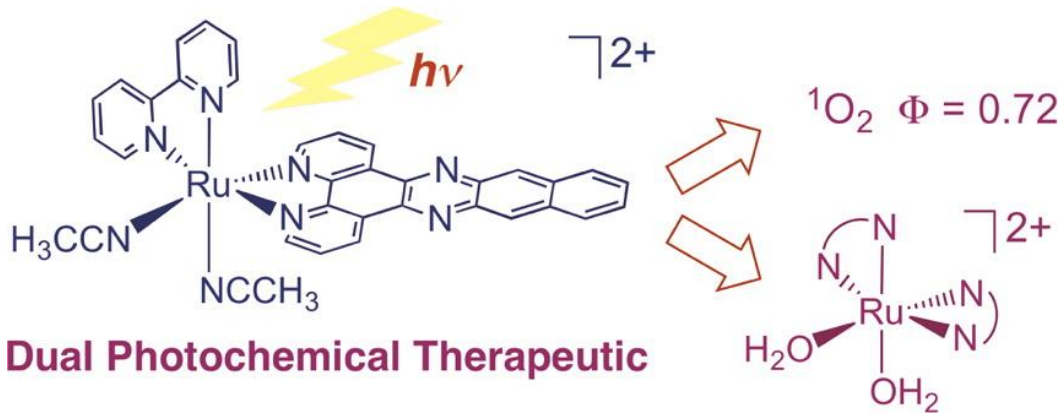

Figure 23. Chemical structure of the tris-heteroleptic Ru complex and its photoreaction. Reproduced by permission of ref 155. Copyright 2014 American Chemical Society.

2.3.3 Ruthenium-containing polymer assemblies for phototherapy

Although Ru complexes are promising metallodrugs for phototherapy, their solubility in aqueous electrolyte is often poor due to the hydrophobicity of their organic ligands.[156] Moreover, most Ru complexes have a short half-life during the circulation and are frequently fast eliminated from the bloodstream, resulting in a small amount of the complexes to reach the tumor.[157, 158] Additionally, uptake of Ru complexes by cancer cells is often insufficient.[159-161] Thus, nanocarriers are needed to realize phototherapy potential of Ru complexes *in vivo*.

Nanocarriers provide several advantages. Physical encapsulation Ru complexes into nanocarriers can increase the water solubility of system (Figure 24a). Nanocarriers restrict the exposure of Ru complexes to healthy tissues and shield them from the immune system, thus limiting the elimination by renal excretion.[162] Besides, nanocarriers can improve the targeting efficiency to cancer cells to increase the availability of Ru complexes. However, the uncontrolled release of drugs, specially the 'burst' release, is one of the major drawbacks using physical encapsulation. What is more, the loading amount of Ru complexes into nanocarriers is often low. Those disadvantages can be addressed by covalently conjugating Ru complexes to the polymer to present a well-defined metallopolymer prodrug.[156, 163]

Ru-containing metallopolymers can self-assemble into nanocarriers in H_2O or under physiological conditions (Figure 24b). This alternative strategy not only inherits all merits of physical encapsulation, but also overcomes its difficulties. Conjugation enables the high loading of Ru complexes into polymer assemblies. Ru complexes remain intact when transported. Then it is able to be activated by light for the controlled release when reaching the target site. Specifically, light can induce the cleavage of Ru complexes or other toxic ligands from polymer assemblies for phototherapy. Polymers

can coordinate to a Ru centre by N-donor ligand or O-donor ligand, in different positions, containing as side group or in the main chain.[156]

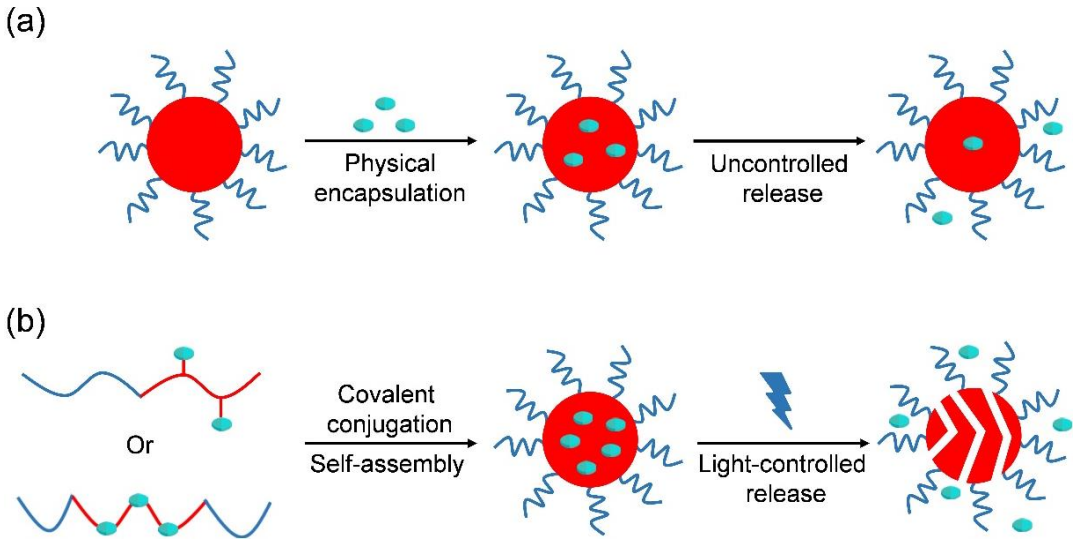

Figure 24. (a) Physical encapsulation and (b) covalently conjugation to load Ru complexes into nanocarriers and their drug release.

2.3.3.1 Ruthenium complexes as side group

For the first time, our group synthesized red-light-activated block copolymers containing Ru complexes as side group and demonstrated their anticancer effect using phototherapy (Figure 25).[164] The block copolymers had a hydrophilic PEG block and a hydrophobic Ru-containing block. The copolymers with three different molecular weights were synthesized. Red light triggered the cleavage of Ru complexes from the polymers as anticancer agent and the production of $^1O_2$ simultaneously. The three polymers with different molecular weights formed various aggregates, such as micelles, vesicles, and large compound micelles. The micelles could be efficiently taken up by cancer cells compared with the two others. Upon red light irradiation, the Ru complexes were released from the nanocarriers for PACT and $^1O_2$ was generated for PDT. The combined PACT and PDT enhanced anticancer activity. No cleavage of Ru complexes from the nanocarriers was observed in the dark, which give hope for less side effect in normal tissue. Therefore, such polymer assemblies containing Ru complexes as side group have potential anticancer effect using phototherapy.

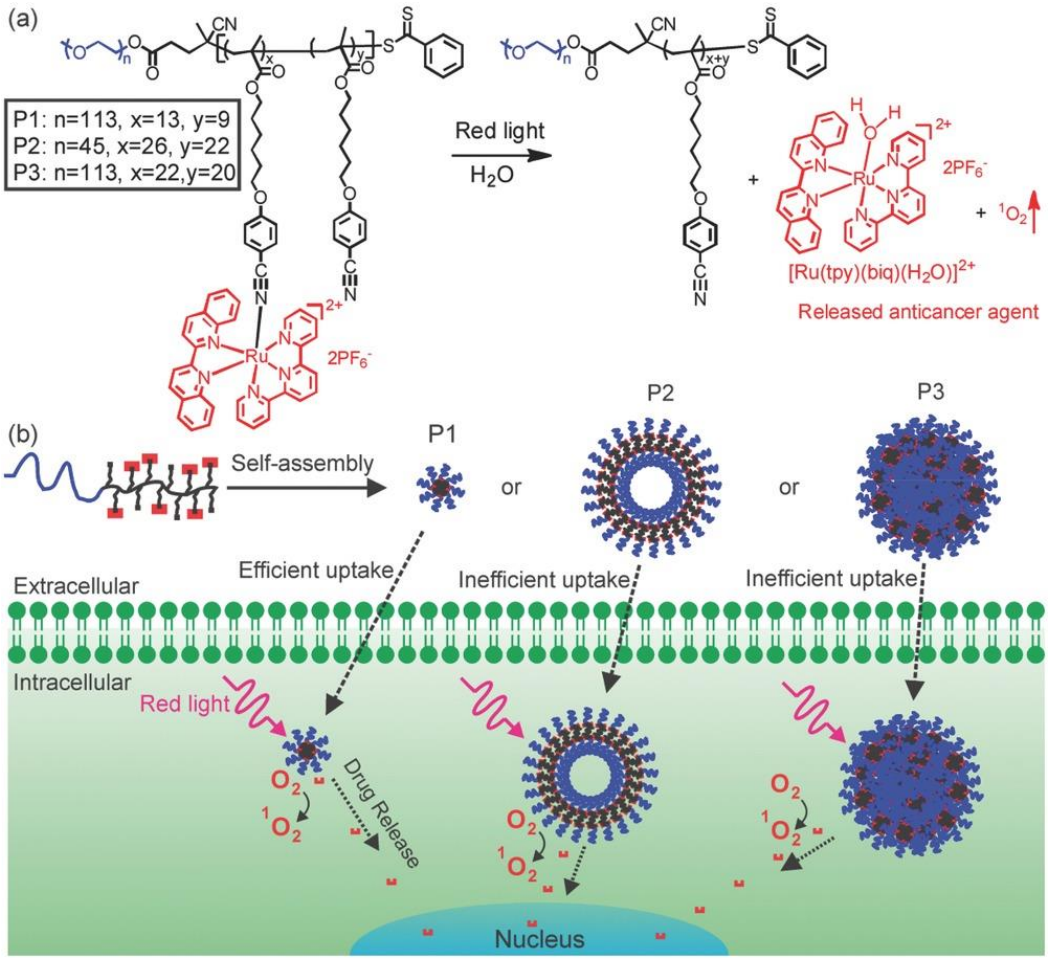

Figure 25. (a) Chemical structures of side-chain Ru-containing block copolymers with three different molecular weights. Irradiation of red light induces the release of Ru complex and generation of singlet oxygen. (b) Schematic illustration of the self-assembly of Ru-containing block copolymers and their anticancer phototherapy. Reproduced by permission of ref 164. Copyright 2016 Wiley-VCH.

Based on above work, our group designed a new red-light-triggered Ru-containing block copolymer, which restrained hypoxic tumors *in vivo* by photochemotherapy (Figure 26).[165] The novel synthesized drug-Ru complex was introduced to polymer side chains as the hydrophobic section. The commercial anticancer drug chlorambucil (CHL) enhanced anticancer efficiency of the drug-Ru complex by conjugation. Red light activated the cleavage of the Ru-N coordination bond to release the drug-Ru complex from the copolymer.

The Ru-containing block copolymer formed micelles by self-assembly. The micelles entered tumor cells by endocytosis. Red light caused the release of the drug-Ru complex *in vivo*, resulting in the inhibition of tumor growth. Because the process of PACT is oxygen-independent, the micelles effectively killed tumor cells in hypoxic environment.

The copolymer that conjugated to the photocleavable drug–Ru complex is a new candidate of PACT to overcome the shortcoming of conventional PDT under hypoxic conditions, which develops an avenue for PACT in polymers against hypoxic tumors.

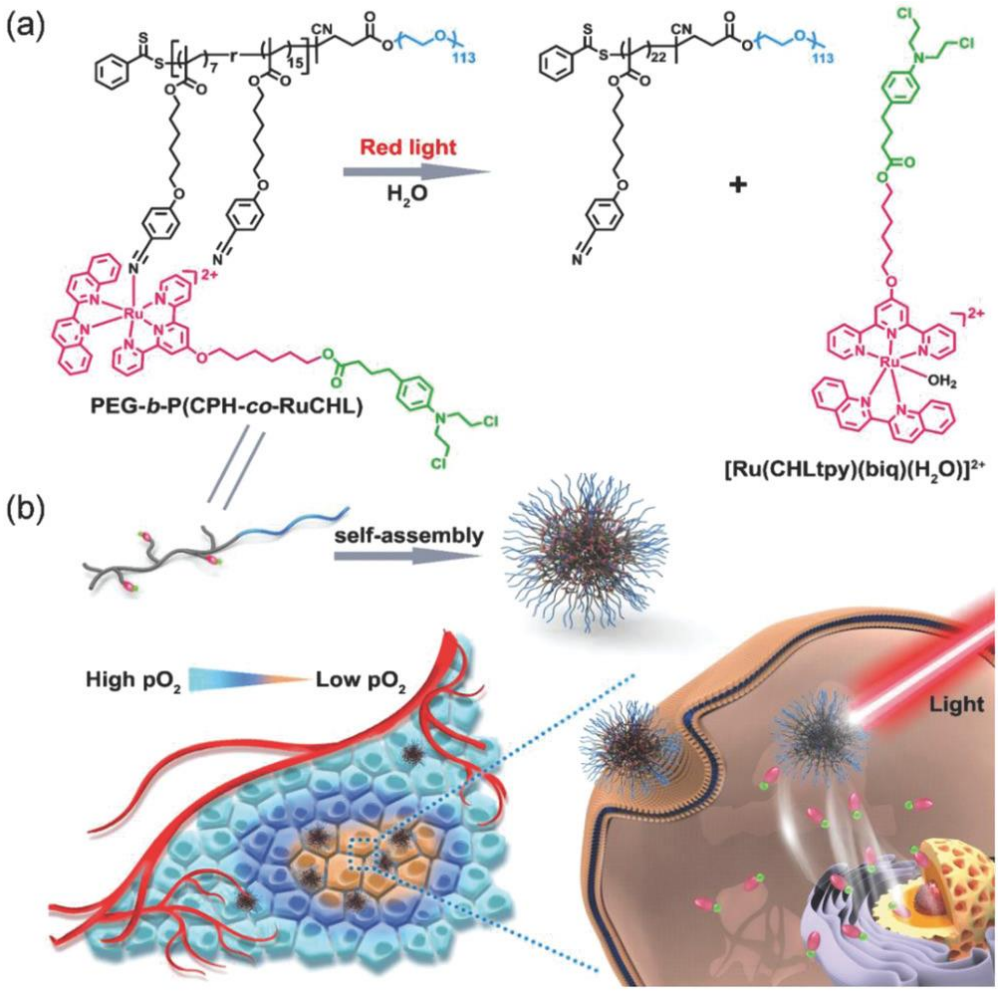

Figure 26. (a) Structure and photoreaction of the Ru-containing block copolymer. Red light induces the release of the drug-Ru complex conjugate. (b) Self-assembly of the Ru-containing block copolymer and its phototherapy in hypoxic tumor environment. Reproduced by permission of ref 165. Copyright 2018 Wiley-VCH.

2.3.3.2 Ruthenium complexes in the main chain

Our group also conjugated Ru complexes in the main chain of block copolymers, which contained two PEG blocks as hydrophilic section and a Ru-containing block as hydrophobic section (Figure 27).[166] The Ru-containing block contributed to more than 50% weight in polymers, indicating a high drug-loading. Red light also activated the cleavage of Ru complexes from the polymers as anticancer agent and the production of $^1O_2$ simultaneously.

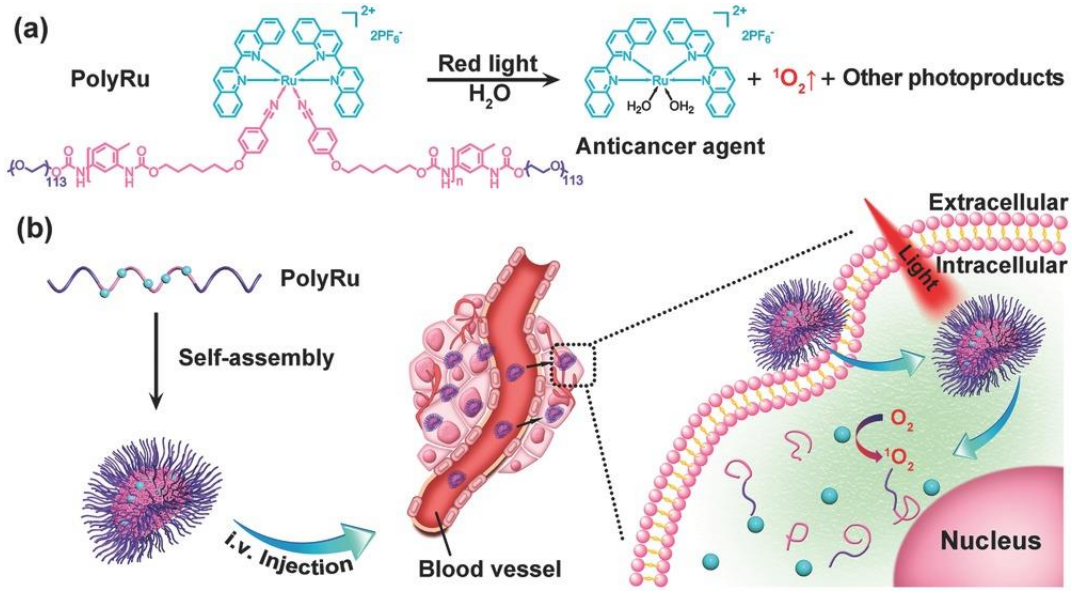

Figure 27. (a) Chemical structure of main-chain Ru-containing block copolymers. Red light induces the degradation to generate the anticancer complex and $^1O_2$. (b) Schematic illustration of self-assembly and phototherapy using Ru-containing block copolymers. Reproduced by permission of ref 166. Copyright 2017 Wiley-VCH.

The polymers spontaneously formed nanoparticles in water. The average diameter of nanoparticles was 180 nm, that could be effectively taken up by cancer cells such as HeLa, HepG2 and PC3. Upon red light irradiation, the photodegradation of nanoparticles was induced to release Ru complexes for PACT and $^1O_2$ was generated for PDT. Combination PACT with PDT can lead to synergetic therapeutic effects, which efficiently killed cancer cells. Moreover, the nanoparticles could accumulate at tumor and inhibit its growth when irradiated with red light. No pathological tissue damage or abnormality was observed during the treatment. Therefore, such nanoparticles containing Ru complexes in the main chain become a perspective of anticancer treatment using phototherapy.

2.4 Challenges

As discussed previously, the entire eradication and cure of cancer remain a tough challenge using nanocarriers alone to overcome MDR. Multifunctional nanocarriers seem to settle this problem. We still want to find a more potential and efficient approach for overcoming MDR. Phototherapy combined nanocarriers may be an ideal choice. Due to unknown toxicity in PTT and oxygen dependence in PDT, PACT is more

superior than the two others in phototherapy. However, current researches on PACT in nanocarriers mainly focus on UV or visible light. Compared to them, red or NIR light is more suitable in biologic applications. Thus, we need adopt Ru complexes, which can respond to red or NIR light in PACT. Constructing Ru-containing polymers can increase the therapeutic efficiency and decrease the side effects of Ru complexes. However, researches using Ru-containing polymers to overcome MDR are rare.

Therefore, the challenge is how to integrate the elements of nanocarriers, red or NIR light-activated PACT, Ru-containing polymers in a system, that can synergistically and sufficiently overcome MDR. In results and discussion chapter, we will show how to design the system and evaluate its efficiency to overcome MDR *in vitro* and *in vivo*.

Chapter 3: Results and discussion

3.1 Nanostructured polymer assemblies stabilize photoactivatable anticancer ruthenium complexes under physiological conditions

Adapted with permission from my publication: M. Chen, et al. *Journal of Inorganic Biochemistry* 207 (2020) 111052. Copyright Elsevier.

Si Wu and Hans-Jürgen Butt led the project. Mingjia Chen synthesized Ru complexes and did the experiments. Wen Sun synthesized Ru-containing polymers. Annika Kretzschmann revised the language. Mingjia Chen and Wen Sun contributed equally to this work.

3.1.1 Introduction

An ideal photoactivatable Ru metallodrug should be non-toxic in the dark but become toxic to cancer cells when they are delivered to tumor tissue and activated by light. Recently, we designed and studied various Ru complexes[77, 167-172] and Ru-containing block polymers,[165, 173] involving polyRu1 (a diblock copolymer containing Ru complexes as side group)[164] and polyRu2 (a triblock copolymer containing Ru complexes in the main chain),[166] which self-assembled into nanostructures in aqueous solutions (Figure 28). Both PolyRu1 and PolyRu2 are responsive to red light. Red light has the advantage that it can penetrate deeply into tissue.[174, 175] After red light irradiation, PolyRu1 and PolyRu2 released Ru moieties as anticancer agents for PACT and sensitized the generation of $^1O_2$ for PDT.

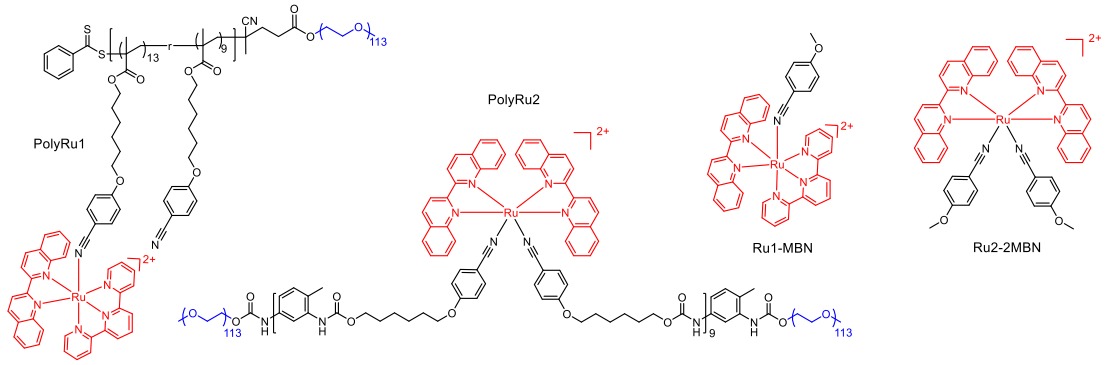

Figure 28. Chemical structures of photoactivatable Ru-containing block polymers (PolyRu1 and PolyRu2) and Ru complexes (Ru1-MBN and Ru2-2MBN).

In the process of drug delivery, Ru-containing materials would go through at least three microenvironments: (a) blood stream, (b) tumor tissue, and (c) cancer cells (Figure 29).[176] However, Ru-containing materials may dissociate in those microenvironments because of the instability of the coordination bonds. Then, the toxic compounds may leak into the blood stream or normal tissues.[177-179] Thus, in this section, we systematically compared the stabilities of PolyRu1 and PolyRu2 and their corresponding building blocks Ru1-MBN ($[Ru(tpy)(biq)(MBN)]^{2+}$, tpy = 2,2′:6′,2″-terpyridine, biq = 2,2'-biquinoline, MBN = 4-methoxybenzonitrile) and Ru2-2MBN ($[Ru(biq)_2(MBN)_2]^{2+}$) (Figure 28) under imitated physiological conditions. Our results demonstrated that Ru-containing block polymers, which self-assembled into nanostructure, were more stable than free Ru complexes under similar conditions. Attaching Ru complexes to suitable polymers therefore protected the active compound.

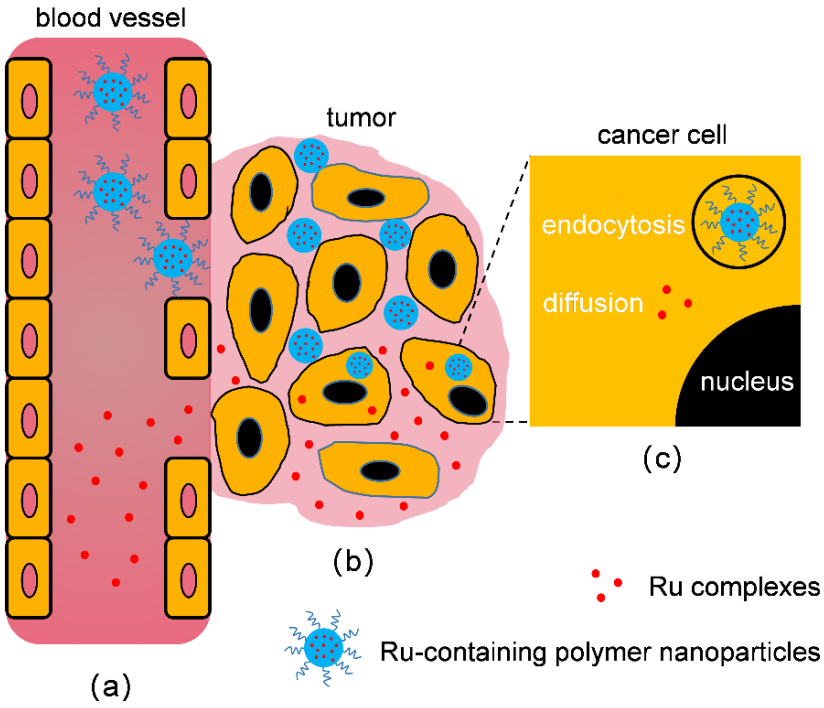

Figure 29. Schematic illustration of the pathways of delivery of Ru complexes or Ru-containing polymer nanoparticles to tumor cells. Three major physiological conditions include (a) blood stream, (b) tumor tissue, and (c) cancer cell environment.

3.1.2 Properties of ruthenium complexes

We synthesized the corresponding building blocks Ru1-MBN and Ru2-2MBN based on PolyRu1 and PolyRu2. The chemical structure of Ru1-MBN was characterized by ^{1}H nuclear magnetic resonance (^{1}H NMR) spectroscopy (Figure 30). Every hydrogen

in Ru1-MBN was clearly marked. Correlation spectroscopy (COSY) further confirmed its chemical structure in aromatic region (Figure 31). The found mass and calculated mass of Ru1-MBN were extremely close in high resolution electrospray ionization mass spectrometry (HR-ESI-MS), showing the successful synthesis (Figure 32).

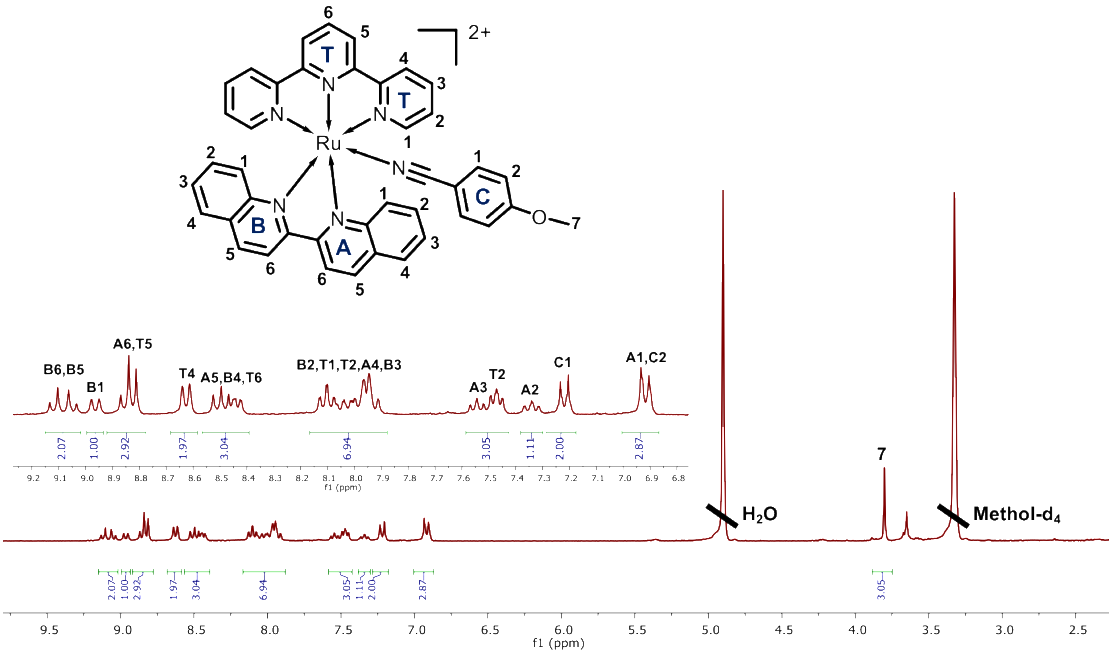

Figure 30. ^{1}H NMR spectrum of Ru1-MBN (methol-d_4, 250 MHz, r.t.).

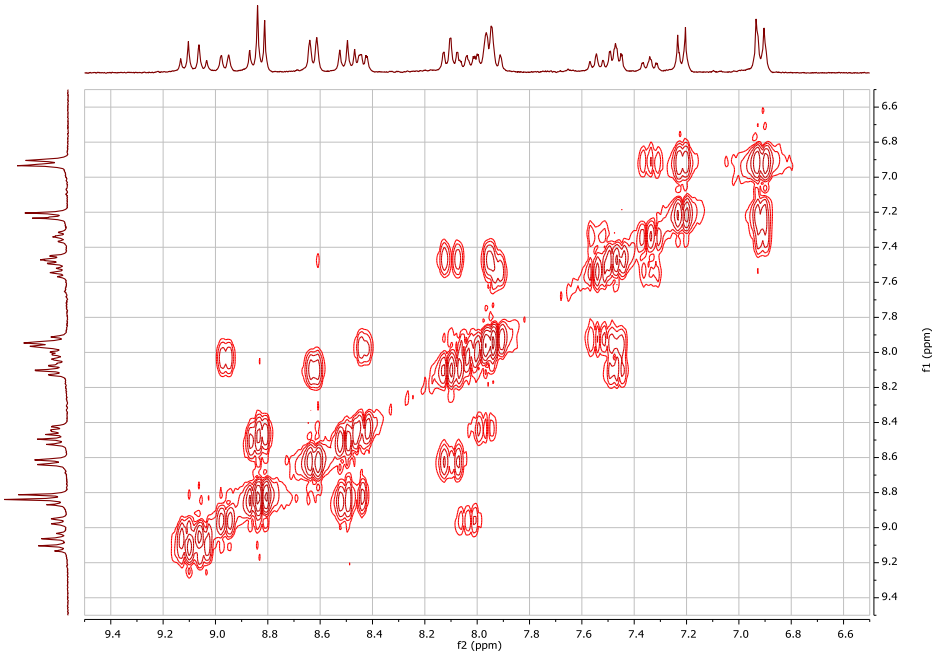

Figure 31. H-H COSY spectrum of Ru1-MBN in aromatic region (methol-d_4, 300 MHz, r.t.).

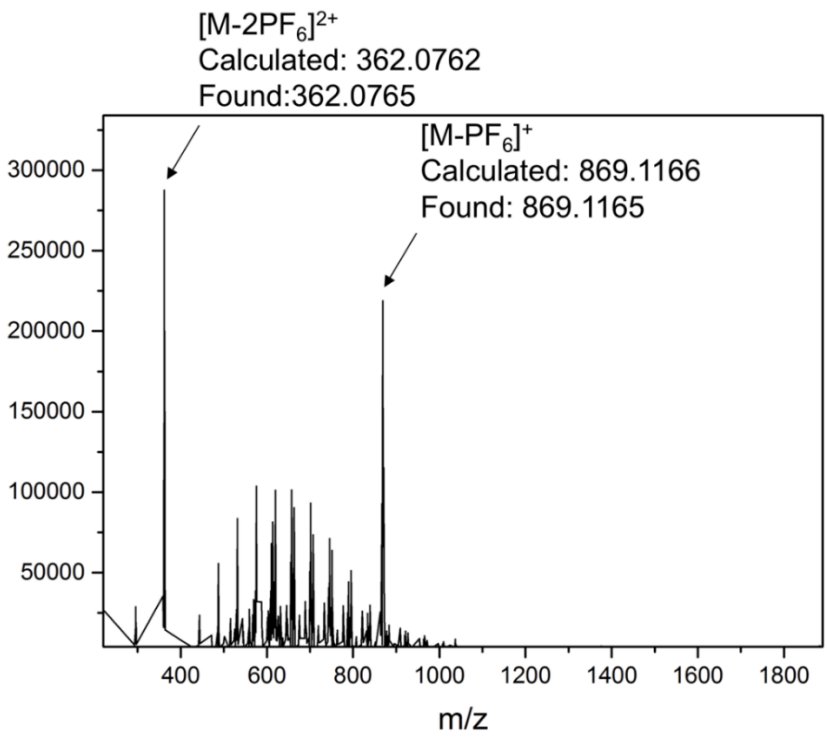

Figure 32. HR-ESI-MS spectrum of Ru1-MBN.

Smilarly, the chemical structure of Ru2-2MBN was also verified by ^{1}H NMR spectroscopy, COSY and HR-ESI-MS (Figures 33–35). To increase the solubility of Ru1-MBN and Ru2-2MBN in the water, the counterion of the Ru complexes was changed to chloride using ion exchange resin (DOWEX 22 Cl).[180]

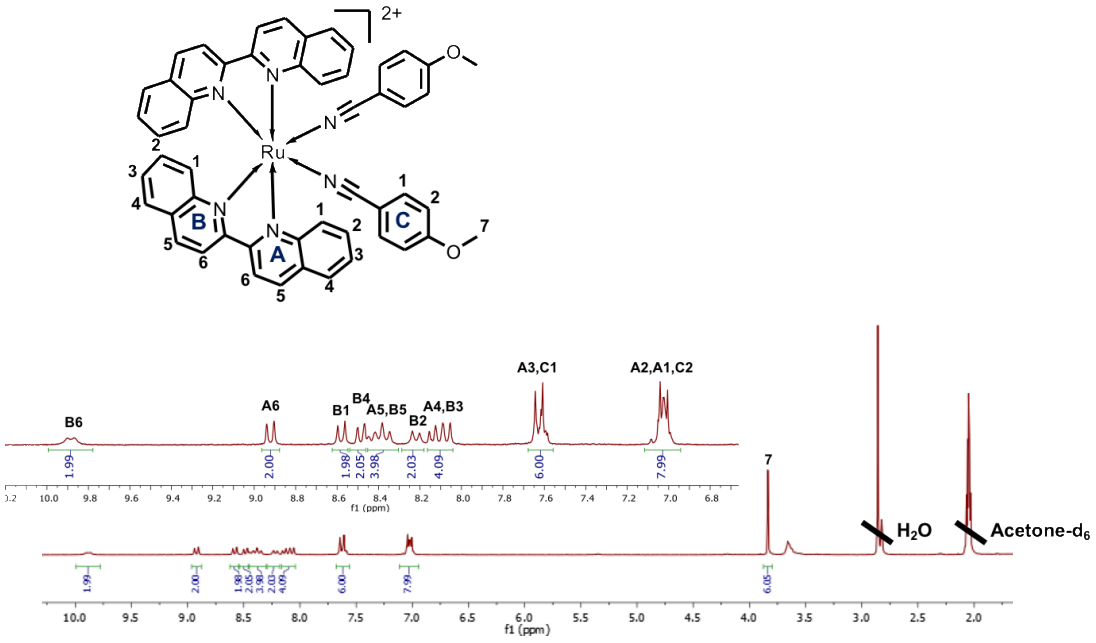

Figure 33. ^{1}H NMR spectrum of Ru2-2MBN (acetone-d_6, 250 MHz, r.t.).

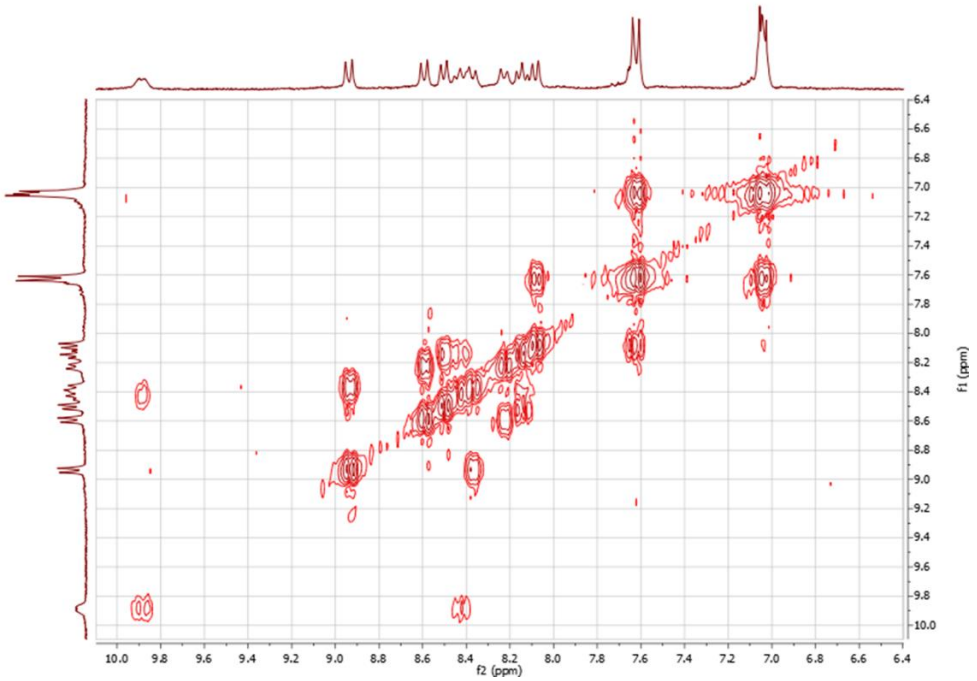

Figure 34. H-H COSY spectrum of Ru2-2MBN in aromatic region (acetone-d_6, 300 MHz, r.t.).

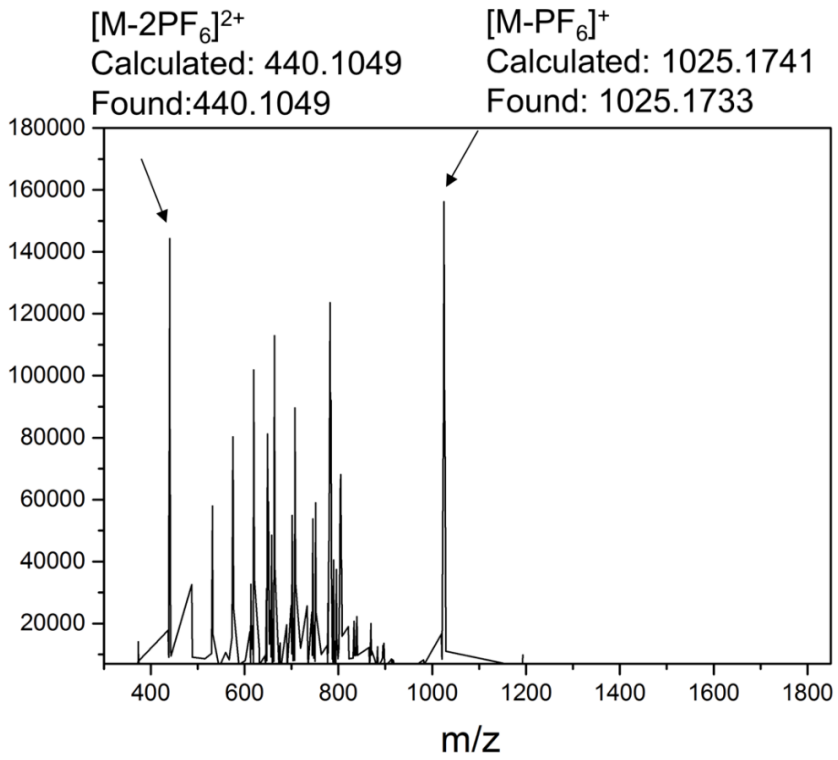

Figure 35. HR-ESI-MS spectrum of Ru2-2MBN.

The properties of polyRu1 and polyRu2 had been systematically researched in our

previous work.[164, 181] The properties of new synthesized Ru1-MBN and Ru2-2MBN should be also figured out. UV/Vis spectroscopy was used to study and compare their stability and photochemistry by ligand exchange.[182] First, we studied the stability of Ru1-MBN in the mixture solution (H_2O/methanol = 7/3, methanol increased solubility) in the dark via monitoring the absorption changes (Figures 36, 37a). The MLCT band at 511 nm gradually deceased and a new peak at ~547 nm appeared during incubation. More than half of MBN replaced by H_2O after 24 h. The hydrolysis suggested that Ru1-MBN was instable in aqueous solution within one day. Subsequently, the photosubstitution of Ru1-MBN was studied under the same condition (Figure 36, 37b). Red light (656 nm, 30 mW cm^{-2}) irradiation of Ru1-MBN for 140 s transformed the MLCT band from 511 nm to 550 nm. The absorption and the isosbestic point were similar to the reaction of Ru1-MBN in the dark.

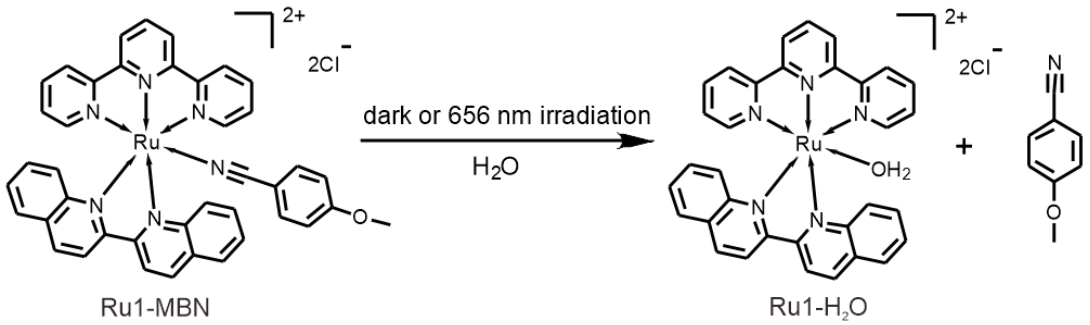

Figure 36. Reaction of Ru1-MBN in the dark or under light irradiation.

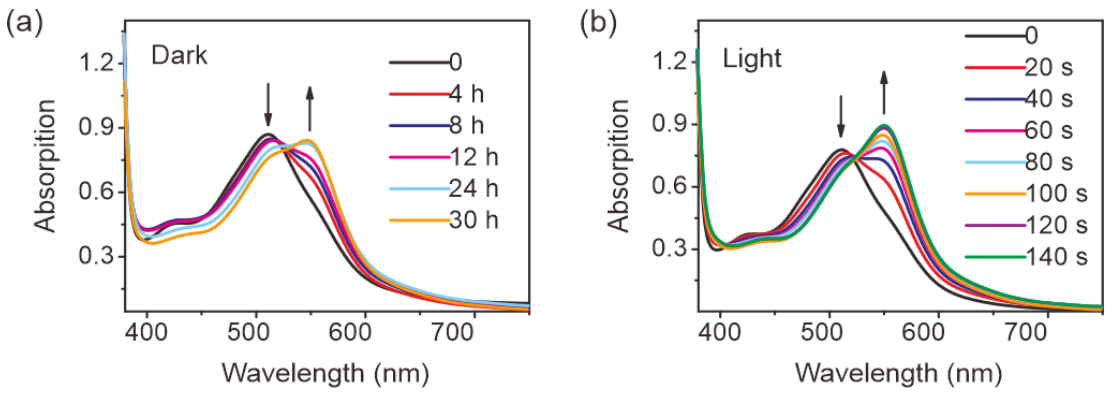

Figure 37. UV/Vis absorption spectroscopy of Ru1-MBN (a) in the dark and (b) under red light irradiation (656 nm, 30 mW cm^{-2}) for different time periods.

We further kept Ru1-MBN in the dark or irradiated it under red light until their spectra did not change anymore (Figure 38a). The spectra of Ru1-MBN after the reaction overlapped well with that of Ru1-H_2O ($[Ru(tpy)(biq)(H_2O)]^{2+}$). Additionally,

the retention time of Ru1-MBN in the dark and after irradiation was the same on high-performance liquid chromatography (HPLC) measurements (Figure 38b). All the results demonstrated that the dissociation procedure of Ru1-MBN in the dark was identical to that of Ru1-MBN under light; the final product of both processes was Ru1-H_2O. HPLC measurements with UV/Vis detection (Figure 39) further confirmed the conclusion, illustrating that free Ru1-MBN was unstable when stored in aqueous solution for one day or more, even in the dark.

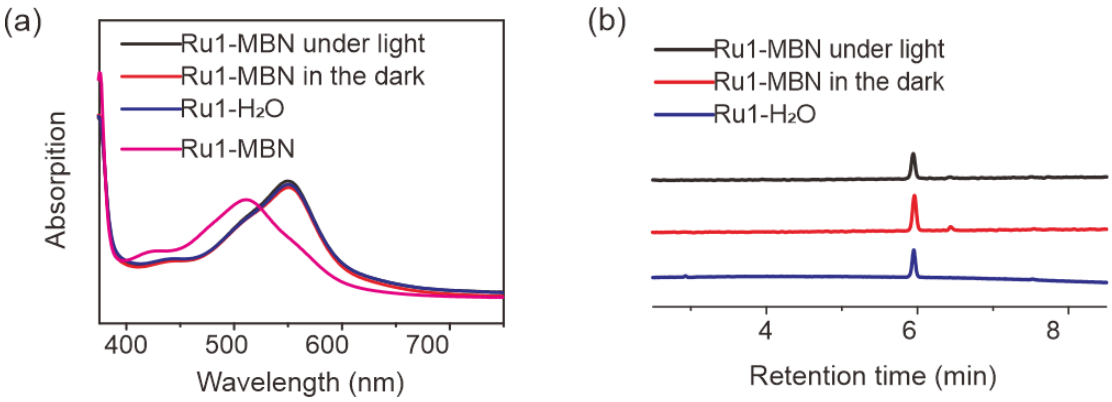

Figure 38. Comparison of Ru1-MBN in the dark and under red light irradiation (30 mW cm^{-2}) after complete reaction using (a) UV/Vis absorption spectroscopy and (b) HPLC.

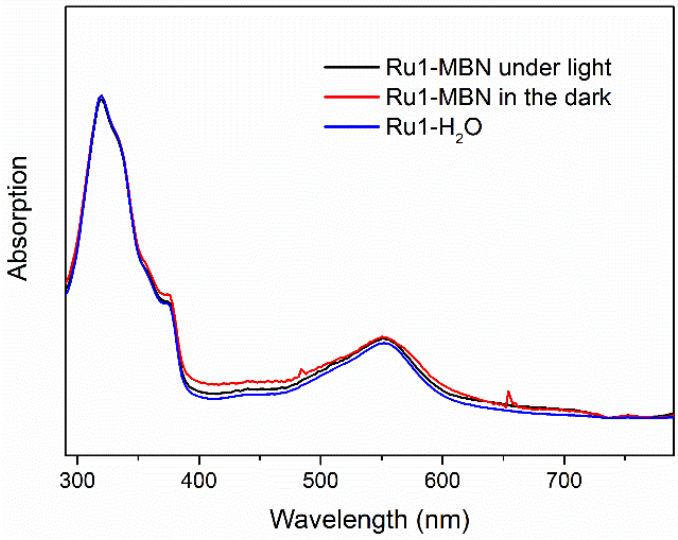

Figure 39. UV/Vis absorption spectroscopy of Ru1-MBN in the dark and under red light irradiation (30 mW cm^{-2}) after complete reaction in HPLC measurements in Figure 38b. The spectroscopy was measured by the UV/Vis detector of the HPLC system.

We also tested the stability of Ru2-2MBN under the same condition (Figure 40). UV/Vis absorption spectroscopy (Figure 41a) was used to monitor the reaction of Ru2-

2MBN in the H_2O/methanol (=7/3) mixture in the dark. I observed an isosbestic point at ~562 nm. The MLCT band at 529 nm gradually deceased and a new peak at ~ 610 nm appeared after 30 h. The results suggested that Ru2-2MBN was unstable in the mixture in the dark.

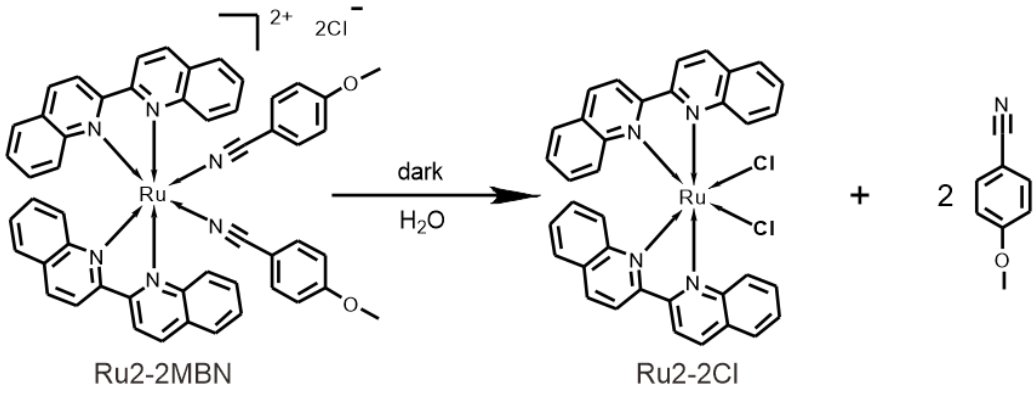

Figure 40. Instability of Ru2-2MBN in the dark.

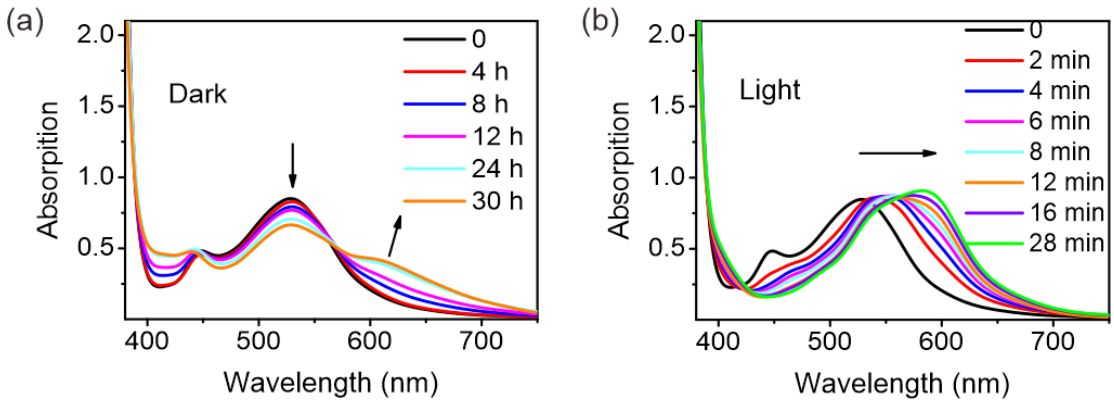

Figure 41. UV/Vis absorption spectroscopy of Ru2-2MBN (a) in the dark and (b) under red light irradiation (656 nm, 30 mW cm^{-2}) for different time periods.

Photosubstitution of Ru2-2MBN was studied under the same condition using UV/Vis absorption spectroscopy (Figure 41b, 42). Different from the reaction of Ru2-2MBN in the dark, the MLCT band of Ru2-2MBN gradually red shifted from 529 nm to 585 nm under 656 nm red light (30 mW cm^{-2}) irradiation for 28 min. No isosbestic point was observed during the process, suggesting that the two ligands were not replaced simultaneously but stepwise.

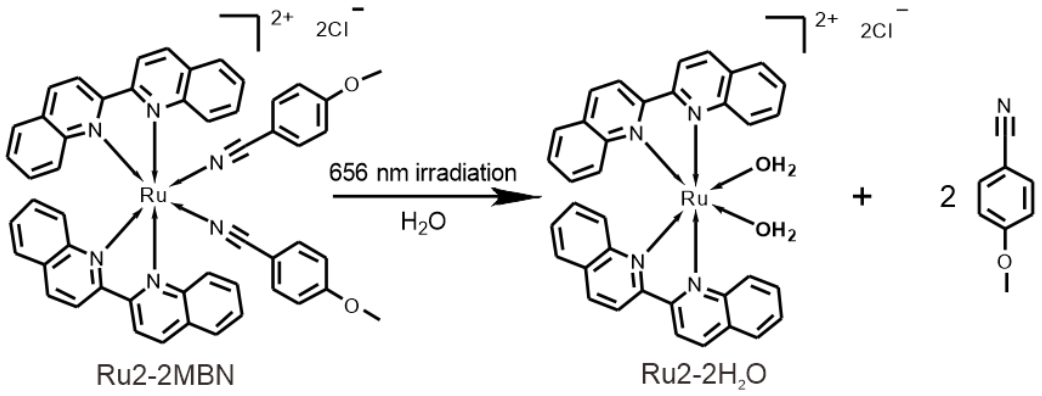

Figure 42. Photosubstitution of Ru2-2MBN.

We kept Ru2-2MBN in the dark or irradiated it using red light until their spectra did not change anymore (Figure 43a). The MLCT band of Ru2-2MBN after the reaction in the dark was identical to that of Ru2-2Cl ($Ru(biq)_2Cl_2$). The MLCT band of Ru2-2MBN after light irradiation was the same as Ru2-2H_2O ($[Ru(biq)_2(H_2O)_2]^{2+}$). Subsequently, HPLC measurements were also performed to prove the reaction (Figure 43b). The retention time of Ru2-2MBN after reaction in the dark was equal to that of Ru2-2Cl, indicating that the reaction product was Ru2-2Cl. However, the retention time of Ru2-2MBN after light irradiation was identical to that of Ru2-2H_2O. Combining HPLC measurements with UV/Vis detection (Figure 44), the results demonstrated that the process of Ru2-2MBN in the dark was different from that of Ru2-2MBN under light irradiation. This phenomenon may occur due to the difference in the sizes of potential surrounding ligands. The structure of the ligands in Ru2-2MBN was big, resulting in acute steric effects. The smaller chloride could more easily coordinate to Ru at a relatively long time compared to the water molecule.

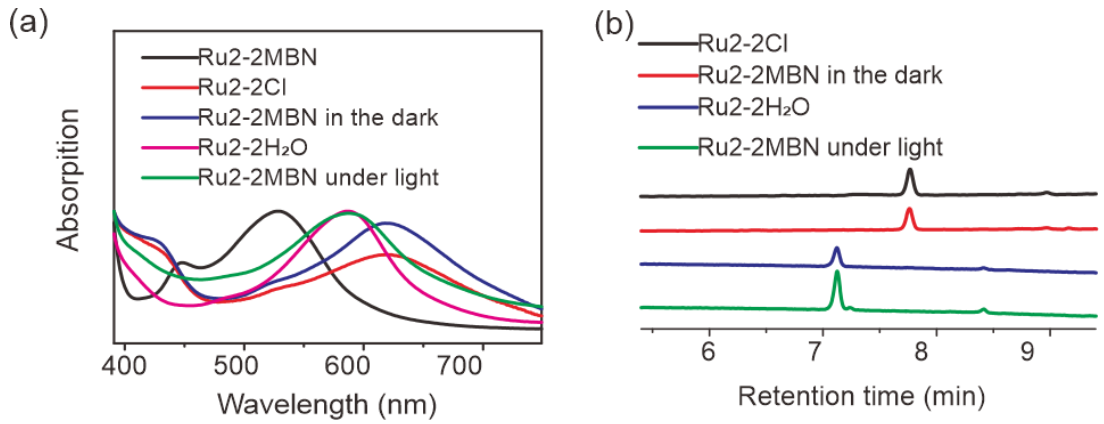

Figure 43. Comparison of Ru2-2MBN in the dark and under red light irradiation (30 mW cm^{-2}) after complete reaction using (a) UV/Vis absorption spectroscopy and (b) HPLC.

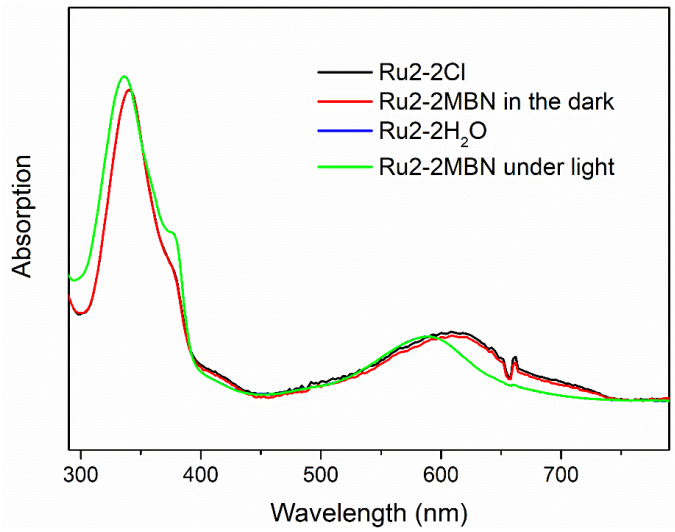

Figure 44. UV/Vis absorption spectroscopy of Ru2-2MBN in the dark and under red light irradiation (30 mW cm^{-2}) after complete reaction in HPLC measurements in Figure 43b. The spectroscopy was measured by the UV/Vis detector of the HPLC system.

3.1.3 Morphologies of ruthenium-containing polymer assemblies

PolyRu1 contains a PEG-b-PCPH (poly(ethylene glycol)-block-poly(6-(4-cyanophenoxy) hexyl methacrylate) as AB-type diblock copolymer with Ru complexes ($[Ru(tpy)(biq)]^{2+}$) as side group (Figure 28). The molecular weight (*Mn*) and polydispersity (*Mw/Mn*) of PEG-b-PCPH determined by gel permeation chromatography (GPC) were 13.3 kg/mol and of 1.17. The degree of polymerization (DP) determined by ^{1}H NMR was 22. More than half of the 6-(4-cyanophenoxy) hexyl methacrylate (CPH) repeat units are coordinated with Ru complexes, whose contents in PolyRu1 were 41 wt%. PolyRu2 is an ABA-type triblock copolymer containing Ru complexes ($[Ru(biq)_2]^{2+}$) in the main chain (Figure 28). The molar mass of PolyRu2 measured by ^{1}H NMR was 22 kg/mol. The polydispersity (*Mw/Mn*) of PolyRu2 determined by GPC is 1.22. The repeat units of the Ru-containing block in each polymer chain is 8, corresponding to more than 50% weight fraction in PolyRu2. Both PolyRu1 and PolyRu2 contain PEG blocks as hydrophilic section and Ru-containing blocks as hydrophobic section. Due to the amphiphilic structures, they self-assemble into nanostructures in aqueous solution. The morphologies of PolyRu1 and PolyRu2 assemblies were observed using transmission electron microscopy (TEM) (Figure 45). PolyRu1 formed homogeneous nanoparticles with a mean diameter of 12 nm (Figure 45a). The hydrodynamic radii of PolyRu1 assemblies measured by dynamic light scattering (DLS) was 22 nm.[164] The difference in sizes was caused by the different states of assemblies.[183] PolyRu2 formed hollow nanostructures with a diameter of ~ 180 nm (Figure 45b). The bowl-shaped morphology in a unequilibrium state was

formed by kinetic control. The similar morphology of assemblies was reported by Eisenberg and Riegel.[184] The average hydrodynamic radii of PolyRu2 assemblies determined by DLS was ~180 nm.[166]

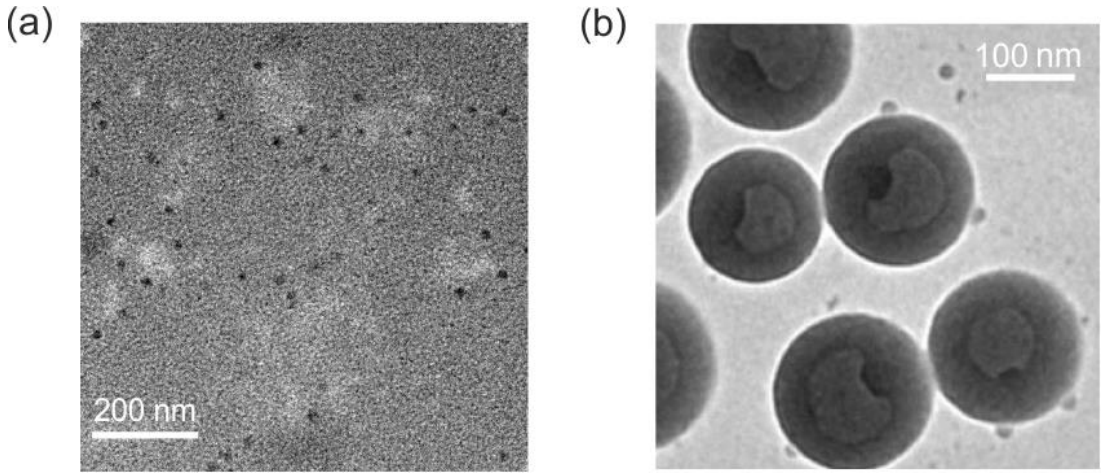

Figure 45. TEM images of PolyRu1 assemblies (a) and PolyRu2 assemblies (b).

3.1.4 Stability of ruthenium-containing materials

To compare the stabilities of Ru complexes (Ru1-MBN and Ru2-2MBN) and Ru-containing polymer nanoparticles (PolyRu1 and PolyRu2) under imitated physiological conditions, we monitored UV/Vis absorption spectra in saline (0.9% w/v of NaCl) (Figure 46) and bovine serum albumin (BSA) aqueous solution (Figure 47) imitating the conditions during blood circulation.

In saline solution, the MLCT band of Ru1-MBN shifted from 510 nm to ~551 nm (Figure 46a). Most of Ru1-MBN hydrolyzed after 30 h. For Ru2-2MBN (Figure 46b), the MLCT band at 526 nm decreased a little. A new peak at ~604 nm was observed after 30 h, which was similar to the situation in aqueous solution in the dark. In contrast, the MLCT band of PolyRu1 only showed slight reduction at 512 nm even after 29 h incubation, verifying a good stability of PolyRu1 in saline solution (Figure 46c). Also, the MLCT band of PolyRu2 showed almost no change in the UV/Vis absorption spectra within 30 h, suggesting its excellent stability (Figure 46d). The big size and wide dispersion of PolyRu2 assemblies induced the light scattering in spectroscopy. These results demonstrated the improved stabilities of PolyRu1 and PolyRu2 as compared to their corresponding Ru complexes. Because PEG blocks in PolyRu1 and PolyRu2 possessed excellent water solubility, good biocompatibility and non-immunogenicity. PEGylated nanoparticles showed long blood circulation times than unmodified nanoparticles.[45, 185, 186] We inferred that the hydrophobic cores of the nanoparticles

isolated Ru moieties from the external water environment and thus improved their stability.

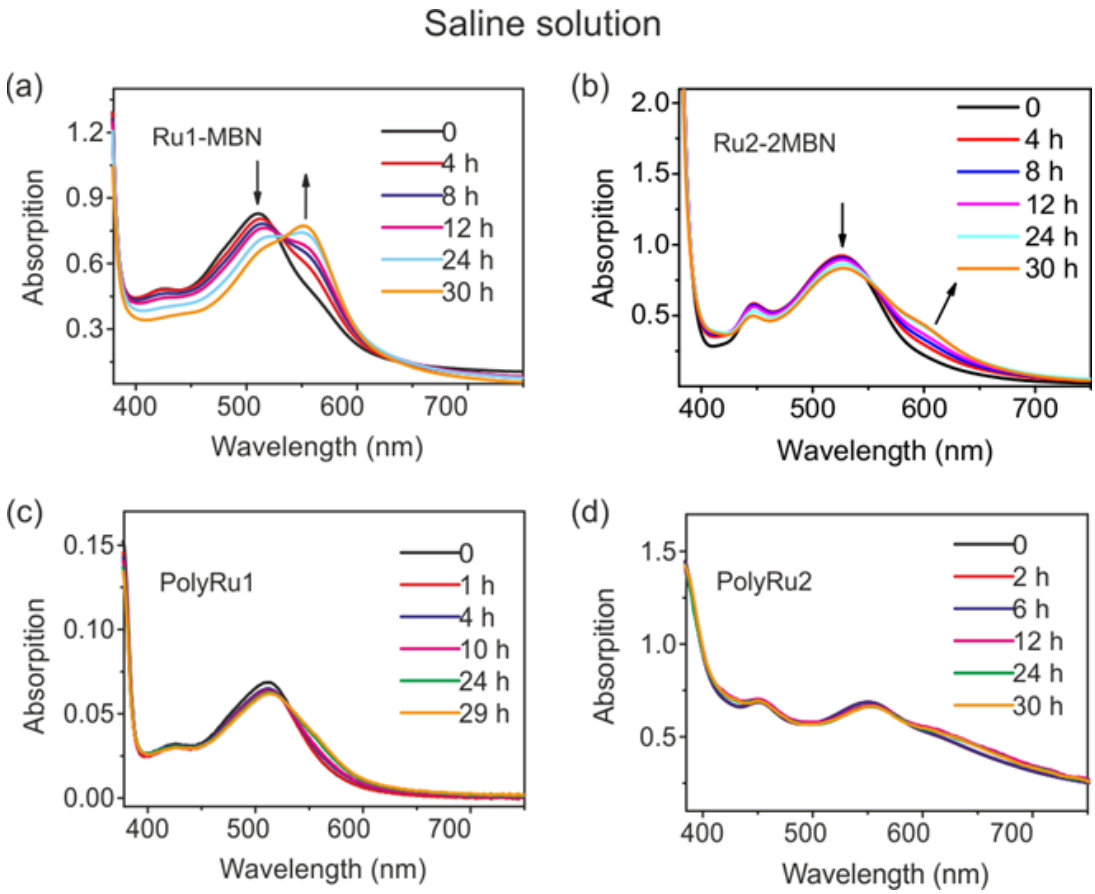

Figure 46. UV/Vis absorption spectroscopy of (a) Ru1-MBN, (b) Ru2-2MBN, (c) PolyRu1, and (d) PolyRu2 in the dark for different time periods in saline solution.

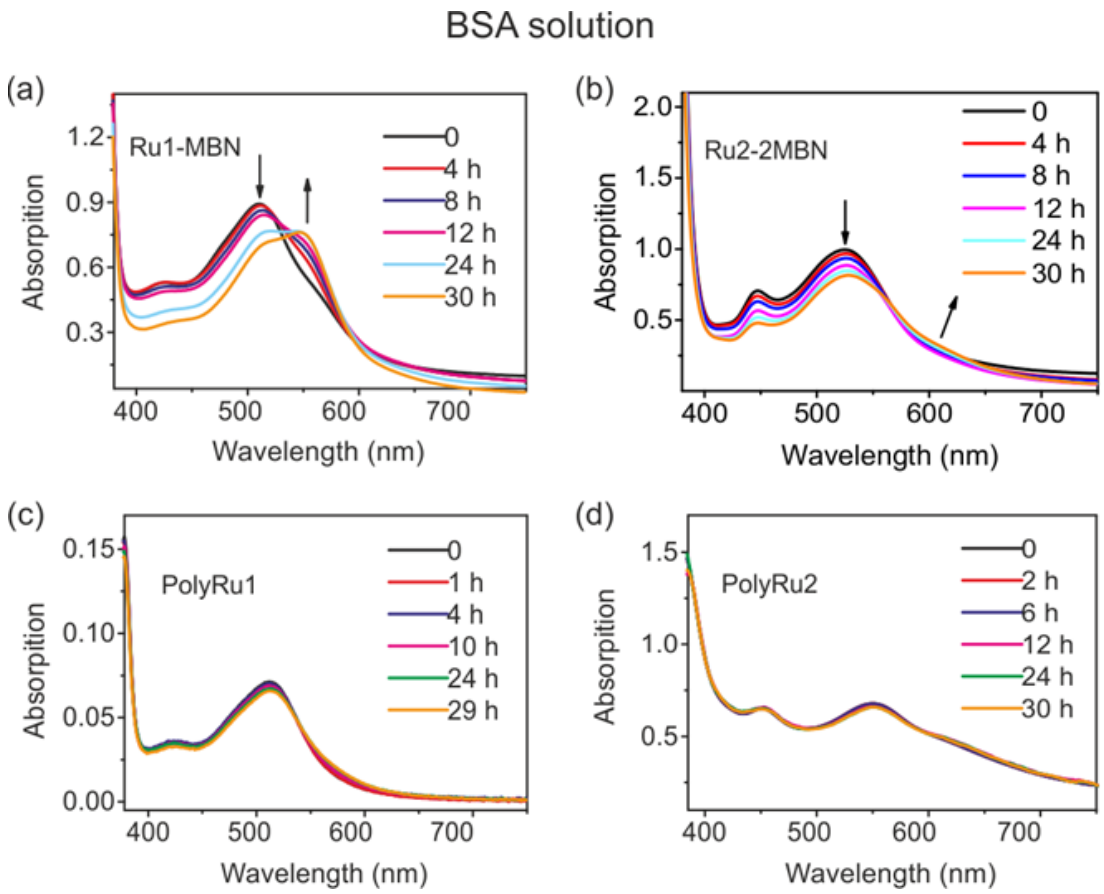

Figure 47. UV/Vis absorption spectroscopy of (a) Ru1-MBN, (b) Ru2-2MBN, (c) PolyRu1, and (d) PolyRu2 in the dark for different time periods in BSA aqueous solution.

In BSA aqueous solution (1.5×10^{-5} M), the hydrolysis of most Ru1-MBN still was observed within 30 h (Figure 47a). We noted that the absorption varied irregularly after 12 h; this variation may be caused by the limited solubility of Ru1-MBN in BSA aqueous solution. The MLCT band of Ru2-2MBN at 525 nm gradually reduced within 30 h (Figure 47b). In contrast, the absorption spectra of PolyRu1 and PolyRu2 showed almost no change (Figure 47c,d), demonstrating their good stability in protein solution.

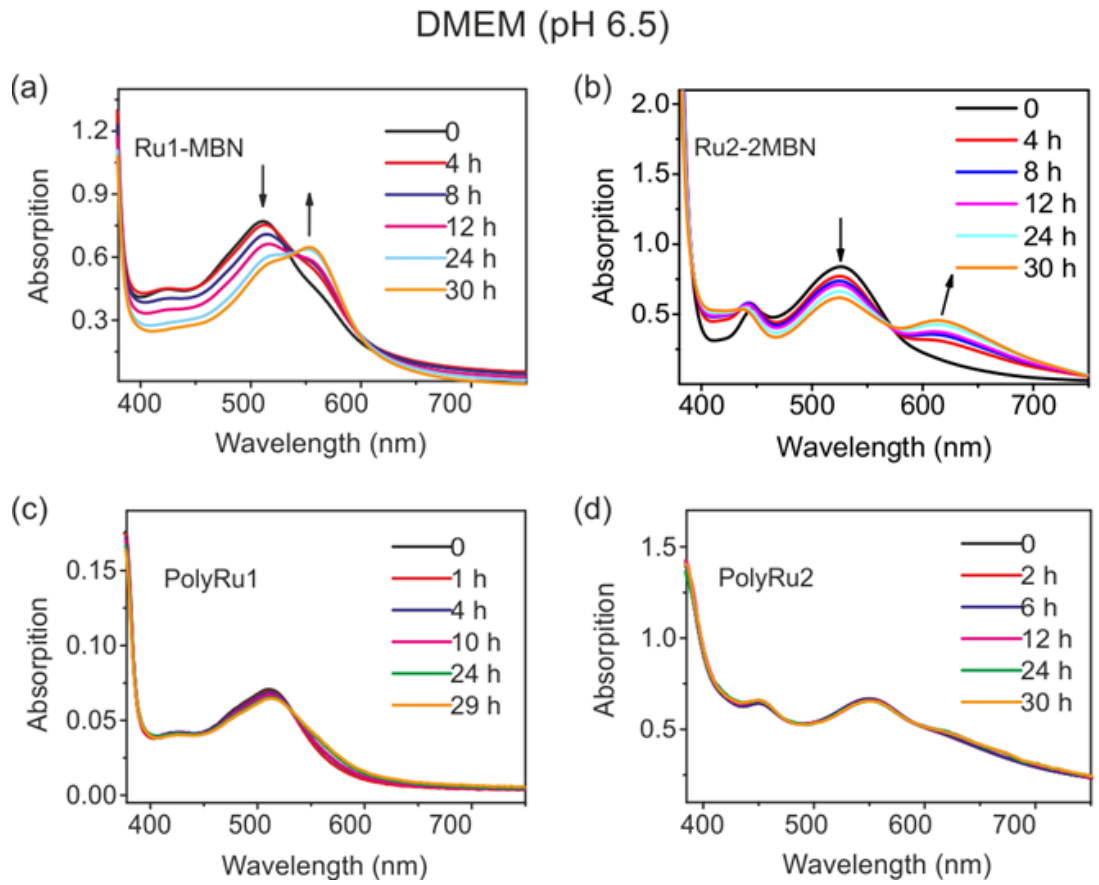

Figure 48. UV/Vis absorption spectroscopy of (a) Ru1-MBN, (b) Ru2-2MBN, (c) PolyRu1, and (d) PolyRu2 in the dark for different time periods in DMEM at pH 6.5.

Subsequently, the variations of the materials were investigated by UV/Vis absorption spectroscopy in Dulbecco's Modified Eagle's Medium (DMEM) at pH 6.5, imitating the internal acidic environment of tumor tissue but outside of cancer cells (Figure 48). The MLCT bands of Ru1-MBN (Figure 48a) and Ru2-2MBN (Figure 48b) changed quickly from 511 nm to ~553 nm and from 526 nm to ~615 nm, respectively, within 30 h. Thus both complexes dissociate spontaneously in DMEM at pH 6.5. For PolyRu1 and PolyRu2 (Figure 48c,d), the spectra demonstrated nearly no change, suggesting their good stability in DMEM at pH 6.5.

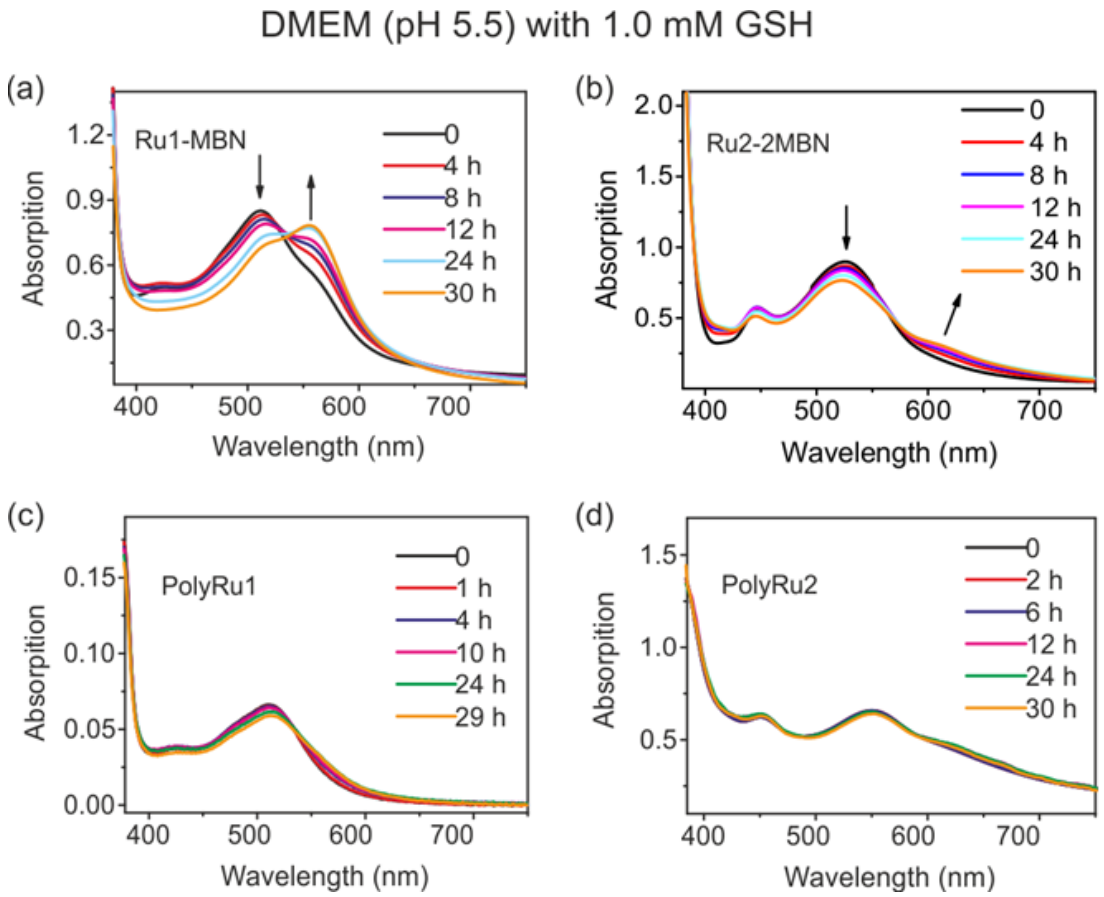

Figure 49. UV/Vis absorption spectroscopy of (a) Ru1-MBN, (b) Ru2-2MBN, (c) PolyRu1, and (d) PolyRu2 in the dark for different time periods in DMEM at pH 5.5 with 1.0 mM GSH.

We further studied the stabilities of Ru-containing materials in DMEM (pH 5.5) containing 1.0 mM L-glutathione reduced (GSH), which was used to imitate the reductive environment of cancer cells (Figure 49). The MLCT band of Ru1-MBN shifted from 511 nm to ~555 nm after 1 day incubation (Figure 49a). The MLCT band of Ru2-2MBN at 527 nm decreased in parallel (Figure 49b). In contrast, the MLCT bands of PolyRu1 and PolyRu2 did not change in the dark, at least not within 29 h, demonstrating their good stability in the reductive environment (Figure 49c,d). In addition, the conversion of Ru-containing materials was calculated in the dark at 24 h by UV/Vis absorption spectroscopy results (Figure 50).[186] We concluded that Ru-containing polymer assemblies stabilized their corresponding Ru complexes under different conditions.

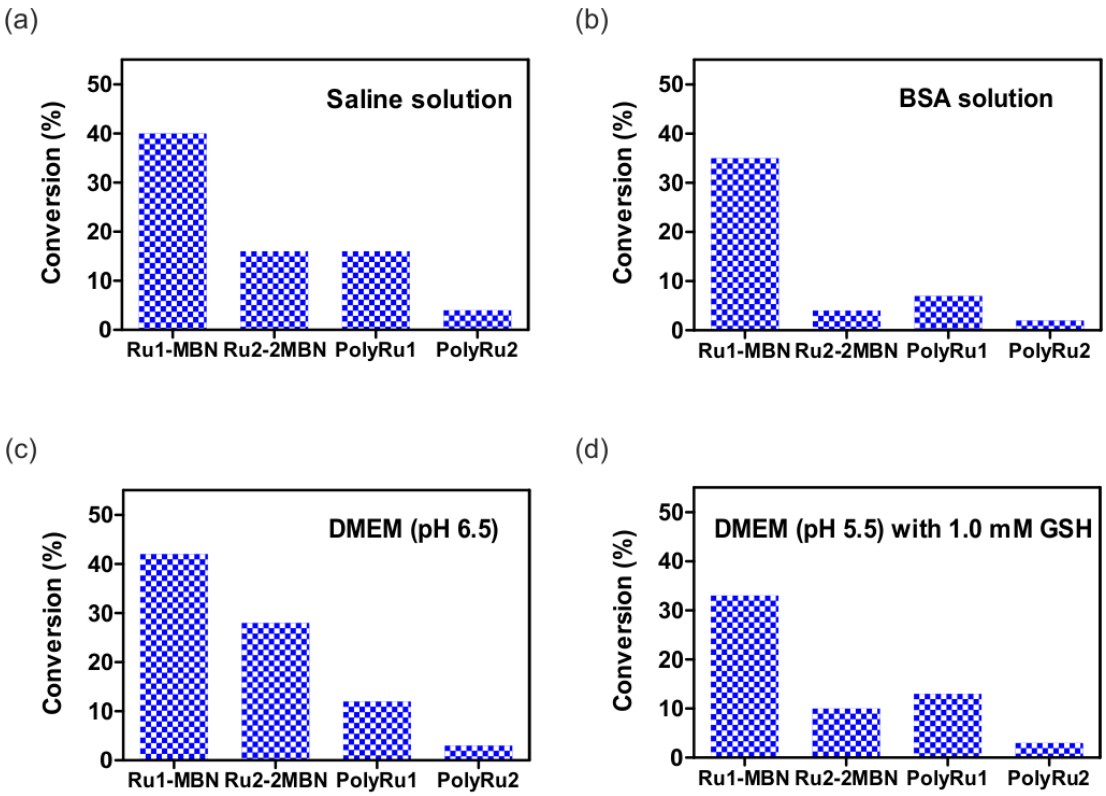

Figure 50. Conversion of Ru1-MBN, Ru2-2MBN, PolyRu1, and PolyRu2, when the samples were in the dark at 24 h in (a) saline solution, (b) BSA aqueous solution, (c) DMEM at pH 6.5, and (d) DMEM at pH 5.5 with 1.0 mM GSH, respectively. We assume conversion reached 100% when the absorption did not change in the dark.

3.1.5 Photoactivation of ruthenium-containing polymer assemblies

Ru-containing polymer assemblies should be controlled by red light to release Ru complexes in cancer cells. Therefore, in the end, photoreaction of Ru-containing polymer assemblies was studied in DMEM (pH 5.5) containing 1.0 mM GSH (Figure 51). Red-light irradiation (656 nm, 30 mW cm^{-2}) of PolyRu1 for 100 min caused a red shift of the MLCT band from 512 nm to ~550 nm (Figure 51a). These spectral variations were identical to photosubstitution of Ru1-MBN. The MLCT band of PolyRu2 at 553 nm deceased and a new peak at ~617 nm appeared under red-light irradiation (656 nm, 30 mW cm^{-2}) for 3 h (Figure 51b). Besides, precipitates gradually appeared in PolyRu2 nanoparticle dispersion after red light irradiation, suggesting that the destabilizing of the dispersion by photocleavage. The results demonstrated that PolyRu1 and PolyRu2 assemblies could be activated by red light under the imitated environment of cancer cells.

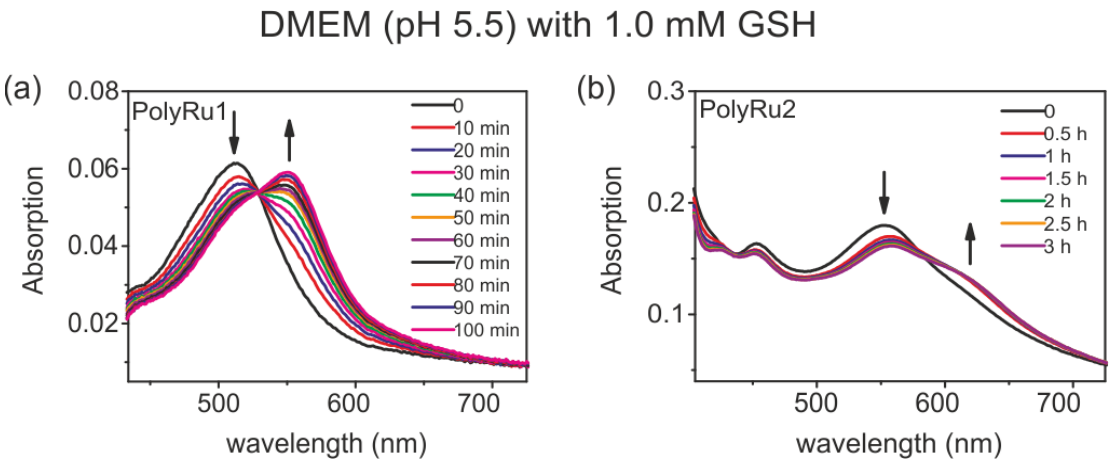

Figure 51. UV/Vis absorption spectroscopy of (a) PolyRu1 and (b) PolyRu2 in DMEM (pH 5.5) containing 1.0 mM GSH under 656 nm red light irradiation (30 mW cm^{-2}) for different time periods.

3.2 Preparation of ruthenium-containing polymer micelles and their co-release of dual drugs by red light

Si Wu, Hans-Jürgen Butt and Xing-Jie Liang led the project. Mingjia Chen did the experiments. Wen Sun synthesized Ru-containing polymers. Ningqiang Gong did TEM measurements. Mingjia Chen and Wen Sun contributed equally to this work.

3.2.1 Introduction

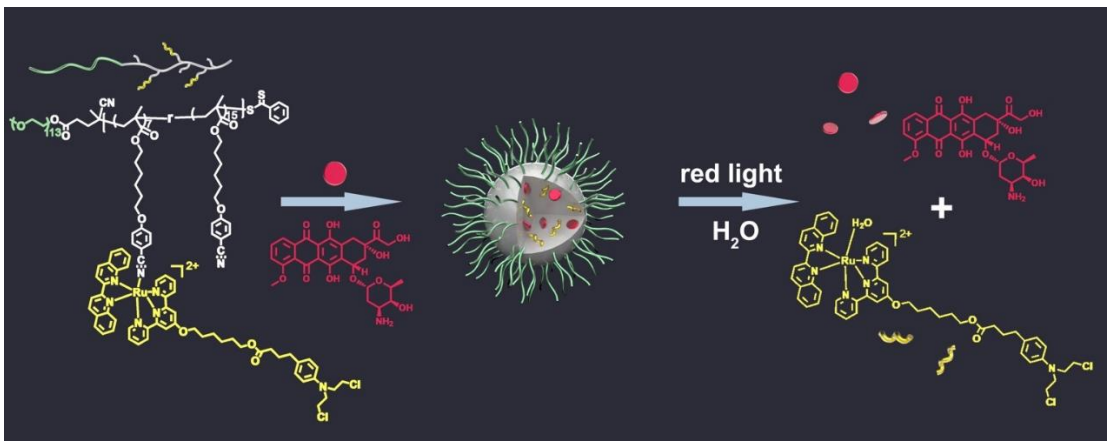

Figure 52. Chemical structure of the Ru-containing block copolymer and its micelle loading with DOX for co-release of dual drugs upon red light irradiation.

In this section, we prepared amphiphilic red-light-responsive Ru-containing block copolymers (PEG-*b*-P(CPH-*co*-RuCHL))(Figure 52). Due to their amphiphilic

structure, in water they self-assembled into micelles with the core available for DOX encapsulation to form DOX@PEG-*b*-P(CPH-*co*-RuCHL). The properties of micelles were characterized by TEM, DLS, fluorescence spectroscopy and UV/vis absorption spectroscopy, respectively. The cleavage of Ru complexes from the polymer chains by red light irradiation induced the disintegration of micelles in cell culture medium and resulted in the simultaneous co-release of dual drugs.

3.2.2 Preparation of micelles

The amphiphilic Ru-containing block copolymers (PEG-*b*-P(CPH-*co*-RuCHL)) used in this work (chemical structure in Figure 52) were synthesized by grafting $[Ru(CHLtpy)(biq)(H_2O)]^{2+}$ (CHLtpy = 4-hydroxyhexyloxy-2,2′:6′,2″-terpyridine ester of chloroambucil) to PEG-b-PCPH via the cyano–Ru coordination.[165] In particular, the Ru-containing units was synthesized by conjugating $[Ru(tpy)(biq)(H_2O)]^{2+}$ with anticancer drug chlorambucil to increase cytotoxicity. 22 CPH units in the polymer coordinated with 7 Ru-containing units was determined by ^{1}H NMR. The molecular weight of PEG-*b*-P(CPH-*co*-RuCHL) was 20.3 kg/mol. Comparing conventional metallodrug-loaded polymer carriers with less than 10% metallodrug content,[187, 188] the weight fraction of Ru complexes in this system reached up to ≈45%, expecting to increase therapeutic efficiency. The DOX@PEG-*b*-P(CPH-*co*-RuCHL) micelles and PEG-*b*-P(CPH-*co*-RuCHL) micelles were prepared through adding water to the organic solution. After getting rid of the organic solvents, the micelles water solution was collected from the dialysis tube. PEG-*b*-P(CPH-*co*-RuCHL) micelles almost were not fluorescent. According to the fluorescence of free DOX as standard, the amount of DOX encapsulated in the micelles could be measured using fluorescence spectroscopy (Figure 53).

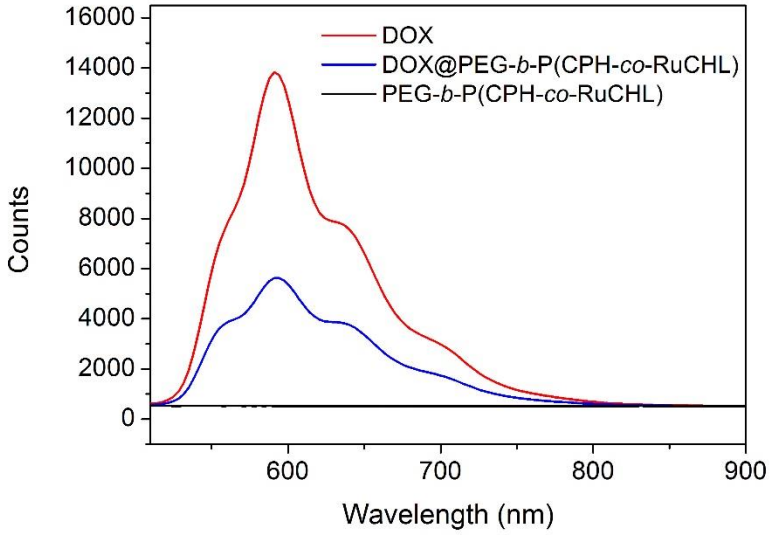

Figure 53. Fluorescence spectra of free DOX and DOX@PEG-*b*-P(CPH-*co*-RuCHL) micelles in H_2O/dimethylformamide mixture, λ_{ex} = 483 nm. PEG-*b*-P(CPH-*co*-RuCHL) micelles was non-fluorescent.

3.2.3 Characterization of micelles

DOX@PEG-*b*-P(CPH-*co*-RuCHL) micelles contained PEG blocks as the hydrophilic outer shell and CPH-co-RuCHL blocks as the hydrophobic inner core, which could encapsulate DOX inside (Figure 54).

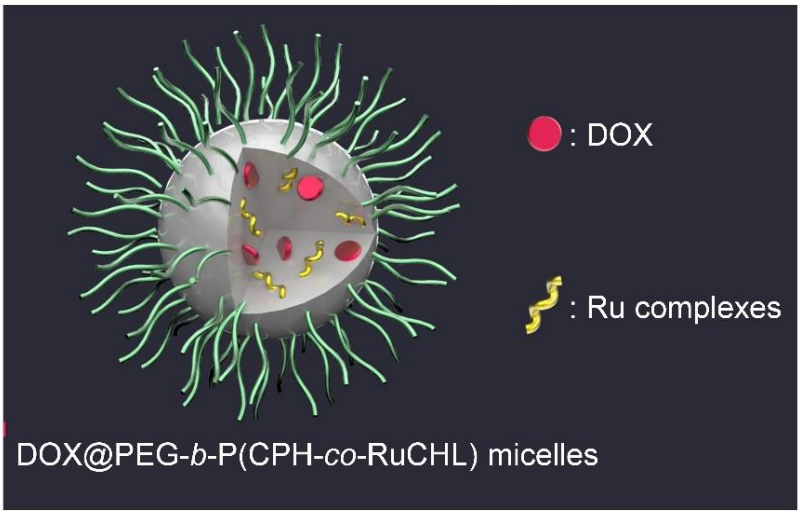

Figure 54. Schematic illustration of DOX@PEG-*b*-P(CPH-*co*-RuCHL) micelles.

TEM image displayed that the morphology of PEG-*b*-P(CPH-*co*-RuCHL) micelles was spherical and monodisperse with a diameter of ~15 nm (Figure 55a). The diameter of DOX@PEG-*b*-P(CPH-*co*-RuCHL) micelles increased to ~22 nm after DOX

encapsulation, still showing a relatively monodisperse size distribution (Figure 55b). DLS similarly indicated that the hydrodynamic diameter of DOX@PEG-*b*-P(CPH-*co*-RuCHL) micelles rised from ~22 nm to ~27 nm with a narrow size distribution after DOX loading (Figure 56).

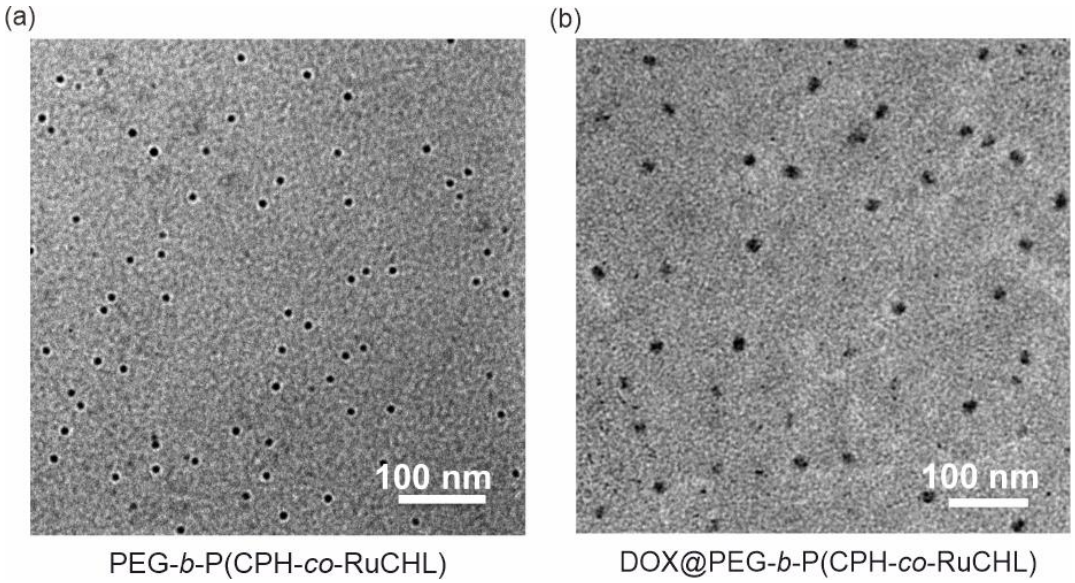

Figure 55. TEM images of (a) PEG-*b*-P(CPH-*co*-RuCHL) micelles and (b) DOX@PEG-*b*-P(CPH-*co*-RuCHL) micelles.

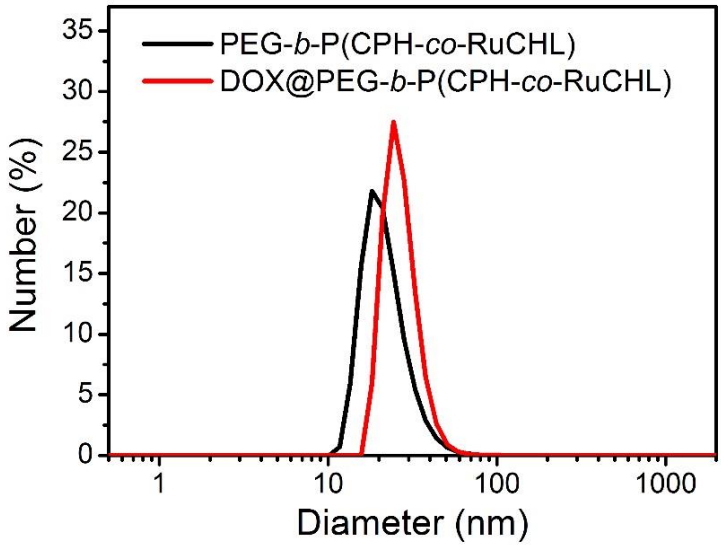

Figure 56. DLS analysis of PEG-*b*-P(CPH-*co*-RuCHL) micelles and DOX@PEG-*b*-P(CPH-*co*-RuCHL) micelles in water. Concentration of micelles was ~100 μg/mL.

The size of DOX@PEG-*b*-P(CPH-*co*-RuCHL) micelles was unchanged even after

incubation for 48 h in water and saline solution in the dark (Figure 57). No fluorescence was observed from dialysate at least for 9 h, after dialysis of DOX@PEG-*b*-P(CPH-*co*-RuCHL) micelle dispersion, suggesting no leakage of DOX from the micelles (Figure 58). These results demonstrated that the well dispersed DOX@PEG-*b*-P(CPH-*co*-RuCHL) micelles had good stability in aqueous solution.

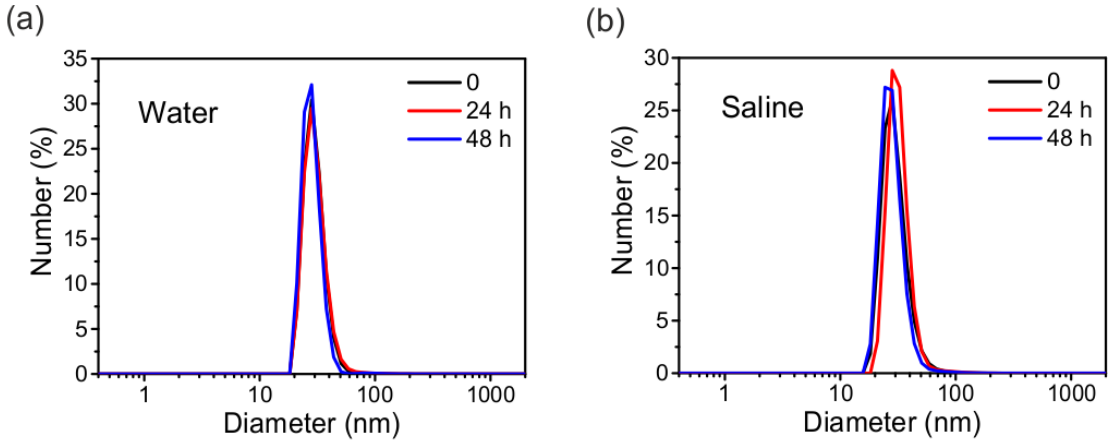

Figure 57. Diameters of DOX@PEG-*b*-P(CPH-*co*-RuCHL) micelles when incubated in (a) water and (b) saline solution for 48 h in the dark.

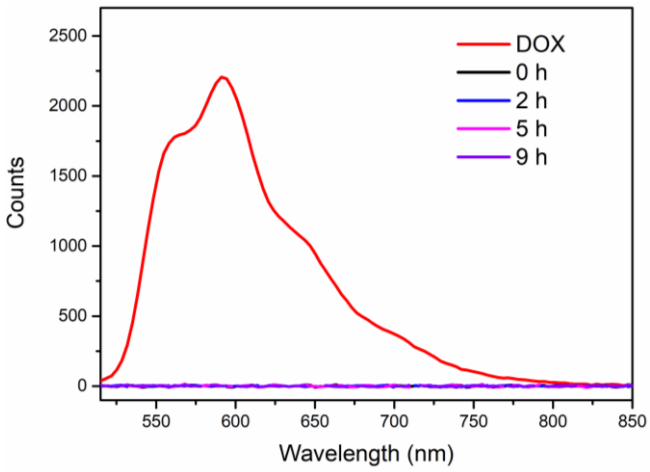

Figure 58. Fluorescence spectra of free DOX (red curve), and fluorescence spectra of dialysate after dialysis of DOX@PEG-*b*-P(CPH-*co*-RuCHL) in saline solution for 0, 2, 5 and 9 h.

3.2.4 Drug release

A wide MLCT band of PEG-*b*-P(CPH-*co*-RuCHL) micelles could be excited using red light in the "therapeutic window" (e.g., 650–900 nm). [165] The photoresponse of micelles was set in DMEM, imitating the internal environment of cancer cells. 656 nm

red light (30 mW cm^{-2}) irradiation of PEG-*b*-P(CPH-*co*-RuCHL) micelles for different time periods induced the red shift of the MLCT band from 519 nm to 576 nm (Figure 59). This indicates that Ru complexes were indeed cleaved by red light.

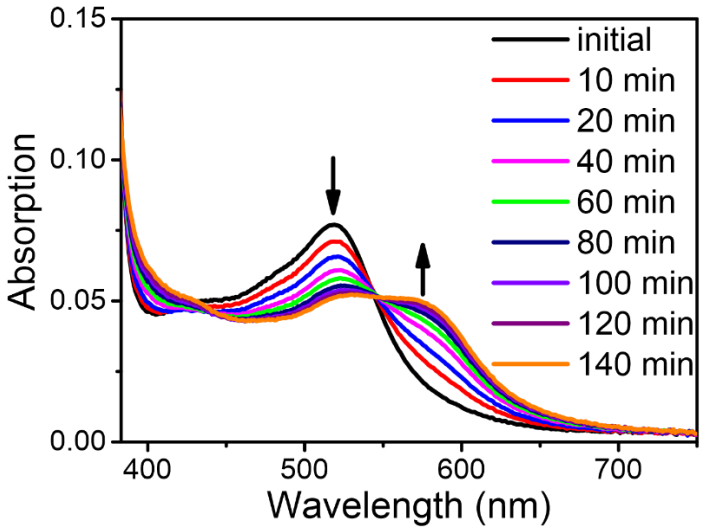

Figure 59. UV/vis absorption spectroscopy of PEG-*b*-P(CPH-*co*-RuCHL) micelles in cell culture medium (DMEM) after 656 nm red light (30 mW cm^{-2}) irradiation for different time periods.

The release of Ru complexes from DOX@PEG-*b*-P(CPH-*co*-RuCHL) micelles after 656 nm red light (30 mW cm^{-2}) irradiation was quantified by inductively coupled plasma mass spectrometry (ICP-MS), which could calculate the contents of Ru element (Figure 60a). After red light (30 mW cm^{-2}) irradiation, the 64% of Ru complexes was acceleratingly released at 9 h, while less than 10% of Ru complexes was released at the same time in the dark because of spontaneous hydrolysis. Thus the release of Ru complexes was controlled by light irradiation. The percentage of released DOX from DOX@PEG-*b*-P(CPH-*co*-RuCHL) micelles after 656 nm red light (30 mW cm^{-2}) irradiation was determined by fluorescence spectroscopy (Figure 60b). Because of the breakdown of micelles in DMEM solution under light irradiation, the 50% of DOX was released within 1 h. In contrast, a little DOX was slowly released in the dark; most likely DOX was protonated in the acidic environment.[189] Moreover, TEM images showed stable micelles in DMEM solution. In contrast, micelles were rarely observed after 660 nm laser (120 mW cm^{-2}, 50 min) irradiation (Figure 61). All the results demonstrated the remaining block copolymers could not stabilize the structure of micelles after the removal of Ru complexes in DMEM solution. Micelles collapsed under red light irradiation, leading to simultaneously controllable release of Ru

complexes and DOX.

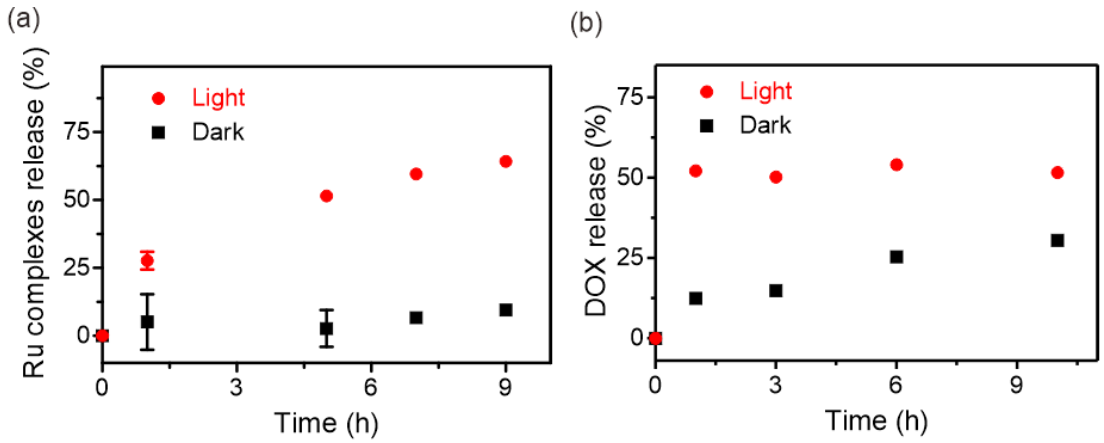

Figure 60. The release percentage of (a) Ru complexes and (b) DOX from DOX@PEG-*b*-P(CPH-*co*-RuCHL) micelles at pH 5.5 under 656 nm red light (30 mW cm^{-2}) irradiation or in the dark. Concentration of micelles was ~100 μg/mL.

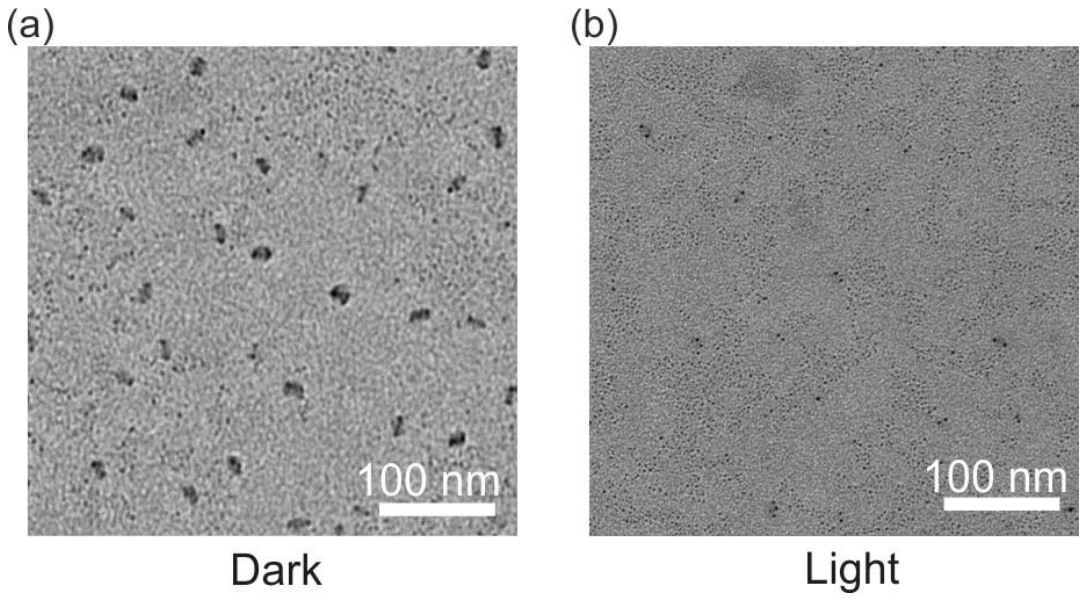

Figure 61. TEM images of PEG-*b*-P(CPH-*co*-RuCHL) micelles in DMEM cell medium culture (a) in the dark and (b) after 660 nm laser irradiation (120 mW cm^{-2}, 50 min).

3.3 Ruthenium-containing polymer micelles for photochemotherapy to overcome multidrug resistance

Si Wu, Hans-Jürgen Butt and Xing-Jie Liang led the project. Mingjia Chen, Ningqiang Gong did the experiments and contributed equally to this work.

3.3.1 Introduction

Encouraged by the controllable co-release of dual drugs from DOX@PEG-*b*-P(CPH-*co*-RuCHL) micelles, in this section, we applied them *in vitro* and *in vivo* to overcome MDR (Figure 62). DOX@PEG-*b*-P(CPH-*co*-RuCHL) micelles were efficiently taken up into drug-resistant breast cancer cells (MCF-7R cells) via endocytosis. Unlike free DOX that would be pumped out from cancer cells, they overcame drug resistance through bypassing P-gp. The structure of micelles was damaged upon red light irradiation in cellular environment, simultaneously releasing Ru complexes and DOX. Integrating of Ru complexes crosslinked with DNA by photobinding and DOX interacted with DNA by intercalation, the synergetic effects enhanced the death of MCF-7R cells. Besides, MCF-7R tumor-bearing mice were treated with DOX@PEG-*b*-P(CPH-*co*-RuCHL) micelles, showing the significant inhibition of the tumor growth after light irradiation, suggesting the promising application in cancer chemotherapy for combating MDR.

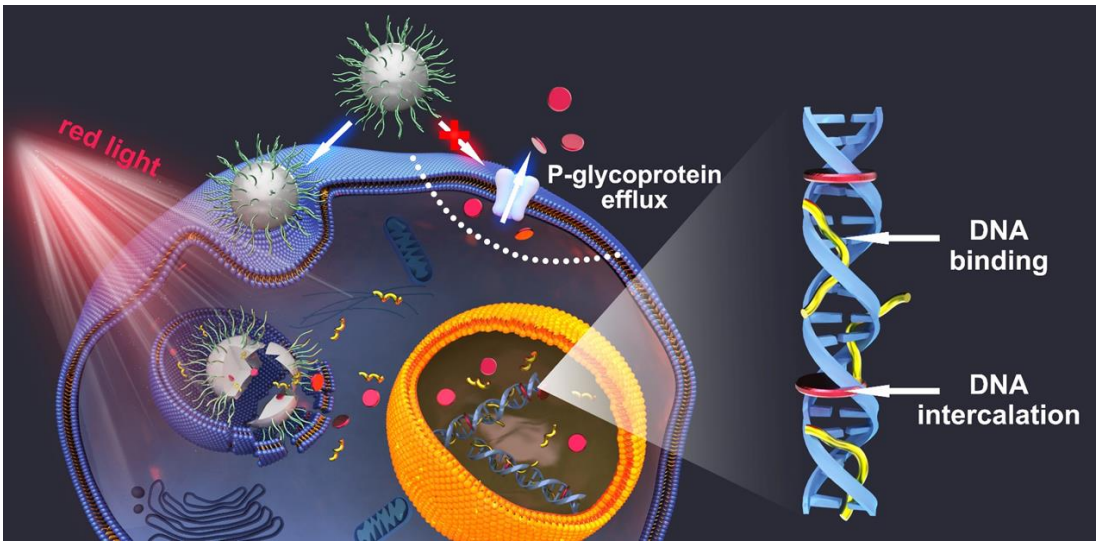

Figure 62. Schematic illustration of endocytosis and photochemotherapy using DOX@PEG-*b*-P(CPH-*co*-RuCHL) micelles in drug-resistant cancer cells (MCF-7R cells) of a nude mouse.

3.3.2 Cellular uptake and accumulation

Cellular uptake of free DOX or DOX@PEG-*b*-P(CPH-*co*-RuCHL) micelles at a final DOX concentration of 1.0 μM and 2.0 μM was measured using flow cytometry by MCF-7R cells, which overexpressed P-gp on their cell membrane. Since PEG-*b*-P(CPH-*co*-RuCHL) micelles were none-fluorescent, the uptake efficiency was evaluated by the count of DOX fluorescence. After incubation with MCF-7R cells for 0.5 h, cellular uptake of both free DOX and DOX@PEG-*b*-P(CPH-*co*-RuCHL)

micelles was low (Figure 63a). After 2 h, the fluorescence of the cells treated with DOX@PEG-*b*-P(CPH-*co*-RuCHL) strongly increased, while free DOX did not lead to an increase of cellular fluorescence (Figure 63b). We conclude that DOX@PEG-*b*-P(CPH-*co*-RuCHL) micelles are efficiently taken up by the cells which free Dox is kept outside.

Intracellular fluorescence of DOX@PEG-*b*-P(CPH-*co*-RuCHL) micelles was considerably enhanced when the concentration of encapsulation DOX increased from 1.0 µM to 2.0 µM (Figure 64). In particular DOX@PEG-*b*-P(CPH-*co*-RuCHL) micelles could be quickly taken up by MCF-7R cells and accumulated in the cells. Conversely, the uptake of free DOX by MCF-7R cells was nearly null. The membrane protein of P-gp overexpressed on MCF-7R cells decreased the drug influx, objecting to the cellular uptake of free DOX.[51, 190, 191] Because of bypassing P-gp, the uptake of DOX@PEG-*b*-P(CPH-*co*-RuCHL) micelles in MCF-7R cells was rapid and effective.

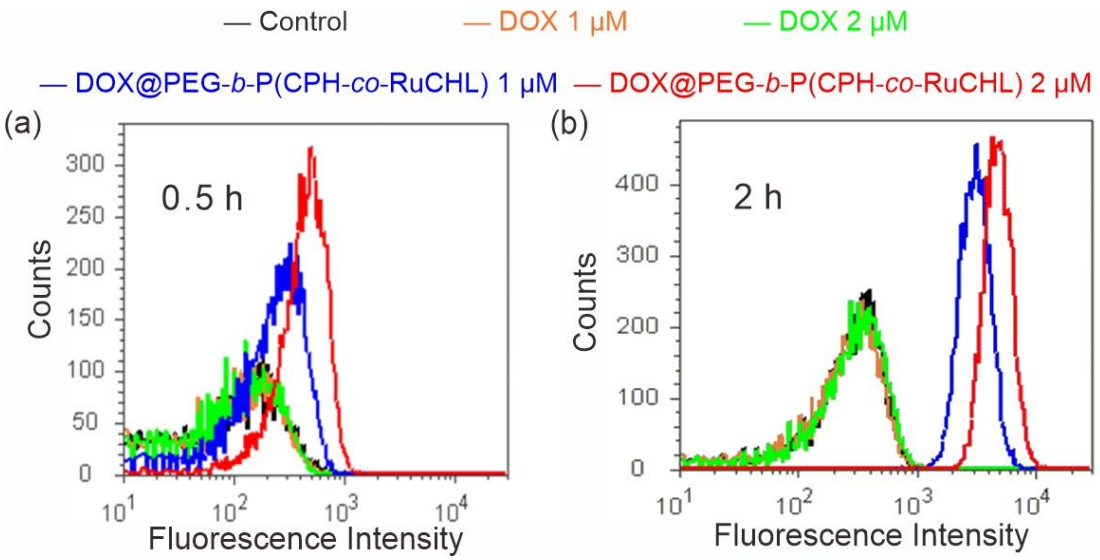

Figure 63. Quantitative analysis of DOX@PEG-*b*-P(CPH-*co*-RuCHL) micelles or free DOX uptake by MCF-7R cells for (a) 0.5 h and (b) 2 h using acoustic focusing cytometer.

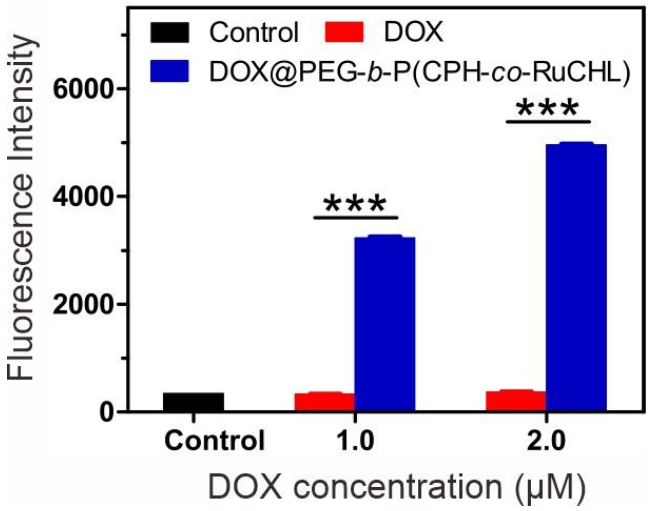

Figure 64. Fluorescence intensity of MCF-7R cells treatment with DOX@PEG-*b*-P(CPH-*co*-RuCHL) micelles or free DOX after 2 h incubation. The asterisk (***) represented the data had an extremely significant difference ($p < 0.001$; two-way ANOVA test)

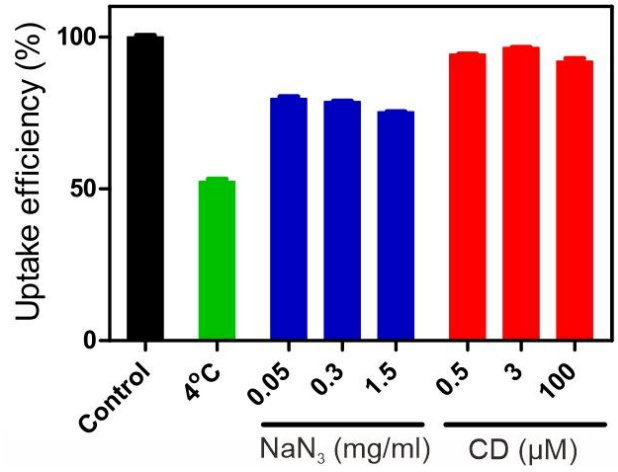

Figure 65. Inhibition of the uptake of DOX@PEG-*b*-P(CPH-*co*-RuCHL) micelles into MCF-7R cells using endocytosis inhibitors. 4°C: inhibition of energy dependent endocytosis; NaN_3: inhibitor of ATP metabolites; Cytochalasin D (CD): inhibitor of micropinocytosis.

We further investigated the uptake mechanism of DOX@PEG-*b*-P(CPH-*co*-RuCHL) micelles in MCF-7R cells using endocytosis inhibitors, which could restrict different endocytosis modes (Figure 65). The mean uptake of DOX@PEG-*b*-P(CPH-*co*-RuCHL) micelles decreased by 47% at 4°C and 22% using sodium azide, respectively, indicating that the endocytosis of DOX@PEG-*b*-P(CPH-*co*-RuCHL) micelles was an energy-dependent procedure.[64] Inhibition of DOX efflux from MCF-7R cells was assessed

using flow cytometry (Figure 66). Almost all free DOX was pumped out within 1 h, whereas the amount of DOX carried by micelles nearly unchanged even after 4 h, demonstrating micelles assisted DOX to escape the drug efflux of P-gp.

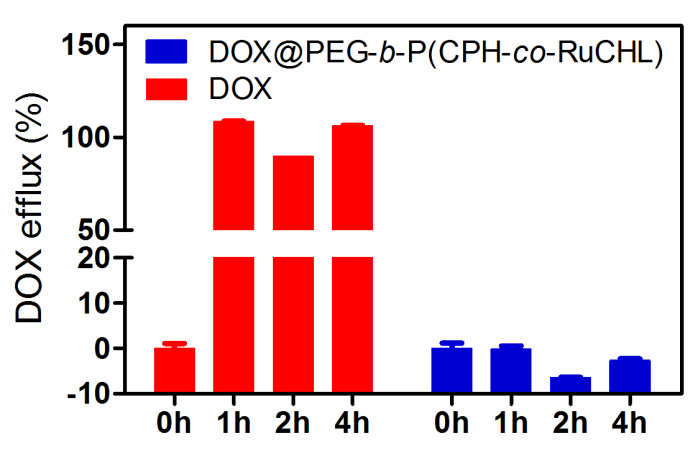

Figure 66. Inhibition of DOX efflux from MCF-7R cells using DOX@PEG-*b*-P(CPH-*co*-RuCHL) micelles or free DOX.

The intracellular distribution of free DOX or DOX@PEG-*b*-P(CPH-*co*-RuCHL) micelles was detected using confocal laser scanning microscopy (CLSM) in MCF-7R cells (Figure 67). Practically no red fluorescence of DOX was observed in cells incubated with free DOX for 270 min because of the efflux by overexpressed P-gp. In contrast, remarkable red fluorescence of DOX was found in the cytoplasm incubated with DOX@PEG-*b*-P(CPH-*co*-RuCHL) micelles due to bypassing P-gp. Besides, some red fluorescence of DOX was detected in the nucleus incubated with DOX@PEG-*b*-P(CPH-*co*-RuCHL) micelles after 660 nm laser (50 mW cm^{-2}) irradiation of 10 min. Prolonging irradiation for 30 min and keeping incubation time consistent, significant red fluorescence was noticed in the nucleus, illustrating the release and the entrance of DOX to nucleus were controlled by red light irradiation. After removing Ru complexes from polymer chains under light irradiation, the structure of micelles was disturbed in cells, thus resulting in the release of DOX and Ru complexes at the same time.

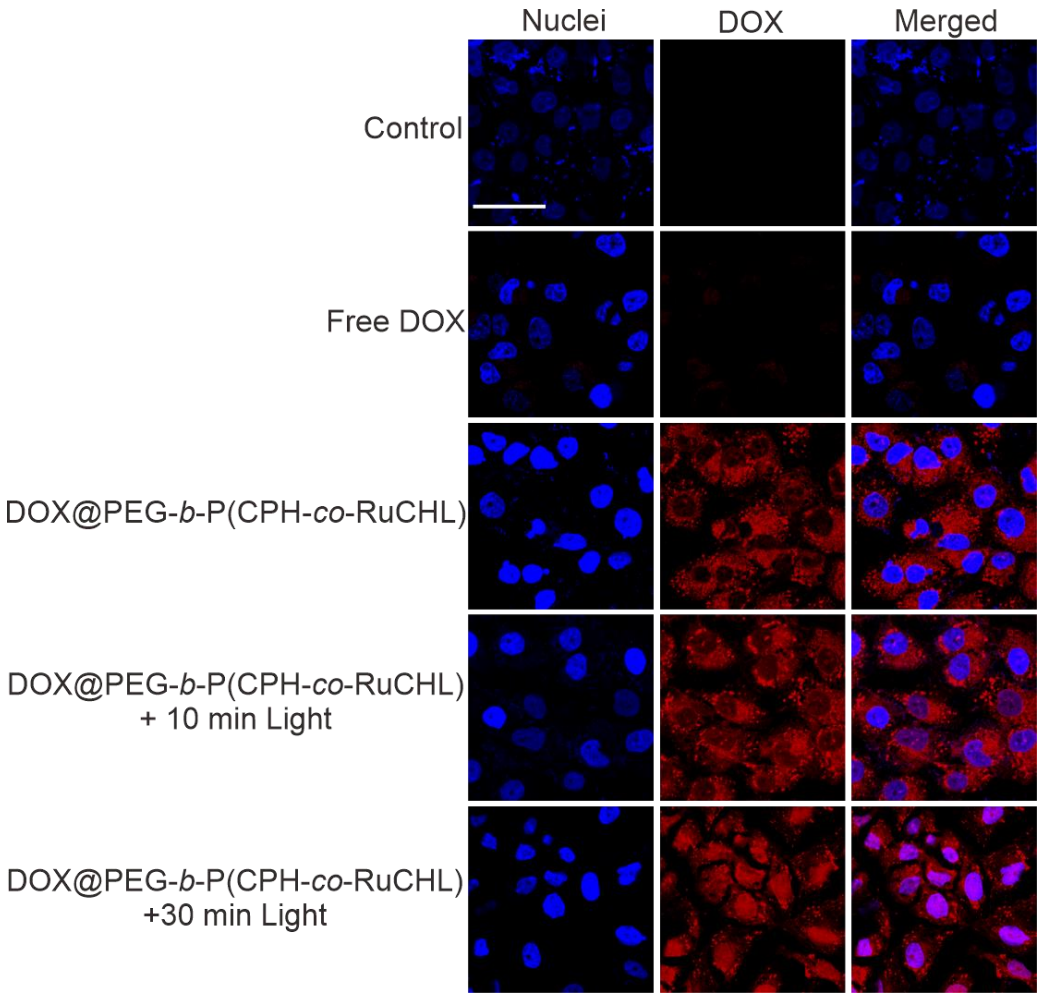

Figure 67. CLSM images of MCF-7R cells incubated with DOX@PEG-*b*-P(CPH-*co*-RuCHL) micelles or free DOX. After 120 min uptake, MCF-7R cells with DOX@PEG-*b*-P(CPH-*co*-RuCHL) micelles were irradiated under 660 nm laser (50 mW cm^{-2}) for 10 min or 30 min, then sequentially incubation for 140 min or 120 min. The incubation time of each group was the same (270 min). Nuclei were stained with Hoechst 33342 (blue). Scale bar: 50 μm.

3.3.3 DNA damage

DNA damage was assessed using agarose gel electrophoresis (Figure 68). The mechanism of common photoresponsive Ru complexes acting on pUC19 plasmid DNA after exposure included DNA photocleavage, DNA photobinding, and combination of these two mechanisms.[192] Specifically, photocleavage induced the break of DNA single strand and deceased its mobility, resulting in the migration from supercoiled DNA (lane 2) to between linear DNA (lane 3) and relaxed circular DNA (lane 4). Photobinding induced the crosslinking of DNA and further deceased its mobility, casuing the migration above the relaxed circular DNA.

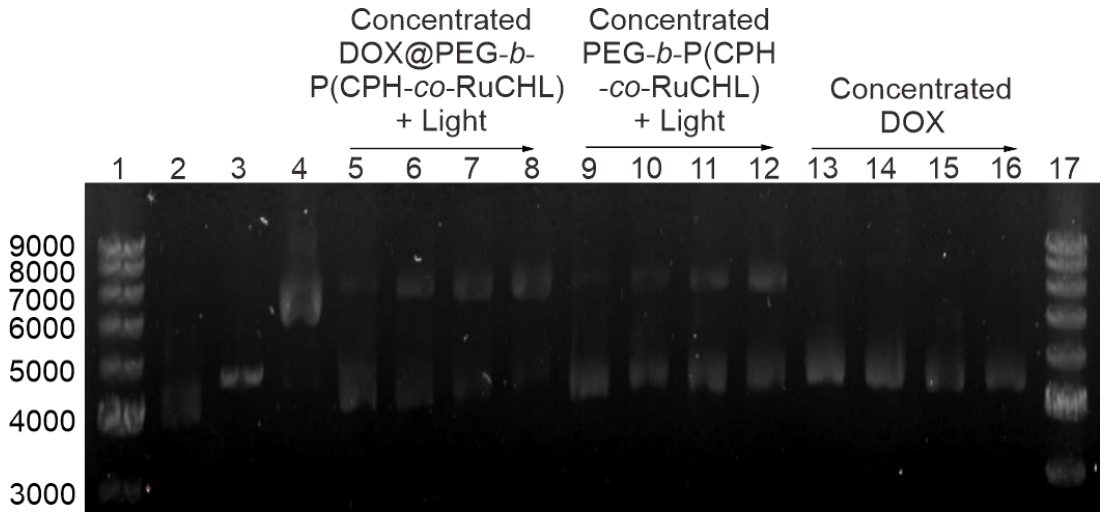

Figure 68. Agarose gel electrophoresis of 40 μg mL^{-1} pUC19 plasmid with different treatments under light. Lane 1,17: DNA molecular weight standard; lane 2: supercoiled DNA (~4000 bp); lane 3: linear DNA (~5000 bp); lane 4: relaxed circle DNA (~6000 bp, $Cu(phen)_2$ reaction with supercoiled DNA); lanes 5−8: supercoiled DNA were prior incubated with 5, 20, 50 and 100 μg ml^{-1} DOX@PEG-*b*-P(CPH-*co*-RuCHL) micelles for 30 min then to 656 nm red light (50 mW cm^{-2}) activation for 1 h; lanes 9−12: supercoiled DNA were prior incubated with 5, 20, 50 and 100 μg ml^{-1} PEG-*b*-P(CPH-*co*-RuCHL) micelles for 30 min then to 656 nm red light (50 mW cm^{-2}) activation for 1 h; lanes 13−16: supercoiled DNA were incubated with 5, 10, 20 and 50 μg ml^{-1} DOX. The samples were incubated overnight after light activation before gel analysis.

Dose responses were performed with pUC19 plasmid using different treatments. Incubation with free DOX (lane 13-16), the mobility of the DNA adducts was slightly reduced compared to supercoiled DNA. DOX interacted with DNA by intercalation and caused radiation-induced unwinding of DNA.[193-195] When incubated with PEG-*b*-P(CPH-*co*-RuCHL) micelles (lane 9-12) after red light (50 mW cm^{-2}, 1 h) irradiation, a dose-dependent effect was shown on the DNA mobility. The migration of the DNA was slower than the relaxed circular DNA with the increasing concentration of micelles, suggesting the crosslinking of DNA adducts. Light prompted the crosslinking of DNA with Ru complexes from PEG-*b*-P(CPH-*co*-RuCHL) micelles by photobinding. The new designed Ru complexes with anticancer drug chlorambucil increased the ability of DNA binding. The integrity of DNA adducts appeared above the relaxed circular DNA at the high concentration of DOX@PEG-*b*-P(CPH-*co*-RuCHL) micelles (lane 8) after red light irradiation, indicating combination Ru complexes with DOX synergistically enhanced the restriction of DNA movement and led to the damage of DNA. In contrast, when incubated with PEG-*b*-P(CPH-*co*-RuCHL) micelles (lane 6−9) or DOX@PEG-

b-P(CPH-*co*-RuCHL) micelles (lane 2−5) without light irradiation (Figure 69), their mobility was no significant different compare to supercoiled DNA (lane 10). No DNA adducts was observed, suggesting no DNA binding in the dark.

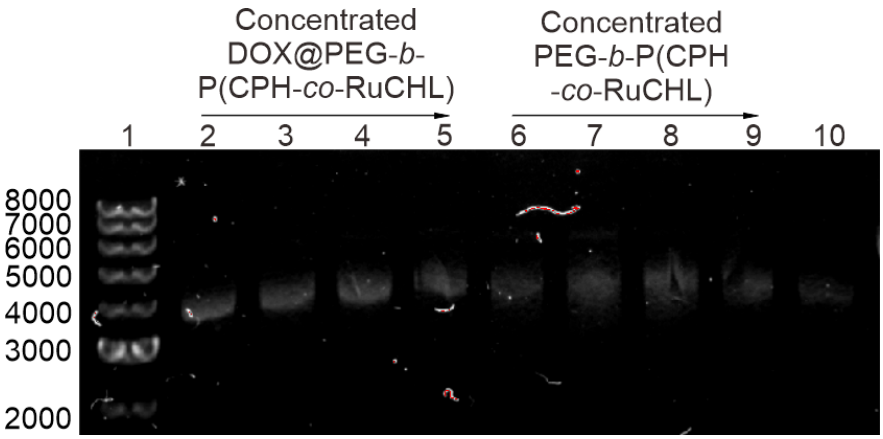

Figure 69. Agarose gel electrophoresis of 40 μg mL^{-1} pUC19 plasmid with different treatments in the dark. Lane 1: DNA molecular weight standard; lane 10: supercoiled DNA (~4000 bp); lanes 2−5: supercoiled DNA were incubated with 5, 20, 50 and 100 μg ml^{-1} DOX@PEG-*b*-P(CPH-*co*-RuCHL) micelles; lanes 6−9: supercoiled DNA were incubated with 5, 20, 50 and 100 μg ml^{-1} PEG-*b*-P(CPH-*co*-RuCHL) micelles. The samples were incubated overnight for the same time period before gel analysis.

3.3.4 Anticancer assessment *in vitro*

The viability of MCF-7R cells after different treatments was studied by cell counting kit-8 (CCK-8) assay (Figure 70). First, the cells were incubated with materials for 4 h and then irradiated by red light for 30 min (50 mW cm^{-2}). Continuing to incubate, the whole process took 24 h. The treatments separately used free DOX or DOX@PEG-*b*-P(CPH-*co*-RuCHL) micelles in the dark or PEG-*b*-P(CPH-*co*-RuCHL) micelles with light irradiation. They did not kill the MCF-7R cells when setting the concentration of DOX from 2.2 to 17.5 μg mL^{-1} or the concentration of micelles from 12.5 to 100 μg mL^{-1}. Specifically, the cell viability merely decreased to 72%, 73%, and 62% by the above measurements at the highest set concentration, respectively. However, the MCF-7R cells were effectively killed, when incubated with DOX@PEG-*b*-P(CPH-*co*-RuCHL) micelles with light irradiation at the same concentration. The cell viability sharply decreased to 22% at the highest set concentration because of the co-release of Ru complexes and DOX under red light irradiation. The new Ru complexes was conjugate of $[Ru(tpy)(biq)(H_2O)]^{2+}$ and the commercial anticancer drug chlorambucil, both of which could inhibit cancer cell growth and thus enhance anticancer efficiency.

[165, 196] The novel design was different from the other photoactived Ru complexes.[197] Moreover, when the Ru complexes was cleaved from polymers by light, our group proved that no $^1O_2$ was generated. The PACT process was oxygen independent, which was suited for hypoxic tumor treatment.[165] Combined with the release of DOX, those synergetic effects induced the death of MCF-7R cells.

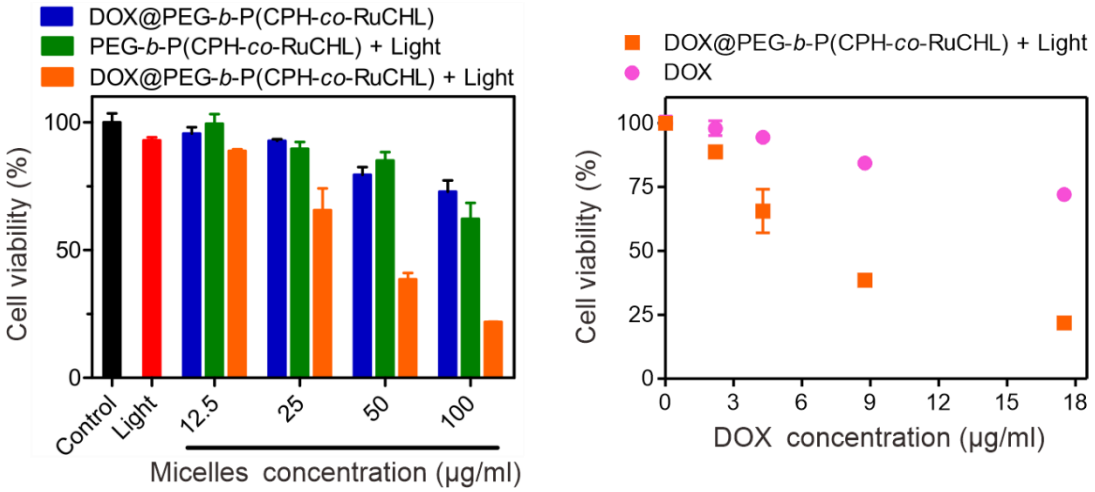

Figure 70. Viability of MCF-7R cells after different treatments. Control group: cells without any treatment; Light group: cells irradiated with 656 nm red light (50 mW cm^{-2}, 30 min); DOX@PEG-*b*-P(CPH-*co*-RuCHL) micelles group: cells incubated with DOX@PEG-*b*-P(CPH-*co*-RuCHL) micelles; PEG-*b*-P(CPH-*co*-RuCHL) micelles + Light group: after incubation with PEG-*b*-P(CPH-*co*-RuCHL) micelles for 4 h, cells irradiated with 656 nm red light (50 mW cm^{-2}, 30 min); DOX@PEG-*b*-P(CPH-*co*-RuCHL) micelles + Light group: after incubation with DOX@PEG-*b*-P(CPH-*co*-RuCHL) micelles for 4 h, cells irradiated with 656 nm red light (50 mW cm^{-2}, 30 min); DOX group: cells incubated with free DOX. Cell viability was tested after incubating the cells for 24 h.

3.3.5 Antitumor evaluation *in vivo*

Inspired by the promising results *in vitro*, experiments *in vivo* to assess the antitumor efficacy were performed using DOX@PEG-*b*-P(CPH-*co*-RuCHL) micelles in BALB/c nude mice bearing tumors derived from MCF-7R cells (Figure 71).

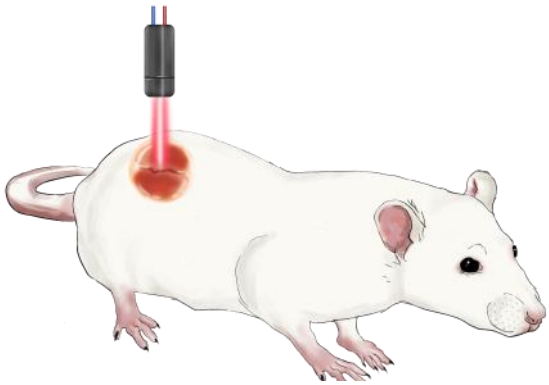

Figure 71. Schematic illustration of antitumor photochemotherapy using DOX@PEG-*b*-P(CPH-*co*-RuCHL) micelles in a tumor-bearing mouse model. Red light activated the micelles at the tumor site.

MCF-7R tumor-bearing mice were divided into six groups with different treatments: the control group, the group treated with light, the group administered with DOX, the group of DOX@PEG-*b*-P(CPH-*co*-RuCHL) micelles, the group of PEG-*b*-P(CPH-*co*-RuCHL) micelles with light irradiation, and the group of DOX@PEG-*b*-P(CPH-*co*-RuCHL) micelles with light irradiation, respectively. The material solution was injected into the neoplastic center, that was hypoxic.[198] Waiting for 4 h, the tumors (only for groups that need light irradiation) were exposed to 660 nm laser (200 mW cm^{-2}) for 30 min.

The antitumor effects of each group were evaluated through monitoring the tumor volumes over 12 days (Figure 72). Treatment with the group of DOX@PEG-*b*-P(CPH-*co*-RuCHL) micelles with light irradiation efficiently retarded the tumor growth. Conversely, neither light treatment nor DOX treatment showed a significant reduction in tumor growth compared to the control. The tumor volumes increased at varying degrees after treatment with DOX@PEG-*b*-P(CPH-*co*-RuCHL) micelles or PEG-*b*-P(CPH-*co*-RuCHL) micelles with light irradiation. During the treatment period, the mice did not show any unusual behavior for all six groups, and no distinct variation of mice body weight was found (Figure 73).

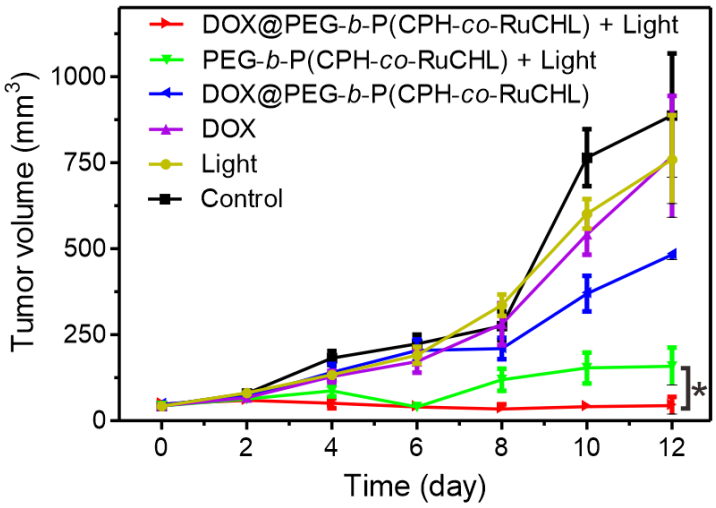

Figure 72. The mice were deal with different treatments at the same time period. Average volume of tumors was measured every two days, *p < 0.05 (two-tailed Student's t-test), n = 5.

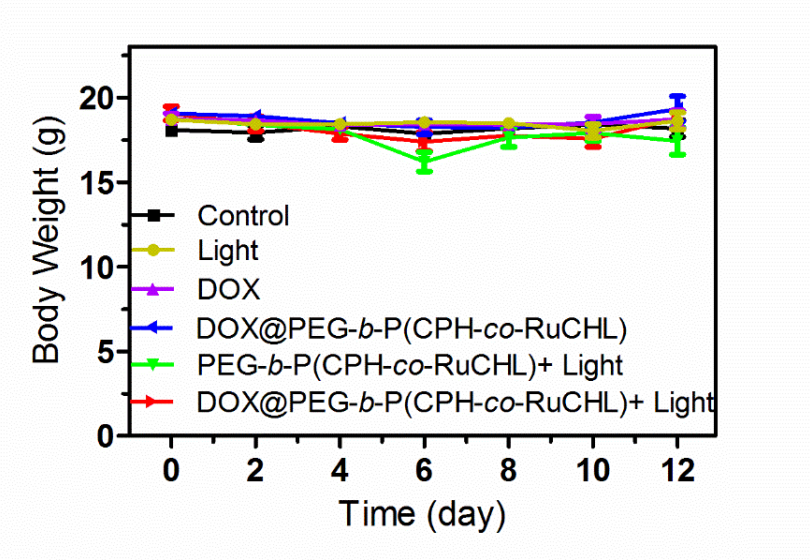

Figure 73. Mice body weight during different treatments were measured every two days (n = 5).

The weight and the representative image of the tumors at day 12 further confirmed the excellent treatment efficacy of the group of DOX@PEG-*b*-P(CPH-*co*-RuCHL) micelles with light irradiation. (Figures 74-75). Compared to other five groups, it effectually inhibited the growth of the drug-resistant tumor.

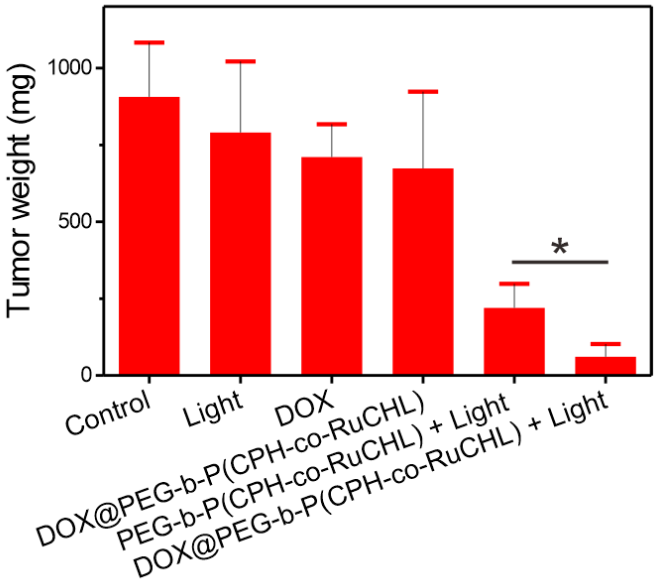

Figure 74. Average weight of tumors was measured at day 12 for different treatments. The mice were sacrificed and the tumors were harvested to weigh, *p < 0.05, n = 5.

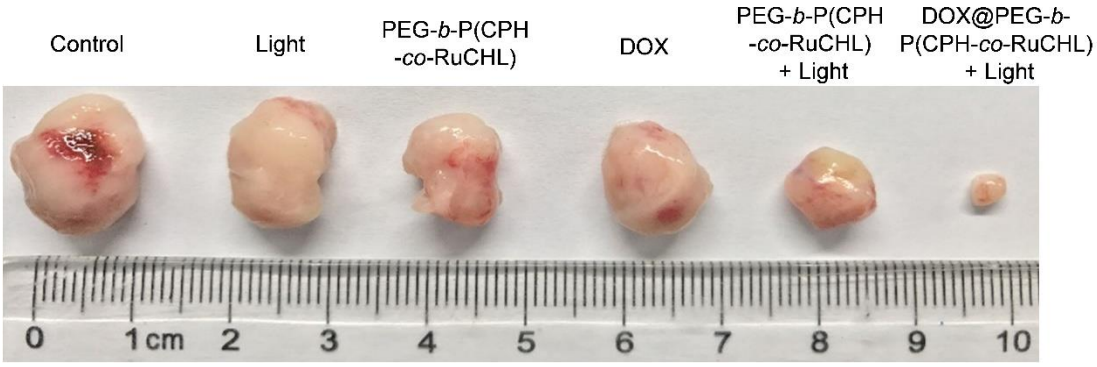

Figure 75. Representative image of the harvested MCF-7R tumors for different treatments.

Moreover, to evaluate the antitumor efficacy of different treatments, the tumor tissues were analyzed by hematoxylin and eosin (H&E) staining (Figure 76a), which could diagnose a broad range of histopathologic conditions.[199] A great quantity of apoptotic and nonproliferative cells were observed in the H&E staining image of the group of DOX@PEG-*b*-P(CPH-*co*-RuCHL) micelles with light irradiation. However, most living cells were still detected in the other five groups. Similarly, Ki-67 immunohistochemical (IHC) staining was used to assess tumor cell proliferation (Figure 76b). The Ki-67 level in the group of DOX@PEG-*b*-P(CPH-*co*-RuCHL) micelles with light irradiation was much lower than that in other five groups, demonstrating the higher antitumor activity of DOX@PEG-*b*-P(CPH-*co*-RuCHL)

micelles after light irradiation.

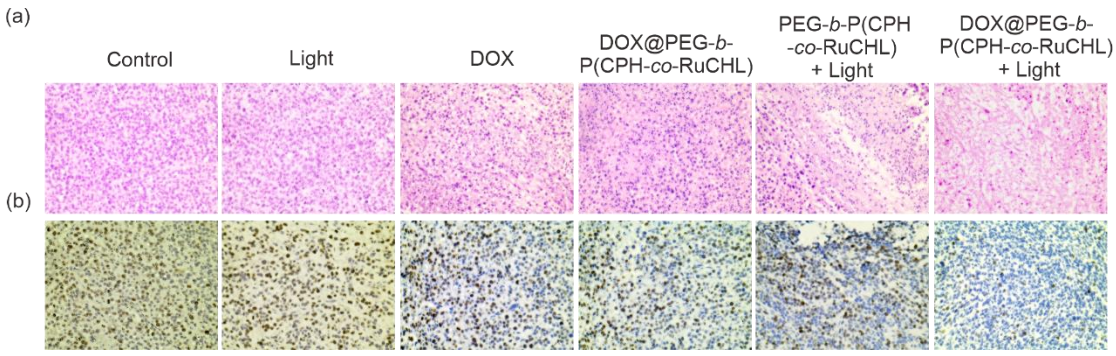

Figure 76. Evaluation of the antitumor efficacy of each treatment modality by histological analysis: (a) H&E staining and (b) Ki-67 IHC staining of the tumor tissues.

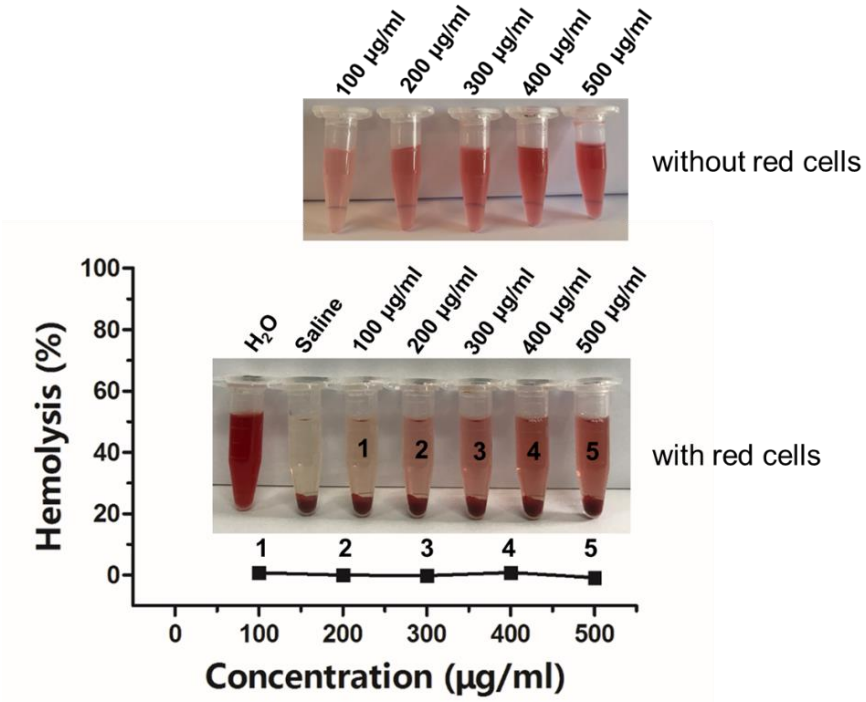

Figure 77. No hemolysis was observed with red blood cells after treated with DOX@PEG-*b*-P(CPH-*co*-RuCHL) micelles at concentrations of 100, 200, 300, 400 and 500 μg/mL, using water as a positive control and saline as a negative control. Samples without red cells setting as references indicated that the red color was from DOX@PEG-*b*-P(CPH-*co*-RuCHL) micelle solutions.

Hemolysis analysis was studied by DOX@PEG-*b*-P(CPH-*co*-RuCHL) micelles (100–500 μg mL^{-1}) incubated with red blood cells to evaluate their blood compatibility (Figure 77). No hemolytic effect was observed compared to the control group of saline,

when the concentration of micelles was as high as 500 μg/mL. That demonstrated that the micelles were good compatible with red blood cells. Additionally, the blood of the mice after different treatments over 12 days was analyzed to evaluate the biological safety (Figure 78). All the investigated parameters in the group of DOX@PEG-*b*-P(CPH-*co*-RuCHL) micelles with light irradiation were normal, showing insignificant difference compared to the group of control. That demonstrated negligible side effects after DOX@PEG-*b*-P(CPH-*co*-RuCHL) micelles treatment with light irradiation. The results *in vivo* suggested red-light-triggered synchronous release of Ru complexes and DOX from DOX@PEG-*b*-P(CPH-*co*-RuCHL) micelles exhibited the superior antitumor efficiency in drug-resistant tumors.

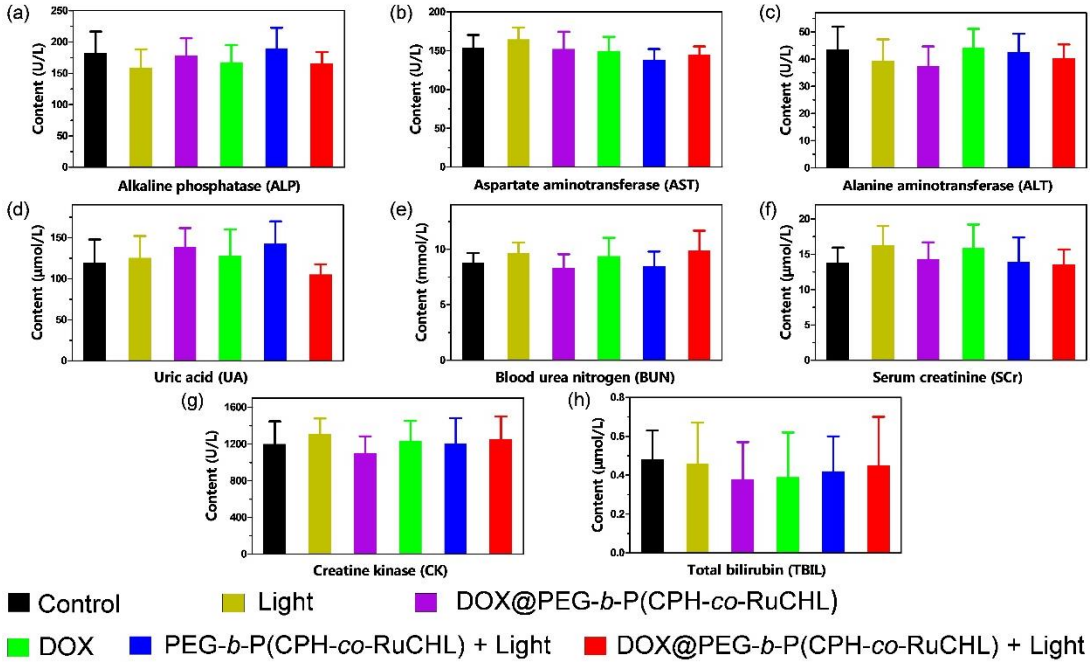

Figure 78. Biological safety evaluation. Blood biochemistry data of the mice of different treatments over 12 days: (a) alkaline phosphatase (ALP), (b) aspartate aminotransferase (AST), (c) alanine aminotransferase (ALT), (d) Uric acid (UA), (e) Blood urea nitrogen (BUN), (f) Serum creatinine (SCr), (g) Creatine kinase (CK), and (h) Total bilirubin (TBIL), respectively.

Chapter 4: Experimental section

4.1 Experimental details for chapter 3.1

Adapted with permission from my publication: M. Chen, et al. *Journal of Inorganic Biochemistry* 207 (2020) 111052. Copyright Elsevier.

4.1.1 Materials

$RuCl_3 \cdot xH_2O$ (99.9%), MBN (99%), tpy (97%) and biq (98%) were purchased from Alfa Aesar. Potassium hexafluorophosphate (98%), silver hexafluorophosphate (98%), lithium chloride, DOWEX 22 Cl anion exchange resin, BSA and GSH were purchased from Sigma–Aldrich. Saline (0.9% w/v of NaCl) was purchased from VWR International GmbH. DMEM was purchased from Gibco, USA. Sodium acetate buffer solution (3M, pH 5.5) was purchased from Life Technologies GmbH. Tris buffer solution (1M, pH 6.5) was purchased from Thermo Fisher GmbH. All other solvents were purchased from Fisher Scientific or Sigma–Aldrich. Dialysis tubing (3.5K MWCO) was purchased from SERVA Electrophoresis GmbH. Milli-Q water with a resistivity of 18.2 MΩ·cm was used in this study.

4.1.2 Methods

^1H NMR spectroscopy and COSY were recorded on a Bruker NMR AV250 spectrometer and AV300 spectrometer, respectively. HR-ESI-MS measurements were recorded with a Micromass Q-TOF-Ultima spectrometer (Johannes Gutenberg University, Mainz, Germany). UV/Vis absorption spectrum was obtained on a Lambda 900 spectrometer (Perkin Elmer). An LED (LCS-0656-03-22, Mightex Systems) with an output controller (SLC-MA04-MU, Mightex Systems) was used as a wavelength of 656 nm to induce the photosubstitution. HPLC analysis was performed on an Agilent HPLC system armed with a Merck Chromolith Performance RP18e 100-3 mm HPLC column, a 1100 Series Quaternary pump and a 1200 Series Diode detector. The detector was set at the wavelength of 260 nm for the system of MBN, the wavelength of 550 nm for the system of Ru1-MBN and the wavelength of 620 nm for the system of Ru2-2MBN, separately. TEM images were recorded on a FEI Tecnai^{TM} F20 TEM.

The chloride salt of each Ru complexes was dissolved in water or physiological solution with 30% methanol or acetone to increase the solubility. The solution concentrations of Ru-containing polymer nanoparticles and Ru complexes were from 2.7×10^{-6} to 2.1×10^{-4} M. Under imitated physiological conditions, saline and DMEM

were directly used. The concentration of sodium acetate buffer solution and tris buffer solution was 0.1 M. The concentration of BSA aqueous solution used in the experiment was 1.5×10^{-5} M. The concentration of GSH used in the experiment was 10^{-3} M.

4.1.3 Synthesis

Ru1-H_2O and Ru2-$2H_2O$ were synthesized according to the procedure described in literature.[164, 166] Ru1-MBN was synthesized according to literature with some modifications.[164] Generally, Ru1-H_2O (90 mg, 0.1 mmol) and MBN (16 mg, 0.12 mmol) were mixed in 10 mL acetone. The solution was degassed for 10 min. Then, the mixture was stirred in the dark under reflux overnight. After that, the solvent was removed by rotary evaporation under reduced pressure. Then, the crude product was purified by column chromatography (eluent: methanol/dichloromethane) with silica gel. Finally, the solvent was evaporated to obtain the product as a red solid (46 mg, 45%). The synthesis of Ru2-2MBN was described below. Briefly, Ru2-$2H_2O$ (103 mg, 0.12 mmol) and MBN (32 mg, 0.25 mmol) were mixed in acetone (10 mL). The solution was degassed for 10 min. After that, the mixture was stirred in the dark under reflux overnight. Then, the solvent was evaporated under reduced pressure. Finally, the crude product was purified using column chromatography (eluent: methanol/dichloro-methane) to obtain the product as a red solid (58 mg, 42%).

4.1.4 Preparation of polymer assemblies

Ru-containing block polymers (PolyRu1 and PolyRu2) were synthesized according to our previous work.[164, 166] To prepare polymer assemblies, 1 mg Ru-containing polymers was dissolved in 0.2 mL THF/DMF mixture (4/1=v/v) and stirred for 10 min. Then, 1.8 mL Milli-Q water was gently added to the polymer solution. The colloidal dispersion was continuously stirred for 20 min. Subsequently, the mixture was placed in a dialysis tube (MWCO 3500 Da) against Milli-Q water for two days to remove the organic solvents, Milli-Q water was replaced approximately every 8 h.

4.2 Experimental details for chapter 3.2

4.2.1 Materials

PEG-*b*-P(CPH-*co*-RuCHL) were synthesized according to our previous work.[165] DOX hydrochloride was purchased from Beijing Huafeng United Technology Co., Ltd. Saline (0.9% w/v of NaCl) was purchased from VWR International GmbH. DMEM was purchased from Gibco, USA. Sodium acetate buffer solution (3M, pH 5.5) was

purchased from Life Technologies GmbH. All other solvents were purchased from Fisher Scientific or Sigma–Aldrich. Milli-Q water with a resistivity of 18.2 MΩ·cm was used in this study. Dialysis tubing (3.5K MWCO) was purchased from SERVA Electrophoresis GmbH. D-Tube^{TM} Dialyzer MiNi (MWCO 6-8kDa) was purchased from EDM Millipore Corp., Billerica, MA USA. Slide-A-Lyzer MINI Dialysis Device (MWCO 10K) was purchased from Thermo Fisher Scientific.

4.2.2 Preparation of micelles

DOX@PEG-*b*-P(CPH-*co*-RuCHL) micelles were prepared through adding water to the organic mixture. Briefly, 0.9 mg DOX hydrochloride was dissolved in 0.1 mL DMF, adding 3 equiv. of trimethylamine to obtain hydrophobic DOX. 2.2 mg PEG-*b*-P(CPH-*co*-RuCHL) was dissolved in 0.3 mL THF/DMF mixture (4/1=v/v) and stirred for 10 min. Then, DOX solution was added to PEG-*b*-P(CPH-*co*-RuCHL) solution and stirred for 20 min. After that, 3.2 mL Milli-Q water was gently added to the polymer solution and continuously stirred for another 20 min. Subsequently, the mixture was purified in a dialysis tube (MWCO 3.5 K) against Milli-Q water for two days to remove the organic solvents. At last, the solution was collected from the dialysis tube. The amount of DOX encapsulated in the micelles was measured using fluorescence spectroscopy (TIDAS II spectrometer, J&M). PEG-*b*-P(CPH-*co*-RuCHL) micelles were prepared by the same procedures without adding DOX.

4.2.3 Physicochemical properties

The size and morphology of PEG-*b*-P(CPH-*co*-RuCHL) micelles and DOX@PEG-*b*-P(CPH-*co*-RuCHL) micelles were obtained using TEM (HT7700, Hitachi). The size distribution of micelles was determined by DLS on a Nano ZS90 particle size analyzer, Malvern (UK). The scattering angles were set to 90° for each sample. A laser with wavelength of 660 nm (120 mW cm^{-2}) was used as the light source for the physicochemical characterization experiments. The output power of the laser was controlled through a fiber coupled laser system (FC-655-1W, Changchun New Industries Optoelectronics Technology) and measured through a power meter (LP100/TS15, Changchun New Industries Optoelectronics Technology).

4.2.4 Photochemistry

Photoreaction of PEG-*b*-P(CPH-*co*-RuCHL) micelles was studied by UV/vis absorption spectroscopy. UV/vis detector was set at the wavelength of 260 nm for data collection and analysis. UV/Vis absorption spectrum was obtained on a Lambda 900

spectrometer (Perkin Elmer). An LED with wavelength of 656 nm (device type LCS-0656-03-22, Mightex Systems) was used to induce the Photoreaction. An LED controller (device type SLC-MA04-MU, Mightex Systems) was used to control the output power of the LED.

4.2.5 Release of ruthenium complexes

The LED at wavelength of 656 nm was used as the light source for Ru complexes release measurement. Generally, after red light (30 mW cm^{-2}) irradiation for 270 J cm^{-2} dose, the solution of DOX@PEG-*b*-P(CPH-*co*-RuCHL) micelles was transferred to D-Tube^{TM} mini dialyzers. These dialyzers were suspended onto 2 L of buffer solution (pH 5.5) containing 0.5% v/v tween-80 and shaken at room temperature. At different time point, the solution in the dialyzers was collected. The release of Ru complexes was quantified using ICP-MS (NexION 300X, Perkinelmer).

4.2.6 Release of doxorubicin

The LED at wavelength of 656 nm was used as the light source for DOX release measurement. Briefly, the solution of DOX@PEG-*b*-P(CPH-*co*-RuCHL) micelles was placed in DMEM solution red light (30 mW cm^{-2}) irradiation for 270 J cm^{-2} dose. Then, the mixture was transferred to Slide-A-Lyzer MINI Dialysis Devices, which were suspended onto 2 L of buffer solution (pH 5.5) containing 0.5% v/v tween-80 and shaken at room temperature. At different time point, the solution in the dialyzers was collected. The percentage of released DOX was determined by fluorescence spectroscopy.

4.3 Experimental details for chapter 3.3

4.3.1 Materials

Hoechst 33342 for Flow Cytometry was purchased from Life Technologies. Sodium azide, cytochalasin D, dithiothreitol, dichloro(1,10-phenanthroline)copper(II), ethidium bromide and CCK-8 were purchased from Sigma-Aldrich. Plasmid pUC19 and EcoRI restriction enzyme was purchased from New England Biolabs (Beijing) Ltd.

4.3.2 Cell culture

Cell culture medium RPMI 1640 and MEM nonessential amino acids, ANTI−ANTI, Hepes, and trypsin were purchased from Life Technologies, USA. MCF-7R cells were cultured in RPMI 1640 medium supplemented with 10% fetal bovine serum (FBS,

Lonza Group Ltd.), insulin Humalog, MEM nonessential amino acids, ANTI−ANTI, Hepes, and incubated at 37 °C in CO_2-incubator with 95% humidity and 5% CO_2. To detach adherent cells, MCF-7R cells were trypsinized with 0.25% trypsin for 5 min for further assays.

4.3.3 Internalization

The internalization of free DOX or DOX@PEG-*b*-P(CPH-*co*-RuCHL) micelles was determined in MCF-7R cells using flow cytometer. Briefly, 1.5×10^5 cells per well were seeded into 6-well plates and incubated overnight at 37 °C. After that, the medium was replaced by free DOX or DOX@PEG-*b*-P(CPH-*co*-RuCHL) micelles at a final DOX concentration of 1.0 μM and 2.0 μM for 0.5 h or 2 h under 37 °C. Cells were harvested and washed with PBS (pH 7.4, 1×) three times and subsequently analyzed by an Attune® acoustic focusing cytometer (Applied Biosystems, Life Technologies, Carlsbad, CA).

4.3.4 Endocytotic mechanism

Specific inhibition of endocytosis pathways was evaluated by MCF-7R cells to survey the possible endocytosis mechanism of DOX@PEG-*b*-P(CPH-*co*-RuCHL) micelles, with non-treatment as control. Briefly, 1.0×10^5 cells per well were seeded into 12-well plates and incubated in complete medium overnight. Then, the cells were washed using PBS three times, followed by preincubating at 37 °C with the inhibitor (sodium azide or cytochalasin D) or at 4 °C in serum-free RPMI 1640 medium for 1 h. After that, the medium was replaced by complete RPMI 1640 medium containing free DOX or DOX@PEG-*b*-P(CPH-*co*-RuCHL) micelles at a final DOX concentration of 2.0 μM and treated with respective inhibition for another 2 h. Subsequently, the medium was removed and the cells were washed by PBS three times. The cells were harvested and analyzed by the Attune® acoustic focusing cytometer.

4.3.5 Inhibition of drug efflux

Drug efflux of free DOX and DOX@PEG-*b*-P(CPH-*co*-RuCHL) micelles was evaluated using MCF-7R cells (overexpressing P-gp protein) to examine the potential drug efflux inhibition of DOX@PEG-*b*-P(CPH-*co*-RuCHL) micelles.[51] Generally, 1.5×10^5 cells per well were seeded into 6-well plates and incubated overnight at 37 °C. The cells were incubated with free DOX or DOX@PEG-*b*-P(CPH-*co*-RuCHL) micelles at a final DOX concentration of 10 μM for 4 h. After that, the medium was removed and the cells were washed by PBS three times, and then incubated with

complete RPMI 1640 medium for different time. Subsequently, the cells were washed, collected, and analyzed using the Attune® acoustic focusing cytometer.

4.3.6 Cell imaging

The intracellular distribution of free DOX or DOX@PEG-*b*-P(CPH-*co*-RuCHL) micelles was detected in MCF-7R cells by CLSM (LSM760, Carl Zeiss). Briefly, 2 × 10^4 cells per well were seeded into a Nunc Lab-Tek 8-well plate (Thermo Fisher, USA) and cultured in complete RPMI 1640 medium overnight at 37 °C. Then, the medium was washed and incubated with fresh medium containing free DOX or DOX@PEG-*b*-P(CPH-*co*-RuCHL) micelles at a final DOX concentration of 10 μM for 270 or 120 min, respectively. After that, MCF-7R cells containing DOX@PEG-*b*-P(CPH-*co*-RuCHL) micelles were divided into three groups: (1) incubation for another 150 min; (2) after irradiating the cells under 660 nm laser (50 mW cm^{-2}) for 10 min, incubation for another 140 min; (3) after irradiating the cells under 660 nm laser (50 mW cm^{-2}) for 30 min, incubation for another 120 min. The total incubation time of each group was the same (270 min). Subsequently, the cells were washed by PBS twice, followed by Hoechst 33342 staining to the nuclei, and then observed using CLSM. Excitation and detection was performed for the CLSM studies as follows: DOX was excited with a 483 nm laser, detected in the range from 520 to 620 nm. The cell nucleus stained with Hoechst 33342 was excited with a 405 nm laser, detected in the range from 425 to 475 nm.

4.3.7 Gel electrophoresis analysis

Agarose gel electrophoresis of plasmid was performed according to the literature.[192] Plasmid pUC19 amounts were quantified by UV/Vis absorption spectra (Lambda 900, Perkin Elmer). Briefly, 40 μg ml^{-1} of plasmid was incubated with free DOX or PEG-*b*-P(CPH-*co*-RuCHL) micelles or DOX@PEG-*b*-P(CPH-*co*-RuCHL) micelles, respectively, at various concentrations in 96-well plate. The plasmids containing micelles were prior incubated for 30 min then to red light activation for 1 h using the LED at 656 nm (50 mW cm^{-2}). Controls were performed by keeping PEG-*b*-P(CPH-*co*-RuCHL) micelles or DOX@PEG-*b*-P(CPH-*co*-RuCHL) micelles with plasmids in the dark. Then, all the samples were incubated overnight for the same time period before gel analysis. To identify the type of damaging the plasmid by DOX@PEG-*b*-P(CPH-*co*-RuCHL) micelles, linear plasmid and relaxed circle plasmid were prepared and run side-by-side with experimental samples. Linear plasmid was prepared by the EcoRI restriction enzyme following the manufacturers' protocol, while relaxed circle

plasmid, single cut, was prepared by adding plasmid, dithiothreitol, hydrogen peroxide, and copper phenanthroline into PBS (pH 7.5) for reaction. The final concentration of linear plasmid and relaxed circle plasmid was 40 μg ml^{-1}. Samples were resolved on a 1% non-ethidium bromide agarose gel, then stained with 0.5 μg ml^{-1} ethidium bromide for 40 min in tris-acetate buffer followed by destaining for 40 min in tris-acetate before imaging.

4.3.8 Cell viability

In vitro cytotoxicity/phototoxicity against MCF-7R cells were evaluated by CCK-8 assay. The measurement was determined calorimetrically by a multi reader (TECAN, Infinite M200, Germany) following the manufacturers protocol and based on the absorbance at 450 nm. The viability of cell growth was calculated as the following formula: Cell viability (%) = (mean of absorbance value of treatment group/mean absorbance value of control) × 100%. Specifically, 5×10^3 cells per well were seeded into 96-well plates and incubated for 24 h at 37 °C. Then, cells were divided into six groups. (1) Control: treatment with the culture medium; (2) Light: after treatment with the culture medium for 4 h, light irradiation for 30 min; (3) DOX@PEG-*b*-P(CPH-*co*-RuCHL) micelles: treatment with the culture medium containing various concentrations of DOX@PEG-*b*-P(CPH-*co*-RuCHL) micelles; (4) PEG-*b*-P(CPH-*co*-RuCHL) micelles + Light group: after treatment with the culture medium containing various concentrations of PEG-*b*-P(CPH-*co*-RuCHL) micelles for 4 h, light irradiation for 30 min; (5) DOX@PEG-*b*-P(CPH-*co*-RuCHL) micelles + Light group: after treatment with the culture medium containing various concentrations of DOX@PEG-*b*-P(CPH-*co*-RuCHL) micelles for 4 h, light irradiation for 30 min; (6) DOX: treatment with the culture medium containing various concentrations of free DOX. The LED at 656 nm (50 mW cm^{-2}) was used as light source. Cell viability was assessed after a terminal incubation time of 24 h.

4.3.9 Animal and tumor model

BALB/c nude mice (female, 18-20 g, 4-6 weeks) were purchased from Vital River Laboratory Animal Center (Beijing, China). The mice were kept under specific pathogen-free conditions with free access to standard food and water. All protocols for animal studies conformed to the Guide for the Care and Use of Laboratory Animals. All animal experiments were performed in accordance with guidelines approved by the ethics committee of Peking University.

4.3.10 Antitumor efficacy *in vivo*

1.0×10^7 MCF-7R cells were inoculated subcutaneously into the flank region of each mouse to establish the tumor-bearing mouse model. When the tumor volume reached ~50 mm^3 after implantation, the MCF-7R-tumor-bearing mice were randomly divided into six groups: (1) Control: mice without any treatment; (2) Light: mice exposed to light irradiation by 660 nm laser (200 mW cm^{-2}); (3) DOX: mice injected with free DOX (100 μL, 74 μg mL^{-1}); (4) DOX@PEG-*b*-P(CPH-*co*-RuCHL) micelles: mice injected with DOX@PEG-*b*-P(CPH-*co*-RuCHL) micelles (100 μL, 500 μg mL^{-1}); (5) PEG-*b*-P(CPH-*co*-RuCHL) micelles + Light group: mice injected with PEG-*b*-P(CPH-*co*-RuCHL) micelles (100 μL, 500 μg mL^{-1}) and then exposed to light irradiation by 660 nm laser (200 mW cm^{-2}); (6) DOX@PEG-*b*-P(CPH-*co*-RuCHL) micelles + Light group: mice injected with DOX@PEG-*b*-P(CPH-*co*-RuCHL) micelles (100 μL, 500 μg mL^{-1}) and then exposed to light irradiation by 660 nm laser (200 mW cm^{-2}). DOX or micelles were directly injected into the central part of the tumor of mice at day 1, day 3, and day 5. After 4 h, the mice in groups (2), (5) and (6) were locally irradiated for 30 min, respectively. The weights of mouse body were recorded every two days. Tumor volume was measured using a caliper and calculated as follows: $V=L*W^2/2$, where L and W were the length and width of the tumor, separately. At day 12, mice were sacrificed, and then the tumors were collected, weighed and photographed. The paraffin sections of the tumors were performed with H&E staining and Ki-67 IHC staining by Beijing Lawke Health Laboratory Center for Clinical Laboratory Development. The images were obtained by a fluorescence microscope (EVOS XL Core, Life technologies, USA).

4.3.11 Hemolysis assay

1.0 mL fresh red blood cells were collected from BALB/c nude mice, followed by centrifugation at 2000 rpm for 5 min. The cells were washed by saline for three times and then suspended in 15 mL saline. 0.4 mL red blood cells suspension was added to 0.6 mL saline containing different concentrations of DOX@PEG-*b*-P(CPH-*co*-RuCHL) micelles to obtain samples with the final concentration of 100, 200, 300, 400, 500 μg mL^{-1}. 0.4 mL red blood cells suspension added with 0.6 mL saline or water were used as the negative control and positive control, separately. The suspension was softly mixed, put at 37 °C for 4 h, and then centrifugation at 2000 rpm for 5 min. 100 μL supernatant was transferred into a 96-well plate, and then the absorbance value at 570 nm was measured. The percentage of hemolysis was calculated as follows: Hemolysis % = [(sample absorbance – background absorbance) / (positive control – negative control)]

× 100%.

4.3.12 Blood biochemistry analysis

After all the treatments were finished, the blood samples of mice were collected to detect alkaline phosphatase, aspartate aminotransferase, alanine aminotransferase, Uric acid, Blood urea nitrogen, Serum creatinine, Creatine kinase, and Total bilirubin, respectively, by Beijing Lawke Health Laboratory Center for Clinical Laboratory Development.

Chapter 5: Conclusion and perspective

5.1 Conclusion

We synthesized two well-defined Ru-containing block copolymers (PolyRu1 and PolyRu2): Ru complexes as side group in PolyRu1 and Ru complexes in the main chain in PolyRu2. Their corresponding Ru-building blocks (Ru1-MBN and Ru2-2MBN) were also synthesized and characterized. We investigated the stabilities of Ru1-MBN and Ru2-2MBN in the dark as well as their photoreactions under red light irradiation. Both Ru complexes, Ru1-MBN and Ru2-2MBN, were not stable in the H_2O/methanol (=7/3) mixture, but dissociated after spontaneous cleavage of the coordinated acetonitrile bonds. The dissociation procedure of Ru1-MBN in the dark was identical to that of Ru1-MBN under light irradiation. However, the two procedures were different for Ru2-2MBN.

In the process of drug delivery, Ru-containing materials would go through at least three microenvironments. Therefore, we studied and compared the stabilities of Ru complexes (Ru1-MBN and Ru2-2MBN) as well as Ru-containing polymer nanoparticles (PolyRu1 and PolyRu2) under imitated physiological conditions, involving saline, serum albumin aqueous solution, cell culture medium (DMEM) at pH 6.5 and cell culture medium at pH 5.5 with 1.0 mM glutathione. Ru1-MBN and Ru2-2MBN were labile under these conditions. The instability of these Ru complexes might hinder their biological applications. In contrast, nanostructured PolyRu1 and PolyRu2 were more stable than Ru1-MBN and Ru2-2MBN under imitated physiological conditions. The hydrophobic cores in the nanostructure protected Ru moieties from the external water environment and thus improved their stability. In addition, PolyRu1 and PolyRu2 could be activated with red light. Red light is able to penetrate more deeply into tissue than visible light or UV. The stabilities under physiological conditions and red-light-responsiveness of Ru-containing polymers make them potential candidates for biomedical applications.

Furthermore, a red-light-triggered Ru-containing block copolymer (PEG-*b*-P(CPH-*co*-RuCHL)) was designed. The amphiphilic structure of PEG-*b*-P(CPH-*co*-RuCHL) self-assembled into micelles with the core available for DOX encapsulation to form DOX@PEG-*b*-P(CPH-*co*-RuCHL) micelles. The morphology of PEG-*b*-P(CPH-*co*-RuCHL) and DOX@PEG-*b*-P(CPH-*co*-RuCHL) micelles was spherical and monodisperse by TEM measurements. DLS results showed the size of DOX@PEG-*b*-P(CPH-*co*-RuCHL) micelles increased ~ 5 nm after DOX loading. More importantly,

DOX@PEG-*b*-P(CPH-*co*-RuCHL) micelles could be stable in the dark, but activated by red light irradiation. Red light induced the damage of DOX@PEG-*b*-P(CPH-*co*-RuCHL) micelles in cell culture medium, causing the release of Ru complexes and DOX at the same time.

Finally, we applied DOX@PEG-*b*-P(CPH-*co*-RuCHL) micelles *in vitro* and *in vivo* to overcome multidrug resistance. Flow cytometry measurements displayed that compared to free DOX, DOX@PEG-*b*-P(CPH-*co*-RuCHL) micelles were rapid and effectively taken up by endocytosis into the drug-resistant cancer cells (MCF-7R cells), which overexpressed P-gp on the surface. The micelles were not transported out by P-gp and thus prompted the effective drug accumulation. CLSM experiments illustrated the release of DOX from the micelles and then the entrance to nucleus in MCF-7R cells were controlled by red light. DNA damage experiments showed that after light irradiation, the detached Ru complexes with the commercial anticancer drug chlorambucil increased the ability of DNA photobinding, inducing the DNA crosslinking. Integrating DOX interacted with DNA by intercalation, the synergetic effects in DOX@PEG-*b*-P(CPH-*co*-RuCHL) micelles resulted in the severe DNA damage.

The cytotoxicity experiments *in vitro* demonstrated that the massive MCF-7R cells were killed using DOX@PEG-*b*-P(CPH-*co*-RuCHL) micelles upon red light irradiation. In addition to DOX, both $[Ru(tpy)(biq)(H_2O)]^{2+}$ and chlorambucil in the Ru complexes could inhibit cancer cell growth and thus enhance anticancer efficiency. Moreover, DOX@PEG-*b*-P(CPH-*co*-RuCHL) micelles were used in MCF-7R tumor-bearing mice to overcome multidrug resistance *in vivo*. The mice were divided into six groups with different treatments. DOX@PEG-*b*-P(CPH-*co*-RuCHL) micelles could remarkably inhibit the tumor growth when irradiated with red light, compared to other five groups. In the staining of the tumor tissues, a great quantity of apoptotic and nonproliferative cells were observed in the group of DOX@PEG-*b*-P(CPH-*co*-RuCHL) micelles with light irradiation. Additionally, the micelles have a good blood compatibility without hemolysis. They did not cause any abnormality of blood biochemistry after the treatment. The co-release of dual drugs based on red-light-response DOX@PEG-*b*-P(CPH-*co*-RuCHL) micelles is a new strategy, which shows good therapeutic efficacy and opens a paradigm of combing new designed anticancer drug with conventional anticancer drug for photochemotherapy to overcome multidrug resistance.

5.2 Perspective

There are still open questions and difficulties regarding photoactivable Ru-containing polymers *in vivo* applications. First of all, their stability needs to be further improved. Although Ru-containing polymer assemblies can stabilize their corresponding Ru complexes under physiological conditions, we also notice a little hydrolysis of Ru complexes in their assemblies by UV/Vis absorption spectroscopy results, due to the instability of the coordinated acetonitrile bonds. The coordinated pyridine bonds exhibit more stability, which may develop an alternative approach to settle this problem.

Secondly, the wavelength that activates Ru-containing polymers should be further red-shifted to NIR area, which is the best activation wavelength. Our group has reported some Ru-containing polymers capable of releasing ligands using red light, but their Ru complexes hardly absorb beyond ~700 nm. Although Ru complexes can be activated using NIR light by the methods of two-photon absorption and photon upconversion, they require high-intensity lasers; the non-linear optical processes are inefficient. Therefore, the wavelength directly red-shifts to NIR area and then activates Ru-containing polymers, that is more suitable for biomedical applications in depth tissue.

Thirdly, Ru complexes in the polymers for photochemotherapy are better to be fluorescent. Tracing Ru complexes *in vivo* is difficult due to their non-fluorescence. Especially, once they are taken up by cancer cells and cleaved from the polymers by light, we scarcely know their whereabouts. The amount of Ru complexes that enter and accumulate in the nucleus cannot be observed and calculated. Thus, it is highly desirable to design the fluorescent Ru complexes in the polymers for photochemotherapy.

References

[1] Das M, Mohanty C, Sahoo SK. Ligand-based targeted therapy for cancer tissue. *Expert Opinion on Drug Delivery* **2009**, 6, 285-304.
[2] Mohanty C, Das M, R Kanwar J, K Sahoo S. Receptor mediated tumor targeting: an emerging approach for cancer therapy. *Current Drug Delivery* **2011**, 8, 45-58.
[3] Larsson M, Huang W-T, Liu D-M, Losic D. Local co-administration of gene-silencing RNA and drugs in cancer therapy: State-of-the art and therapeutic potential. *Cancer Treatment Reviews* **2017**, 55, 128-135.
[4] Hanahan D, Weinberg RA. Hallmarks of cancer: the next generation. *Cell* **2011**, 144, 646-674.
[5] Peer D, Karp JM, Hong S, Farokhzad OC, Margalit R, Langer R. Nanocarriers as an emerging platform for cancer therapy. *Nature Nanotechnology* **2007**, 2, 751-760.
[6] Talebian S, Foroughi J, Wade SJ, Vine KL, Dolatshahi-Pirouz A, Mehrali M, Conde J, Wallace GG. Biopolymers for antitumor implantable drug delivery systems: Recent advances and future outlook. *Advanced Materials* **2018**, 30, 1706665.
[7] Parhi P, Mohanty C, Sahoo SK. Nanotechnology-based combinational drug delivery: an emerging approach for cancer therapy. *Drug Discovery Today* **2012**, 17, 1044-1052.
[8] Wolinsky JB, Colson YL, Grinstaff MW. Local drug delivery strategies for cancer treatment: gels, nanoparticles, polymeric films, rods, and wafers. *Journal of Controlled Release* **2012**, 159, 14-26.
[9] Conde J, Shomron N, Artzi N. Cancer Therapy: Biomaterials for Abrogating Metastasis: Bridging the Gap between Basic and Translational Research. *Advanced Healthcare Materials* **2016**, 5, 2452-2452.
[10] Allen TM, Cullis PR. Drug delivery systems: entering the mainstream. *Science* **2004**, 303, 1818-1822.
[11] De Souza R, Zahedi P, Allen CJ, Piquette-Miller M. Polymeric drug delivery systems for localized cancer chemotherapy. *Drug Delivery* **2010**, 17, 365-375.
[12] Persidis A. Cancer multidrug resistance. *Nature Biotechnology* **1999**, 17, 94.
[13] Ayers D, Nasti A. Utilisation of nanoparticle technology in cancer chemoresistance. *Journal of Drug Delivery* **2012**, 2012,
[14] Longley D, Johnston P. Molecular mechanisms of drug resistance. *The Journal of Pathology: A Journal of the Pathological Society of Great Britain and Ireland* **2005**, 205, 275-292.
[15] Fletcher JI, Haber M, Henderson MJ, Norris MD. ABC transporters in cancer: more than just drug efflux pumps. *Nature Reviews Cancer* **2010**, 10, 147-156.

[16] Meng H, Liong M, Xia T, Li Z, Ji Z, Zink JI, Nel AE. Engineered design of mesoporous silica nanoparticles to deliver doxorubicin and P-glycoprotein siRNA to overcome drug resistance in a cancer cell line. *ACS Nano* **2010**, 4, 4539-4550.

[17] Markman JL, Rekechenetskiy A, Holler E, Ljubimova JY. Nanomedicine therapeutic approaches to overcome cancer drug resistance. *Advanced Drug Delivery Reviews* **2013**, 65, 1866-1879.

[18] Yeung J, Esposito MT, Gandillet A, Zeisig BB, Griessinger E, Bonnet D, So CWE. β-Catenin mediates the establishment and drug resistance of MLL leukemic stem cells. *Cancer Cell* **2010**, 18, 606-618.

[19] Copur S, Aiba K, Drake JC, Allegra CJ, Chu E. Thymidylate synthase gene amplification in human colon cancer cell lines resistant to 5-fluorouracil. *Biochemical Pharmacology* **1995**, 49, 1419-1426.

[20] Bradbury PA, Kulke MH, Heist RS, Zhou W, Ma C, Xu W, Marshall AL, Zhai R, Hooshmand SM, Asomaning K. Cisplatin pharmacogenetics, DNA repair polymorphisms, and esophageal cancer outcomes. *Pharmacogenetics and Genomics* **2009**, 19, 613.

[21] Arora S, Kothandapani A, Tillison K, Kalman-Maltese V, Patrick SM. Downregulation of XPF–ERCC1 enhances cisplatin efficacy in cancer cells. *DNA Repair* **2010**, 9, 745-753.

[22] Plati J, Bucur O, Khosravi-Far R. Apoptotic cell signaling in cancer progression and therapy. *Integrative Biology* **2011**, 3, 279-296.

[23] Kushnareva Y, Newmeyer DD. Bioenergetics and cell death. *Annals of the New York Academy of Sciences* **2010**, 1201, 50.

[24] Rolland SG, Conradt B. New role of the BCL2 family of proteins in the regulation of mitochondrial dynamics. *Current Opinion in Cell Biology* **2010**, 22, 852-858.

[25] Gandhi L, Camidge DR, De Oliveira MR, Bonomi P, Gandara D, Khaira D, Hann CL, McKeegan EM, Litvinovich E, Hemken PM. Phase I study of Navitoclax (ABT-263), a novel Bcl-2 family inhibitor, in patients with small-cell lung cancer and other solid tumors. *Journal of Clinical Oncology* **2011**, 29, 909.

[26] Kapse-Mistry S, Govender T, Srivastava R, Yergeri M. Nanodrug delivery in reversing multidrug resistance in cancer cells. *Frontiers in Pharmacology* **2014**, 5, 159.

[27] Szakács G, Paterson JK, Ludwig JA, Booth-Genthe C, Gottesman MM. Targeting multidrug resistance in cancer. *Nature Reviews Drug Discovery* **2006**, 5, 219-234.

[28] Luqmani Y. Mechanisms of drug resistance in cancer chemotherapy. *Medical Principles and Practice* **2005**, 14, 35-48.

[29] Hu C-MJ, Zhang L. Therapeutic nanoparticles to combat cancer drug resistance.

Current Drug Metabolism **2009**, 10, 836-841.
[30] Majidinia M, Mirza-Aghazadeh-Attari M, Rahimi M, Mihanfar A, Karimian A, Safa A, Yousefi B. Overcoming multidrug resistance in cancer: Recent progress in nanotechnology and new horizons. *IUBMB life* **2020**, 72, 855-871.
[31] Wang M, Thanou M. Targeting nanoparticles to cancer. *Pharmacological Research* **2010**, 62, 90-99.
[32] Farokhzad OC, Langer R. Impact of nanotechnology on drug delivery. *ACS Nano* **2009**, 3, 16-20.
[33] Gao Z, Zhang L, Sun Y. Nanotechnology applied to overcome tumor drug resistance. *Journal of Controlled Release* **2012**, 162, 45-55.
[34] Xie X, Zhang Y, Li F, Lv T, Li Z, Chen H, Jia L, Gao Y. Challenges and opportunities from basic cancer biology for nanomedicine for targeted drug delivery. *Current Cancer Drug Targets* **2019**, 19, 257-276.
[35] Prabhakar U, Maeda H, Jain RK, Sevick-Muraca EM, Zamboni W, Farokhzad OC, Barry ST, Gabizon A, Grodzinski P, Blakey DC. Challenges and key considerations of the enhanced permeability and retention effect for nanomedicine drug delivery in oncology. *Cancer Research* **2013**, 73, 2412-2417.
[36] Cho K, Wang X, Nie S, Shin DM. Therapeutic nanoparticles for drug delivery in cancer. *Clinical Cancer Research* **2008**, 14, 1310-1316.
[37] Koziara JM, Whisman TR, Tseng MT, Mumper RJ. In-vivo efficacy of novel paclitaxel nanoparticles in paclitaxel-resistant human colorectal tumors. *Journal of Controlled Release* **2006**, 112, 312-319.
[38] Rouf MA, Vural I, Renoir JM, Hincal AA. Development and characterization of liposomal formulations for rapamycin delivery and investigation of their antiproliferative effect on MCF7 cells. *Journal of Liposome Research* **2009**, 19, 322-331.
[39] Gabizon A, Catane R, Uziely B, Kaufman B, Safra T, Cohen R, Martin F, Huang A, Barenholz Y. Prolonged circulation time and enhanced accumulation in malignant exudates of doxorubicin encapsulated in polyethylene-glycol coated liposomes. *Cancer Research* **1994**, 54, 987-992.
[40] Zhang Y, Zhang H, Wang X, Wang J, Zhang X, Zhang Q. The eradication of breast cancer and cancer stem cells using octreotide modified paclitaxel active targeting micelles and salinomycin passive targeting micelles. *Biomaterials* **2012**, 33, 679-691.
[41] Chen M, Gao C, Lü S, Chen Y, Liu M. Dual redox-triggered shell-sheddable micelles self-assembled from mPEGylated starch conjugates for rapid drug release. *RSC Advances* **2016**, 6, 9164-9174.

[42] Seow WY, Xue JM, Yang Y-Y. Targeted and intracellular delivery of paclitaxel using multi-functional polymeric micelles. *Biomaterials* **2007**, 28, 1730-1740.
[43] Taurin S, Nehoff H, Greish K. Anticancer nanomedicine and tumor vascular permeability; where is the missing link? *Journal of Controlled Release* **2012**, 164, 265-275.
[44] Harris JM, Chess RB. Effect of pegylation on pharmaceuticals. *Nature Reviews Drug Discovery* **2003**, 2, 214-221.
[45] del Pino P, Yang F, Pelaz B, Zhang Q, Kantner K, Hartmann R, Martinez de Baroja N, Gallego M, Möller M, Manshian BB. Basic physicochemical properties of polyethylene glycol coated gold nanoparticles that determine their interaction with cells. *Angewandte Chemie International Edition* **2016**, 55, 5483-5487.
[46] Gottstein C, Wu G, Wong BJ, Zasadzinski JA. Precise quantification of nanoparticle internalization. *ACS Nano* **2013**, 7, 4933-4945.
[47] Rose PG. Pegylated liposomal doxorubicin: optimizing the dosing schedule in ovarian cancer. *The Oncologist* **2005**, 10, 205-214.
[48] Sonneveld P, Hajek R, Nagler A, Spencer A, Bladé J, Robak T, Zhuang SH, Harousseau JL, Orlowski RZ, Investigators DMS. Combined pegylated liposomal doxorubicin and bortezomib is highly effective in patients with recurrent or refractory multiple myeloma who received prior thalidomide/lenalidomide therapy. *Cancer* **2008**, 112, 1529-1537.
[49] Krown SE, Northfelt DW, Osoba D, Stewart JS. Use of liposomal anthracyclines in Kaposi's sarcoma. *Seminars in Oncology* **2004**, 31, 36-52.
[50] Knop K, Hoogenboom R, Fischer D, Schubert US. Poly(ethylene glycol) in drug delivery: pros and cons as well as potential alternatives. *Angewandte Chemie International Edition* **2010**, 49, 6288-6308.
[51] Wei T, Chen C, Liu J, Liu C, Posocco P, Liu X, Cheng Q, Huo S, Liang Z, Fermeglia M. Anticancer drug nanomicelles formed by self-assembling amphiphilic dendrimer to combat cancer drug resistance. *Proceedings of the National Academy of Sciences* **2015**, 112, 2978-2983.
[52] Tang J, Fu H, Kuang Q, Zhang L, Zhang Q, Liu Y, Ran R, Gao H, Zhang Z, He Q. Liposomes co-modified with cholesterol anchored cleavable PEG and octaarginines for tumor targeted drug delivery. *Journal of drug targeting* **2014**, 22, 313-326.
[53] Bar-Zeev M, Livney YD, Assaraf YG. Targeted nanomedicine for cancer therapeutics: towards precision medicine overcoming drug resistance. *Drug Resistance Updates* **2017**, 31, 15-30.
[54] Gottesman MM, Ling V. The molecular basis of multidrug resistance in cancer:

The early years of P-glycoprotein research. *FEBS Letters* **2006**, 580, 998-1009.
[55] Gervasoni JE, Fields SZ, Krishna S, Baker MA, Rosado M, Thuraisamy K, Hindenburg AA, Taub RN. Subcellular distribution of daunorubicin in P-glycoprotein-positive and-negative drug-resistant cell lines using laser-assisted confocal microscopy. *Cancer Research* **1991**, 51, 4955-4963.
[56] Molinari A, Cianfriglia M, Meschini S, Calcabrini A, Arancia G. P-glycoprotein expression in the Golgi apparatus of multidrug-resistant cells. *International Journal of Cancer* **1994**, 59, 789-795.
[57] Calcabrini A, Meschini S, Stringaro A, Cianfriglia M, Arancia G, Molinari A. Detection of P-glycoprotein in the nuclear envelope of multidrug resistant cells. *The Histochemical Journal* **2000**, 32, 599-606.
[58] Wang J, Sun J, Chen Q, Gao Y, Li L, Li H, Leng D, Wang Y, Sun Y, Jing Y. Star-shape copolymer of lysine-linked di-tocopherol polyethylene glycol 2000 succinate for doxorubicin delivery with reversal of multidrug resistance. *Biomaterials* **2012**, 33, 6877-6888.
[59] Jabr-Milane LS, van Vlerken LE, Yadav S, Amiji MM. Multi-functional nanocarriers to overcome tumor drug resistance. *Cancer Treatment Reviews* **2008**, 34, 592-602.
[60] Tang J, Zhang L, Gao H, Liu Y, Zhang Q, Ran R, Zhang Z, He Q. Co-delivery of doxorubicin and P-gp inhibitor by a reduction-sensitive liposome to overcome multidrug resistance, enhance anti-tumor efficiency and reduce toxicity. *Drug Delivery* **2016**, 23, 1130-1143.
[61] Fulda S, Galluzzi L, Kroemer G. Targeting mitochondria for cancer therapy. *Nature Reviews Drug Discovery* **2010**, 9, 447-464.
[62] Weinhouse S. The Warburg hypothesis fifty years later. *Zeitschrift für Krebsforschung und Klinische Onkologie* **1976**, 87, 115-126.
[63] Indran IR, Tufo G, Pervaiz S, Brenner C. Recent advances in apoptosis, mitochondria and drug resistance in cancer cells. *Biochimica et Biophysica Acta (BBA)-Bioenergetics* **2011**, 1807, 735-745.
[64] Chen W-H, Luo G-F, Qiu W-X, Lei Q, Liu L-H, Zheng D-W, Hong S, Cheng S-X, Zhang X-Z. Tumor-Triggered Drug Release with Tumor-Targeted Accumulation and Elevated Drug Retention To Overcome Multidrug Resistance. *Chemistry of Materials* **2016**, 28, 6742-6752.
[65] Creixell M, Peppas NA. Co-delivery of siRNA and therapeutic agents using nanocarriers to overcome cancer resistance. *Nano Today* **2012**, 7, 367-379.
[66] Burnett JC, Rossi JJ. RNA-based therapeutics: current progress and future

prospects. *Chemistry & Biology* **2012**, 19, 60-71.
[67] Chen SH, Zhaori G. Potential clinical applications of siRNA technique: benefits and limitations. *European Journal of Clinical Investigation* **2011**, 41, 221-232.
[68] Khan IU, Khan RU, Asif H, Khalid SH, Asghar S, Saleem M, Shah KU, Shah SU, Rizvi SA, Shahzad Y. Co-delivery strategies to overcome multidrug resistance in ovarian cancer. *International Journal of Pharmaceutics* **2017**, 533, 111-124.
[69] Chen AM, Zhang M, Wei D, Stueber D, Taratula O, Minko T, He H. Co-delivery of doxorubicin and Bcl-2 siRNA by mesoporous silica nanoparticles enhances the efficacy of chemotherapy in multidrug-resistant cancer cells. *Small* **2009**, 5, 2673-2677.
[70] Roointan A, Kianpour S, Memari F, Gandomani M, Gheibi Hayat SM, Mohammadi-Samani S. Poly(lactic-co-glycolic acid): The most ardent and flexible candidate in biomedicine! *International Journal of Polymeric Materials and Polymeric Biomaterials* **2018**, 67, 1028-1049.
[71] Zolnik BS, Burgess DJ. Effect of acidic pH on PLGA microsphere degradation and release. *Journal of Controlled Release* **2007**, 122, 338-344.
[72] Li R, Xie Y. Nanodrug delivery systems for targeting the endogenous tumor microenvironment and simultaneously overcoming multidrug resistance properties. *Journal of Controlled Release* **2017**, 251, 49-67.
[73] Ke C-J, Chiang W-L, Liao Z-X, Chen H-L, Lai P-S, Sun J-S, Sung H-W. Real-time visualization of pH-responsive PLGA hollow particles containing a gas-generating agent targeted for acidic organelles for overcoming multi-drug resistance. *Biomaterials* **2013**, 34, 1-10.
[74] Karimi M, Zangabad PS, Ghasemi A, Hamblin MR. Smart internal stimulus-responsive nanocarriers for drug and gene delivery. **2015**. Morgan & Claypool Publishers.
[75] Karimi M, Ghasemi A, Zangabad PS, Rahighi R, Basri SMM, Mirshekari H, Amiri M, Pishabad ZS, Aslani A, Bozorgomid M. Smart micro/nanoparticles in stimulus-responsive drug/gene delivery systems. *Chemical Society reviews* **2016**, 45, 1457-1501.
[76] Cheng L, Wang C, Feng L, Yang K, Liu Z. Functional nanomaterials for phototherapies of cancer. *Chemical Reviews* **2014**, 114, 10869-10939.
[77] Sun W, Thiramanas R, Slep LD, Zeng X, Mailander V, Wu S. Photoactivation of Anticancer Ru Complexes in Deep Tissue: How Deep Can We Go? *Chemistry – A European Journal* **2017**, 23, 10832-10837.
[78] Fomina N, McFearin C, Sermsakdi M, Edigin O, Almutairi A. UV and near-IR triggered release from polymeric nanoparticles. *Journal of the American Chemical Society* **2010**, 132, 9540-9542.

[79] Wu S, Butt HJ. Near-Infrared-Sensitive Materials Based on Upconverting Nanoparticles. *Advanced Materials* **2016**, 28, 1208-1226.
[80] Juzenas P, Juzeniene A, Kaalhus O, Iani V, Moan J. Noninvasive fluorescence excitation spectroscopy during application of 5-aminolevulinic acid in vivo. *Photochemical & Photobiological Sciences* **2002**, 1, 745-748.
[81] Karimi M, Sahandi Zangabad P, Baghaee-Ravari S, Ghazadeh M, Mirshekari H, Hamblin MR. Smart nanostructures for cargo delivery: uncaging and activating by light. *Journal of the American Chemical Society* **2017**, 139, 4584-4610.
[82] Yu Y, Xu Q, He S, Xiong H, Zhang Q, Xu W, Ricotta V, Bai L, Zhang Q, Yu Z. Recent advances in delivery of photosensitive metal-based drugs. *Coordination Chemistry Reviews* **2019**, 387, 154-179.
[83] Abadeer NS, Murphy CJ. Recent progress in cancer thermal therapy using gold nanoparticles. *The Journal of Physical Chemistry C* **2016**, 120, 4691-4716.
[84] Zou L, Wang H, He B, Zeng L, Tan T, Cao H, He X, Zhang Z, Guo S, Li Y. Current approaches of photothermal therapy in treating cancer metastasis with nanotherapeutics. *Theranostics* **2016**, 6, 762.
[85] Jaque D, Maestro LM, Del Rosal B, Haro-Gonzalez P, Benayas A, Plaza J, Rodriguez EM, Sole JG. Nanoparticles for photothermal therapies. *Nanoscale* **2014**, 6, 9494-9530.
[86] Marangon I, Ménard-Moyon C, Silva AK, Bianco A, Luciani N, Gazeau F. Synergic mechanisms of photothermal and photodynamic therapies mediated by photosensitizer/carbon nanotube complexes. *Carbon* **2016**, 97, 110-123.
[87] Li Z, Wang H, Chen Y, Wang Y, Li H, Han H, Chen T, Jin Q, Ji J. pH-and NIR Light-Responsive Polymeric Prodrug Micelles for Hyperthermia-Assisted Site-Specific Chemotherapy to Reverse Drug Resistance in Cancer Treatment. *Small* **2016**, 12, 2731-2740.
[88] Triesscheijn M, Baas P, Schellens JH, Stewart FA. Photodynamic therapy in oncology. *Oncologist* **2006**, 11, 1034-1044.
[89] Liu K, Liu X, Zeng Q, Zhang Y, Tu L, Liu T, Kong X, Wang Y, Cao F, Lambrechts SA. Covalently assembled NIR nanoplatform for simultaneous fluorescence imaging and photodynamic therapy of cancer cells. *ACS Nano* **2012**, 6, 4054-4062.
[90] Sharman WM, Allen CM, Van Lier JE. Photodynamic therapeutics: basic principles and clinical applications. *Drug Discovery Today* **1999**, 4, 507-517.
[91] O'Connor AE, Gallagher WM, Byrne AT. Porphyrin and nonporphyrin photosensitizers in oncology: preclinical and clinical advances in photodynamic therapy. *Photochemistry and Photobiology* **2009**, 85, 1053-1074.

[92] Jin CS, Lovell JF, Chen J, Zheng G. Ablation of hypoxic tumors with dose-equivalent photothermal, but not photodynamic, therapy using a nanostructured porphyrin assembly. *ACS Nano* **2013**, 7, 2541-2550.
[93] Li Y, Zhang W, Niu J, Chen Y. Mechanism of photogenerated reactive oxygen species and correlation with the antibacterial properties of engineered metal-oxide nanoparticles. *ACS Nano* **2012**, 6, 5164-5173.
[94] Fan W, Huang P, Chen X. Overcoming the Achilles' heel of photodynamic therapy. *Chemical Society reviews* **2016**, 45, 6488-6519.
[95] Ethirajan M, Chen Y, Joshi P, Pandey RK. The role of porphyrin chemistry in tumor imaging and photodynamic therapy. *Chemical Society reviews* **2011**, 40, 340-362.
[96] Plaetzer K, Krammer B, Berlanda J, Berr F, Kiesslich T. Photophysics and photochemistry of photodynamic therapy: fundamental aspects. *Lasers in Medical Science* **2009**, 24, 259-268.
[97] Kamkaew A, Lim SH, Lee HB, Kiew LV, Chung LY, Burgess K. BODIPY dyes in photodynamic therapy. *Chemical Society reviews* **2013**, 42, 77-88.
[98] Zhao J, Wu W, Sun J, Guo S. Triplet photosensitizers: from molecular design to applications. *Chemical Society reviews* **2013**, 42, 5323-5351.
[99] DeRosa MC, Crutchley RJ. Photosensitized singlet oxygen and its applications. *Coordination Chemistry Reviews* **2002**, 233, 351-371.
[100] Macdonald IJ, Dougherty TJ. Basic principles of photodynamic therapy. *Journal of Porphyrins and Phthalocyanines* **2001**, 5, 105-129.
[101] Lucky SS, Muhammad Idris N, Li Z, Huang K, Soo KC, Zhang Y. Titania coated upconversion nanoparticles for near-infrared light triggered photodynamic therapy. *ACS Nano* **2015**, 9, 191-205.
[102] Park H, Park W, Na K. Doxorubicin loaded singlet-oxygen producible polymeric micelle based on chlorine e6 conjugated pluronic F127 for overcoming drug resistance in cancer. *Biomaterials* **2014**, 35, 7963-7969.
[103] Olejniczak J, Carling C-J, Almutairi A. Photocontrolled release using one-photon absorption of visible or NIR light. *Journal of Controlled Release* **2015**, 219, 18-30.
[104] Chen Y, Lei W, Jiang G, Hou Y, Li C, Zhang B, Zhou Q, Wang X. Fusion of photodynamic therapy and photoactivated chemotherapy: a novel Ru (II) arene complex with dual activities of photobinding and photocleavage toward DNA. *Dalton Transactions* **2014**, 43, 15375-15384.
[105] Lovejoy KS, Lippard SJ. Non-traditional platinum compounds for improved accumulation, oral bioavailability, and tumor targeting. *Dalton Transactions* **2009**, 10651-10659.

[106] Sainuddin T, Pinto M, Yin H, Hetu M, Colpitts J, McFarland SA. Strained ruthenium metal–organic dyads as photocisplatin agents with dual action. *Journal of Inorganic Biochemistry* **2016**, 158, 45-54.
[107] Song H, Kang X, Sun J, Jing X, Wang Z, Yan L, Qi R, Zheng M. Nanoparticle delivery of sterically hindered platinum (iv) prodrugs shows 100 times higher potency than that of cisplatin upon light activation. *Chemical Communications* **2016**, 52, 2281-2283.
[108] Zhou L, Wang H, Li Y. Stimuli-responsive nanomedicines for overcoming cancer multidrug resistance. *Theranostics* **2018**, 8, 1059.
[109] Wink DA, Miranda KM, Espey MG, Pluta RM, Hewett SJ, Colton C, Vitek M, Feelisch M, Grisham MB. Mechanisms of the antioxidant effects of nitric oxide. *Antioxidants and Redox Signaling* **2001**, 3, 203-213.
[110] Cole SP, Deeley RG. Transport of glutathione and glutathione conjugates by MRP1. *Trends in Pharmacological Sciences* **2006**, 27, 438-446.
[111] Zhang X, Tian G, Yin W, Wang L, Zheng X, Yan L, Li J, Su H, Chen C, Gu Z. Controllable generation of nitric oxide by near-infrared-sensitized upconversion nanoparticles for tumor therapy. *Advanced Functional Materials* **2015**, 25, 3049-3056.
[112] Ren Z, Gu X, Lu B, Chen Y, Chen G, Feng J, Lin J, Zhang Y, Peng H. Anticancer efficacy of a nitric oxide-modified derivative of bifendate against multidrug-resistant cancer cells. *Journal of Cellular and Molecular Medicine* **2016**, 20, 1095-1105.
[113] Fan J, He Q, Liu Y, Zhang F, Yang X, Wang Z, Lu N, Fan W, Lin L, Niu G. Light-responsive biodegradable nanomedicine overcomes multidrug resistance via NO-enhanced chemosensitization. *ACS Applied Materials & Interfaces* **2016**, 8, 13804-13811.
[114] Galanski M. Recent developments in the field of anticancer platinum complexes. *Recent patents on anti-cancer drug discovery* **2006**, 1, 285-295.
[115] Shaili E. Platinum anticancer drugs and photochemotherapeutic agents: recent advances and future developments. *Science Progress* **2014**, 97, 20-40.
[116] Mcquitty RJ. Metal-based drugs. *Science Progress* **2014**, 97, 1-19.
[117] Hurley LH. DNA and its associated processes as targets for cancer therapy. *Nature Reviews Cancer* **2002**, 2, 188-200.
[118] Hartinger CG, Dyson PJ. Bioorganometallic chemistry—from teaching paradigms to medicinal applications. *Chemical Society reviews* **2009**, 38, 391-401.
[119] Ohmichi M, Hayakawa J, Tasaka K, Kurachi H, Murata Y. Mechanisms of platinum drug resistance. *Trends in pharmacological sciences* **2005**, 26, 113-116.
[120] Bergamo A, Gaiddon C, Schellens J, Beijnen J, Sava G. Approaching tumour

therapy beyond platinum drugs: status of the art and perspectives of ruthenium drug candidates. *Journal of Inorganic Biochemistry* **2012**, 106, 90-99.

[121] Zeng L, Gupta P, Chen Y, Wang E, Ji L, Chao H, Chen Z-S. The development of anticancer ruthenium (II) complexes: from single molecule compounds to nanomaterials. *Chemical Society reviews* **2017**, 46, 5771-5804.

[122] Monro S, Colón KL, Yin H, Roque III J, Konda P, Gujar S, Thummel RP, Lilge L, Cameron CG, McFarland SA. Transition metal complexes and photodynamic therapy from a tumor-centered approach: Challenges, opportunities, and highlights from the development of TLD1433. *Chemical Reviews* **2018**, 119, 797-828.

[123] Thota S, Rodrigues DA, Crans DC, Barreiro EJ. Ru (II) Compounds: Next-Generation Anticancer Metallotherapeutics? *Journal of Medicinal Chemistry* **2018**, 90-99.

[124] Kostova I. Ruthenium complexes as anticancer agents. *Current Medicinal Chemistry* **2006**, 13, 1085-1107.

[125] Artner C, Holtkamp HU, Hartinger CG, Meier-Menches SM. Characterizing activation mechanisms and binding preferences of ruthenium metallo-prodrugs by a competitive binding assay. *Journal of Inorganic Biochemistry* **2017**, 177, 322-327.

[126] Chatlas J, Van Eldik R, Keppler B. Spontaneous aquation reactions of a promising tumor inhibitor *trans*-imidazolium-tetrachlorobis(imidazole)ruthenium(III), *trans*-HIm [$RuCl_4(Im)_2$]. *Inorganica Chimica Acta* **1995**, 233, 59-63.

[127] Bijelic A, Theiner S, Keppler BK, Rompel A. X-ray structure analysis of indazolium *trans*-[tetrachlorobis(1*H*-indazole)ruthenate(III)](KP1019) bound to human serum albumin reveals two ruthenium binding sites and provides insights into the drug binding mechanism. *Journal of Medicinal Chemistry* **2016**, 59, 5894-5903.

[128] Meier-Menches SM, Gerner C, Berger W, Hartinger CG, Keppler BK. Structure-activity relationships for ruthenium and osmium anticancer agents-towards clinical development. *Chemical Society reviews* **2018**, 47, 909-928.

[129] Cetinbas N, Webb MI, Dubland JA, Walsby CJ. Serum-protein interactions with anticancer Ru (III) complexes KP1019 and KP418 characterized by EPR. *JBIC Journal of Biological Inorganic Chemistry* **2010**, 15, 131-145.

[130] Depenbrock H, Schmelcher S, Peter R, Keppler B, Weirich G, Block T, Rastetter J, Hanauske A-R. Preclinical activity of *trans*-indazolium [tetrachlorobisindazoleruthenate(III)] (NSC 666158; IndCR; KP 1019) against tumour colony-forming units and haematopoietic progenitor cells. *European Journal of Cancer* **1997**, 33, 2404-2410.

[131] Rademaker-Lakhai JM, van den Bongard D, Pluim D, Beijnen JH, Schellens JH.

A phase I and pharmacological study with imidazolium-*trans*-DMSO-imidazole-tetrachlororuthenate, a novel ruthenium anticancer agent. *Clinical Cancer Research* **2004**, 10, 3717-3727.

[132] Wachter E, Heidary DK, Howerton BS, Parkin S, Glazer EC. Light-activated ruthenium complexes photobind DNA and are cytotoxic in the photodynamic therapy window. *Chemical Communications* **2012**, 48, 9649-9651.

[133] Huang H, Yu B, Zhang P, Huang J, Chen Y, Gasser G, Ji L, Chao H. Highly Charged Ruthenium(II) Polypyridyl Complexes as Lysosome-Localized Photosensitizers for Two-Photon Photodynamic Therapy. *Angewandte Chemie International Edition* **2015**, 54, 14049-14052.

[134] Choi NW, Verbridge SS, Williams RM, Chen J, Kim JY, Schmehl R, Farnum CE, Zipfel WR, Fischbach C, Stroock AD. Phosphorescent nanoparticles for quantitative measurements of oxygen profiles in vitro and in vivo. *Biomaterials* **2012**, 33, 2710-2722.

[135] Knoll JD, Turro C. Control and utilization of ruthenium and rhodium metal complex excited states for photoactivated cancer therapy. *Coordination Chemistry Reviews* **2015**, 282-283, 110-126.

[136] Wachter E, Zamora A, Heidary DK, Ruiz J, Glazer EC. Geometry matters: inverse cytotoxic relationship for *cis/trans*-Ru(II) polypyridyl complexes from *cis/trans*-$[PtCl_2(NH_3)_2]$. *Chemical Communications* **2016**, 52, 10121-10124.

[137] Albani BA, Pena B, Leed NA, de Paula NA, Pavani C, Baptista MS, Dunbar KR, Turro C. Marked improvement in photoinduced cell death by a new tris-heteroleptic complex with dual action: singlet oxygen sensitization and ligand dissociation. *Journal of the American Chemical Society* **2014**, 136, 17095-17101.

[138] Knoll JD, Albani BA, Turro C. New Ru(II) complexes for dual photoreactivity: ligand exchange and $^1O_2$ generation. *Accounts of Chemical Research* **2015**, 48, 2280-2287.

[139] Zeng L, Gupta P, Chen Y, Wang E, Ji L, Chao H, Chen ZS. The development of anticancer ruthenium(ii) complexes: from single molecule compounds to nanomaterials. *Chemical Society reviews* **2017**, 46, 5771-5804.

[140] Lameijer LN, Ernst D, Hopkins SL, Meijer MS, Askes SH, Le Dévédec SE, Bonnet S. A red light-activated ruthenium-caged NAMPT inhibitor remains phototoxic in hypoxic cancer cells. *Angewandte Chemie International Edition* **2017**, 56, 11549–11553.

[141] Siewert B, Langerman M, Hontani Y, Kennis JTM, van Rixel VHS, Limburg B, Siegler MA, Talens Saez V, Kieltyka RE, Bonnet S. Turning on the red

phosphorescence of a [Ru(tpy)(bpy)(Cl)]Cl complex by amide substitution: self-aggregation, toxicity, and cellular localization of an emissive ruthenium-based amphiphile. *Chemical Communications* **2017**, 53, 11126-11129.

[142] Zayat L, Filevich O, Baraldo LM, Etchenique R. Ruthenium polypyridyl phototriggers: from beginnings to perspectives. *Philosophical Transactions of the Royal Society A: Mathematical, Physical and Engineering Sciences* **2013**, 371, 20120330.

[143] Dickerson M, Howerton B, Bae Y, Glazer E. Light-Sensitive Ruthenium Complex-Loaded Cross-linked Polymeric Nanoassemblies for the Treatment of Cancer. *Journal of Materials Chemistry B* **2016**, 4, 394-408.

[144] Notaro A, Gasser G. Monomeric and dimeric coordinatively saturated and substitutionally inert Ru(ii) polypyridyl complexes as anticancer drug candidates. *Chemical Society reviews* **2017**, 46, 7317-7337.

[145] Mari C, Pierroz V, Ferrari S, Gasser G. Combination of Ru (II) complexes and light: new frontiers in cancer therapy. *Chemical Science* **2015**, 6, 2660-2686.

[146] Scaiano J, Redmond R, Mehta B, Arnason J. EFFICIENCY OF THE PHOTOPROCESSES LEADING TO SINGLET OXYGEN ($^1\delta_g$) GENERATION BY α-TERTHIENYL: OPTICAL ABSORPTION, OPTOACOUSTIC CALORIMETRY AND INFRARED LUMINESCENCE STUDIES. *Photochemistry and Photobiology* **1990**, 52, 655-659.

[147] Scaiano J, MacEachern A, Arnason J, Morand P, Weir D. Singlet oxygen generating efficiency of α-terthienyl and some of its synthetic analogues. *Photochemistry and Photobiology* **1987**, 46, 193-199.

[148] Yin H, Stephenson M, Gibson J, Sampson E, Shi G, Sainuddin T, Monro S, McFarland SA. In vitro multiwavelength PDT with 3IL states: Teaching old molecules new tricks. *Inorganic Chemistry* **2014**, 53, 4548-4559.

[149] Singh TN, Turro C. Photoinitiated DNA binding by *cis*-$[Ru(bpy)_2(NH_3)_2]^{2+}$. *Inorganic Chemistry* **2004**, 43, 7260-7262.

[150] Salassa L, Ruiu T, Garino C, Pizarro AM, Bardelli F, Gianolio D, Westendorf A, Bednarski PJ, Lamberti C, Gobetto R. EXAFS, DFT, Light-induced nucleobase binding, and cytotoxicity of the photoactive complex *cis*-$[Ru(bpy)_2(CO)Cl]^+$. *Organometallics* **2010**, 29, 6703-6710.

[151] Van Rixel V, Siewert B, Hopkins S, Askes S, Busemann A, Siegler M, Bonnet S. Green light-induced apoptosis in cancer cells by a tetrapyridyl ruthenium prodrug offering two trans coordination sites. *Chemical Science* **2016**, 7, 4922-4929.

[152] Bomben PG, Robson KC, Sedach PA, Berlinguette CP. On the viability of

cyclometalated Ru (II) complexes for light-harvesting applications. *Inorganic Chemistry* **2009**, 48, 9631-9643.

[153] Palmer AM, Peña B, Sears RB, Chen O, El Ojaimi M, Thummel RP, Dunbar KR, Turro C. Cytotoxicity of cyclometallated ruthenium complexes: the role of ligand exchange on the activity. *Philosophical Transactions of the Royal Society A: Mathematical, Physical and Engineering Sciences* **2013**, 371, 20120135.

[154] Sgambellone MA, David A, Garner RN, Dunbar KR, Turro C. Cellular toxicity induced by the photorelease of a caged bioactive molecule: Design of a potential dual-action Ru (II) complex. *Journal of the American Chemical Society* **2013**, 135, 11274-11282.

[155] Albani BA, Peña B, Leed NA, De Paula NA, Pavani C, Baptista MS, Dunbar KR, Turro C. Marked improvement in photoinduced cell death by a new tris-heteroleptic complex with dual action: singlet oxygen sensitization and ligand dissociation. *Journal of the American Chemical Society* **2014**, 136, 17095-17101.

[156] Villemin E, Ong YC, Thomas CM, Gasser G. Polymer encapsulation of ruthenium complexes for biological and medicinal applications. *Nature Reviews Chemistry* **2019**, 3, 261-282.

[157] Allardyce CS, Dyson PJ. Ruthenium in medicine: current clinical uses and future prospects. *Platinum Metals Reviews* **2001**, 45, 62.

[158] Allardyce CS, Dorcier A, Scolaro C, Dyson PJ. Development of organometallic (organo-transition metal) pharmaceuticals. *Applied Organometallic Chemistry* **2005**, 19, 1-10.

[159] Koch JH, Rogers W, Dwyer F, Gyarfas EC. The metabolic fate of tris-1,10-phenanthroline 106ruthenium (II) perchlorate, a compound with anticholinesterase and curare-like activity. *Australian Journal of Biological Sciences* **1957**, 10, 342-350.

[160] Dobrucki JW. Interaction of oxygen-sensitive luminescent probes $Ru(phen)_3^{2+}$ and $Ru(bipy)_3^{2+}$ with animal and plant cells in vitro: Mechanism of phototoxicity and conditions for non-invasive oxygen measurements. *Journal of Photochemistry and Photobiology B: Biology* **2001**, 65, 136-144.

[161] Puckett CA, Barton JK. Methods to explore cellular uptake of ruthenium complexes. *Journal of the American Chemical Society* **2007**, 129, 46-47.

[162] Matsumura Y, Maeda H. A new concept for macromolecular therapeutics in cancer chemotherapy: mechanism of tumoritropic accumulation of proteins and the antitumor agent smancs. *Cancer Research* **1986**, 46, 6387-6392.

[163] Ringsdorf H. Structure and properties of pharmacologically active polymers. *Journal of Polymer Science: Polymer Symposia* **1975**, 51, 135-153.

[164] Sun W, Parowatkin M, Steffen W, Butt HJ, Mailander V, Wu S. Ruthenium-Containing Block Copolymer Assemblies: Red-Light-Responsive Metallopolymers with Tunable Nanostructures for Enhanced Cellular Uptake and Anticancer Phototherapy. *Advanced Healthcare Materials* **2016**, 5, 467-473.

[165] Sun W, Wen Y, Thiramanas R, Chen M, Han J, Gong N, Wagner M, Jiang S, Meijer MS, Bonnet S, Butt H-J, Mailänder V, Liang X-J, Wu S. Red-Light-Controlled Release of Drug-Ru Complex Conjugates from Metallopolymer Micelles for Phototherapy in Hypoxic Tumor Environments. *Advanced Functional Materials* **2018**, 28, 1804227.

[166] Sun W, Li S, Haupler B, Liu J, Jin S, Steffen W, Schubert US, Butt HJ, Liang XJ, Wu S. An Amphiphilic Ruthenium Polymetallodrug for Combined Photodynamic Therapy and Photochemotherapy In Vivo. *Advanced Materials* **2017**, 29, 1603702.

[167] Xie C, Sun W, Lu H, Kretzschmann A, Liu J, Wagner M, Butt HJ, Deng X, Wu S. Reconfiguring surface functions using visible-light-controlled metal-ligand coordination. *Nature Communications* **2018**, 9, 3842.

[168] He S, Krippes K, Ritz S, Chen Z, Best A, Butt HJ, Mailander V, Wu S. Ultralow-intensity near-infrared light induces drug delivery by upconverting nanoparticles. *Chemical Communications* **2015**, 51, 431-434.

[169] Chen Z, He S, Butt HJ, Wu S. Photon upconversion lithography: patterning of biomaterials using near-infrared light. *Advanced Materials* **2015**, 27, 2203-2206.

[170] Chen Z, Thiramanas R, Schwendy M, Xie C, Parekh SH, Mailander V, Wu S. Upconversion Nanocarriers Encapsulated with Photoactivatable Ru Complexes for Near-Infrared Light-Regulated Enzyme Activity. *Small* **2017**, 13, 1700997.

[171] Chen Z, Xiong Y, Etchenique R, Wu S. Manipulating pH using near-infrared light assisted by upconverting nanoparticles. *Chemical Communications* **2016**, 52, 13959-13962.

[172] Chen Z, Sun W, Butt HJ, Wu S. Upconverting-nanoparticle-assisted photochemistry induced by low-intensity near-infrared light: how low can we go? *Chemistry – A European Journal* **2015**, 21, 9165-9170.

[173] Sun W, Zeng X, Wu S. Photoresponsive ruthenium-containing polymers: potential polymeric metallodrugs for anticancer phototherapy. *Dalton Transactions* **2018**, 47, 283-286.

[174] Weissleder R, Ntziachristos V. Shedding light onto live molecular targets. *Nature Medicine* **2003**, 9, 123-128.

[175] Wu S, Butt HJ. Near-Infrared-Sensitive Materials Based on Upconverting Nanoparticles. *Advanced Materials* **2016**, 28, 1208-1226.

[176] Chen B, Dai W, He B, Zhang H, Wang X, Wang Y, Zhang Q. Current Multistage Drug Delivery Systems Based on the Tumor Microenvironment. *Theranostics* **2017**, 7, 538-558.

[177] Chen H, Kim S, Li L, Wang S, Park K, Cheng JX. Release of hydrophobic molecules from polymer micelles into cell membranes revealed by Forster resonance energy transfer imaging. *Proceedings of the National Academy of Sciences* **2008**, 105, 6596-6601.

[178] Chen H, Kim S, He W, Wang H, Low PS, Park K, Cheng JX. Fast release of lipophilic agents from circulating PEG-PDLLA micelles revealed by in vivo forster resonance energy transfer imaging. *Langmuir* **2008**, 24, 5213-5217.

[179] Wang H, Tang L, Tu C, Song Z, Yin Q, Yin L, Zhang Z, Cheng J. Redox-responsive, core-cross-linked micelles capable of on-demand, concurrent drug release and structure disassembly. *Biomacromolecules* **2013**, 14, 3706-3712.

[180] San Miguel V, Alvarez M, Filevich O, Etchenique R, del Campo A. Multiphoton reactive surfaces using ruthenium(II) photocleavable cages. *Langmuir* **2012**, 28, 1217-1221.

[181] Sun W, Li S, Häupler B, Liu J, Jin S, Steffen W, Schubert US, Butt HJ, Liang XJ, Wu S. An Amphiphilic Ruthenium Polymetallodrug for Combined Photodynamic Therapy and Photochemotherapy In Vivo. *Advanced Materials* **2016**,

[182] Knoll JD, Albani BA, Durr CB, Turro C. Unusually efficient pyridine photodissociation from Ru(II) complexes with sterically bulky bidentate ancillary ligands. *The Journal of Physical Chemistry A* **2014**, 118, 10603-10610.

[183] Huynh VT, de Souza P, Stenzel MH. Polymeric micelles with pendant dicarboxylato chelating ligands prepared via a michael addition for cis-platinum drug delivery. *Macromolecules* **2011**, 44, 7888-7900.

[184] Riegel IC, Eisenberg A, Petzhold CL, Samios D. Novel bowl-shaped morphology of crew-cut aggregates from amphiphilic block copolymers of styrene and 5-(N,N-diethylamino) isoprene. *Langmuir* **2002**, 18, 3358-3363.

[185] Harris JM, Chess RB. Effect of pegylation on pharmaceuticals. *Nature Reviews Drug Discovery* **2003**, 2, 214-221.

[186] Pelaz B, del Pino P, Maffre P, Hartmann R, Gallego M, Rivera-Fernandez S, de la Fuente JM, Nienhaus GU, Parak WJ. Surface Functionalization of Nanoparticles with Polyethylene Glycol: Effects on Protein Adsorption and Cellular Uptake. *ACS Nano* **2015**, 9, 6996-7008.

[187] Yang J, Liu W, Sui M, Tang J, Shen Y. Platinum (IV)-coordinate polymers as intracellular reduction-responsive backbone-type conjugates for cancer drug delivery.

Biomaterials **2011**, 32, 9136-9143.
[188] Aryal S, Hu C-MJ, Zhang L. Polymer-cisplatin conjugate nanoparticles for acid-responsive drug delivery. *ACS Nano* **2009**, 4, 251-258.
[189] Mazloomi-Rezvani M, Salami-Kalajahi M, Roghani-Mamaqani H. Fabricating core (Au)-shell (different stimuli-responsive polymers) nanoparticles via inverse emulsion polymerization: Comparing DOX release behavior in dark room and under NIR lighting. *Colloids and Surfaces B: Biointerfaces* **2018**, 166, 144-151.
[190] Xu D, Lu Q, Hu X. Down-regulation of P-glycoprotein expression in MDR breast cancer cell MCF-7/ADR by honokiol. *Cancer Letters* **2006**, 243, 274-280.
[191] Holohan C, Van Schaeybroeck S, Longley DB, Johnston PG. Cancer drug resistance: an evolving paradigm. *Nature Reviews Cancer* **2013**, 13, 714.
[192] Howerton BS, Heidary DK, Glazer EC. Strained ruthenium complexes are potent light-activated anticancer agents. *Journal of the American Chemical Society* **2012**, 134, 8324-8327.
[193] Tacar O, Sriamornsak P, Dass CR. Doxorubicin: an update on anticancer molecular action, toxicity and novel drug delivery systems. *Journal of Pharmacy and Pharmacology* **2013**, 65, 157-170.
[194] Fornari FA, Randolph JK, Yalowich JC, Ritke MK, Gewirtz DA. Interference by doxorubicin with DNA unwinding in MCF-7 breast tumor cells. *Molecular Pharmacology* **1994**, 45, 649-656.
[195] Momparler RL, Karon M, Siegel SE, Avila F. Effect of adriamycin on DNA, RNA, and protein synthesis in cell-free systems and intact cells. *Cancer Research* **1976**, 36, 2891-2895.
[196] Vijayashree I, Niranjana P, Prabhu G, Sureshbabu V, Manjanna JJJoCS. Conjugation of Au nanoparticles with chlorambucil for improved anticancer activity. *Journal of Cluster Science* **2017**, 28, 133-148.
[197] Bœuf G, Roullin GV, Moreau J, Van Gulick L, Zambrano Pineda N, Terryn C, Ploton D, Andry MC, Chuburu F, Dukic S. Encapsulated Ruthenium (II) Complexes in Biocompatible Poly($_{D,L}$-lactide-*co*-glycolide) Nanoparticles for Application in Photodynamic Therapy. *ChemPlusChem* **2014**, 79, 171-180.
[198] Brown JM, Wilson WR. Exploiting tumour hypoxia in cancer treatment. *Nature Reviews Cancer* **2004**, 4, 437-447.
[199] Titford M. Progress in the development of microscopical techniques for diagnostic pathology. *Journal of Histotechnology* **2009**, 32, 9-19.

Abbreviations

ATP	adenosine triphosphate
ABC	adenosine triphosphate-binding cassette
Bcl-2	B-cell lymphoma 2
Biq	2,2'-biquinoline
BNN6	*N,N′*-di-sec-Butyl-*N,N′*-dinitroso-1,4-phenylenediamine
BSA	bovine serum albumin
CCK-8	cell counting kit-8
CHL	chlorambucil
CLSM	confocal laser scanning microscopy
CO_2	carbon dioxide
COSY	correlation spectroscopy
CPH	6-(4-cyanophenoxy) hexyl methacrylate
DLS	dynamic light scattering
DMEM	dulbecco's modified eagle's medium
DNA	deoxyribonucleic acid
DOX	doxorubicin
DOX@PEG-b -P(CPH-co-RuCHL)	doxorubicin-loading ruthenium-containing block copolymer
EPR	enhanced permeability and retention
GPC	gel permeation chromatography
GSH	L-glutathione reduced
H&E	hematoxylin and eosin
^{1}H NMR	^{1}H nuclear magnetic resonance
HPLC	high-performance liquid chromatography
HR-ESI-MS	high resolution electrospray ionization mass spectrometry
ICP-MS	inductively coupled plasma mass spectrometry
IHC	immunohistochemical
IR	infrared radiation
MBN	4-methoxybenzonitrile
MCF-7R	drug-resistant Michigan Cancer Foundation-7
MLCT	metal-to-ligand charge transfer
MSNs	mesoporous silica nanoparticles
MDR	multidrug resistance
NIR	near infrared radiation

NO	nitric oxide
$^1O_2$	singlet oxygen
$^3O_2$	triplet oxygen
PACT	photo-activated chemotherapy
PDT	photodynamic therapy
PEG	polyethylene glycol
PEG-b-PCPH	poly(ethylene glycol)-block-poly(6-(4-cyanophenoxy) hexyl methacrylate)
PEG-*b*-P(CPH-*co*-RuCHL)	ruthenium-containing block copolymer
P-gp	permeability glycoprotein
PLGA	poly(lactic-co-glycolic) acid
polyRu1	a diblock copolymer containing Ru complexes as side group
polyRu2	a triblock copolymer containing Ru complexes in the main chain
Pt	platinum
PTT	photothermal therapy
ROS	reactive oxygen species
Ru	ruthenium
Ru1-H_2O	$[Ru(terpyridine)(biquinoline)(H_2O)]^{2+}$
Ru1-MBN	$[Ru(terpyridine)(biquinoline)(methoxybenzonitrile)]^{2+}$
Ru2-2Cl	$Ru(biquinoline)_2Cl_2$
Ru2-2H_2O	$[Ru(biquinoline)_2(H_2O)_2]^{2+}$
Ru2-2MBN	$[Ru(biquinoline)_2(methoxybenzonitrile)_2]^{2+}$
siRNA	small interference ribonucleic acid
TEM	transmission electron microscopy
Tpy	2,2′:6′,2″-terpyridine
UV	ultraviolet

Publications

1. **Mingjia Chen**, Wen Sun, Annika Kretzschmann, Hans-Jürgen Butt, Si Wu. Nanostructured polymer assemblies stabilize photoactivatable anticancer ruthenium complexes under physiological conditions. *Journal of Inorganic Biochemistry*. 2020, 207, 111052.
2. Wen Sun, Yan Wen, Raweewan Thiramanas, **Mingjia Chen**, Jianxiong Han, Ningqiang Gong, Manfred Wagner, Shuai Jiang, Michael S. Meijer, Sylvestre Bonnet, Hans-Jürgen Butt, Volker Mailänder, Xing-Jie Liang, Si Wu. Red-light-Controlled Release of Drug-Ru Complex Conjugates from Metallopolymer Micelles for Phototherapy in Hypoxic Tumor Environments. *Advanced Functional Materials*. 2018, 1804227.
3. **Mingjia Chen**, Ningqiang Gong, Wen Sun, Jianxiong Han, Hans-Jürgen Butt, Xing-Jie Liang, and Si Wu. Red-light-triggered co-release of dual drugs from ruthenium metallopolymer micelles for photochemotherapy to overcome multidrug resistance. *In preparation*.

Acknowledgment

To my grandmother Renliang Yu who I most love, she passed away during my PhD period. Popo, you happily live in heaven now. In my life, the most lucky and proud thing is to be your grandson. Thank you for teaching me how to love. I miss you every day. Love you forever.

I would like to express my sincere gratitude to Prof. Dr. Hans-Jürgen Butt. Thank you so much for providing me the opportunity as a PhD student in your group. My research and this thesis are done under your guidance and encouragement. Your creativity, kindness and patience always inspire me not only in science but also in life. I cannot image a better supervisor like you.

I would like to thank my project leader Prof. Dr. Si Wu. Without your lead, discussion and revise, I cannot publish the paper in the challenging research field.

I would like to thank my colleague Dr. Wen Sun for much help on the synthesis in experiments, the suggestion in projects and the writing in manuscripts.

I also would like to thank Prof. Dr. Xing-Jie Liang to giving me a chance for animal experiments in his lab. With the help of his student Dr. Ningqiang Gong, I can finish the experiments.

I am grateful to my colleagues, Katrin Kirchhoff, Beate Müller in institute and Dr. Elena Berger-Nicoletti in Johannes Gutenberg-Universität Mainz. I appreciate your help in my experiments.

I would like to say thanks to the members of our little group, Annika Kretzschmann, Jianxiong Han, Jiahui Liu, Yazhi Liu and Xiaolong Zeng. I will remember all the enjoyment with you.

Last but not the least, I would like to thank my family, my parents and grandfather for supporting me unconditionally throughout my PhD period and my whole life. Love you.